CHEMICAL ENGINEERING SCIENCE
GENIE CHIMIQUE

VOL. I JULY 1952 NO. 4

Application of the Temkin kinetic equation to ammonia synthesis in large-scale reactors

D. ANNABLE

Research Department, Imperial Chemical Industries Limited, Billingham Division

(Received 1 March 1952)

Summary—The rate of reaction in an industrial, high pressure ammonia synthesis reactor is expressed in terms of the kinetic equation formulated by TEMKIN and PYZHEV. An estimate of catalyst activity is derived, affording a means of comparing different catalysts, and of measuring catalyst deterioration.

Optimum temperatures giving maximum rates of reaction are estimated for certain conditions of catalyst activity and initial gas composition.

A reasonable approach to optimum conditions is calculated for a particular design of catalyst bed, fitted with a means of removing some of the heat of reaction. Incorporation of the design in a plant reactor showed that the best operating conditions conformed closely to those calculated.

Résumé—La vitesse de réaction dans un convertisseur industriel pour la synthèse de l'ammoniac sous haute pression, est exprimée sous la forme de l'équation conétique de TEMKIN et PYZHEV. On obtient une estimation de l'activité catalytique, fournissant un moyen de comparer divers catalyseurs et de mesurer la baisse d'activité d'un catalyseur.

On obtient une valeur approximative des températures optima, donnant les plus grandes vitesses de réaction, pour des conditions données d'activité catalytique et de composition initiale des gaz.

Une approximation raisonnable des conditions optima a été calculée pour une disposition particulière du lit de catalyseur, comportant un moyen d'évacuer une partie des calories fournies par la réaction.

L'introduction de ce dispositif dans un convertisseur industriel a montré que les meilleures conditions opératoires coïncident fort bien avec celles prévues par le calcul.

INTRODUCTION

TEMKIN and PYZHEV [1] formulated a kinetic equation for ammonia synthesis assuming that the rate determining step was the process of activated adsorption of nitrogen. A formula for the latter was postulated on a semi-empirical basis, and the equation for ammonia synthesis in a static system given as:

$$\frac{dP^{*}_{NH_3}}{dt} = \frac{dN_2}{dt} = k_1 \frac{P_{N_2} \cdot P_{H_2}^{1.5}}{P_{NH_3}} - k_2 \frac{P_{NH_3}}{P_{H_2}^{1.5}} \qquad (1)$$

where

N_{N_2} = no. of mols. of N_2, per unit vol. of catalyst after time of contact t hours.

P_{NH_3}, P_{N_2}, P_{H_2} = partial pressures of NH_3, N_2, H_2 after time t.

k_1 and k_2 are the reaction velocity constants for ammonia synthesis and decomposition, respectively.

At pressures above atmospheric, the perfect gas laws are assumed to hold. k_1 and k_2 are related to the equilibrium constant K_p, thus: $\frac{k_1}{k_2} = K_p^2$. As K_p is known accurately [2] over a wide range of temperature and pressure, experimental reaction data can be used to determine values of the reaction velocity constants. k_2 is the constant usually calculated, probably because experimenters, such as WINTER [3], first concentrated on the kinetics of ammonia decomposition. k_2 should obey the Arrhenius equation:

$$k_2 = b_2 e^{-E_{dec}/RT}$$

where

E_{dec} = apparent activation energy for ammonia decomposition cals/mol N_2 reacting.

R = gas constant.

T = absolute temperature °K.

b_2 = frequency factor.

TEMKIN and PYZHEV [1] and EMMETT and KUMMER [4] have applied the kinetic equation to experimental data at pressures up to 100 atm for various space velocities, H_2/N_2 ratios and degrees of approach to equilibrium. The data were obtained at three temperatures, 370, 400 and 450° C. The equation was found to interpret the data satisfactorily, except that k_2 decreased with increasing pressure, and some variation: 40000 to 55000—was observed in E_{dec}**.

* TEMKIN omitted the factor 2 between the rate of N_2 adsorption and NH_3 synthesis, and neglected the change, at constant pressure, of the total volume of gas with reaction [see eq. (2) and (3)].

** See Tables 4 and 5.

The present paper describes the fitting of the equation to approximate plant data, to find a measure of catalyst activity and a means of estimating the best practical reaction conditions. The data were obtained at 245 and 300 atm pressure, and covered a temperature range of 370 to 550° C.

EXPERIMENTAL

The plant reactor, from which the data at 245 atm were obtained, was an upright cylindrical forging, containing a single vertical catalyst bed. The basket holding the catalyst was lagged and measurements showed the heat loss from the converter to be only about 2% of the total heat evolved. The catalyst bed was therefore considered as adiabatic.

Gas at 245 atm pressure, and of constant (initial) gas composition flowed continuously into the reactor. After being heated to reaction temperature, the gas passed down over the catalyst bed, where it was partially converted to ammonia, with a rise in temperature due to the heat of reaction. Conditions were steady, and the pressure constant, so that at each level in the catalyst bed, there was a constant temperature and also a constant ammonia concentration, both quantities increasing with the amount of catalyst traversed.

After leaving the catalyst, the gas gave up some of its heat to the incoming gas, before flowing out of the reactor.

The variables measured were the pressure, the inlet gas rate and composition, the concentration of ammonia in the exit gas, and temperatures taken at short intervals through the catalyst bed by a thermocouple which could be moved in a vertical sheath near the axis of the reactor.

Except for a more comprehensive exploration of temperature in the catalyst bed, the measurements were the normal plant readings, and no great accuracy for them is claimed.

The data at 300 atm were obtained from a reactor similar to the above, but containing several adiabatic beds in series, between each of which was provision for adding cold unconverted gas. The measurements used were the pressure, the initial gas composition, the amounts and temperatures of the gas added before each bed, the total amount of ammonia made in the reactor, and the temperatures at the exit of each bed.

TREATMENT OF DATA

As the catalyst beds were adiabatic, various simplifying assumptions could be made. Radial conduction of heat was taken to be negligible, so that catalyst temperatures over any cross-section were considered uniform. Gas and catalyst temperatures were assumed equivalent and longitudinal conduction of heat was neglected.

In the case of the single bed reactor, for the purposes of analysis, the catalyst bed, of total depth 13 ft, was considered as a series of small horizontal sections, of depth 6″ or 1 ft, such that there were temperature measurements at the beginning and end of each section.

Since all the heat of reaction appeared as increased heat content of the reaction gas, the amount of reaction in each of the above sections could be found from the rise in temperature of the gas over the section, using specific heat and heat of reaction data. The calculation was commenced at the top section, as the rate and composition of the gas were known only at the inlet of the bed. The result for the top section provided inlet gas data for the second section. Repeating the calculation for successive sections gave a series of amounts of ammonia synthesised, the sum of which should agree with the total ammonia made in the reactor, as given by the gas rate and the inlet and exit ammonia analyses. The agreement actually obtained was usually within ±6%.

In the case of the multi-bed reactor, each bed was considered as one catalyst section. The amounts of reaction and the gas concentrations were calculated by the same method as above, making allowance for the extra gas added before each bed. The initial reaction temperatures in the beds subsequent to the first were calculated from the exit temperatures of the preceding beds and the amounts of cooling produced by the added cold gas. The agreement between the calculated amount of ammonia made in the reactor and the total amount measured was usually between 0 and −7%.

The kinetic equation was adapted to the continuous flow system and became:

$$\frac{dA}{dw} = 2\left[k_1 \frac{P_{N_2} P_{H_2}^{1.5}}{P_{NH_3}} - k_2 \frac{P_{NH_3}}{P_{H_2}^{1.5}}\right]. \qquad (2)$$

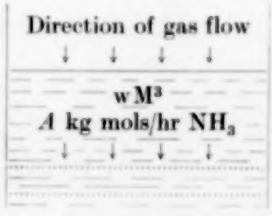

where A = flow of ammonia in kg mols/hr after the gas has traversed w, M^3 of catalyst.

The partial pressures of the gases were expressed in terms of total pressure P atm, and z the mol fraction of NH_3 in the gas after flowing over w, M^3 of catalyst, and the equation was rearranged explicitly in k_2, viz.

$$k_2 = \frac{P^{0.5}a^{1.5}V}{48} \frac{z(1-bz)^{1.5}}{(1+z)[L^2(1-bz)^4 - z^2]} \frac{dz}{dw} \qquad (3)$$

where, after traversing w, M^3 of catalyst, the gas rate is V, M^3/hr, measured at 1 atm and 20° C, the temperature is T° K and the composition in mol fraction is:

z of NH_3, $a(1-bz)$ of H_2, and $\frac{a}{3}(1-bz)$ of N_2.

$$L = \frac{z_{eq}}{(1-bz_{eq})^2}$$

where z_{eq} is the equilibrium mol fraction of NH_3 at pressure P atm, and temperature T° K. a and b are constants determined from the initial gas composition.

As integration of the equation for an adiabatic system, where z is a function of T, would be extremely complex, the following approximation was adopted. The average reaction velocity over each catalyst section, given by $\Delta z/\Delta w$, was assumed equal to the actual velocity dz/dw at the arithmetical average temperature of the section, for the concentrations of reactants and products corresponding to that temperature.

The errors thus involved were, for the case of the single bed reactor, generally less than 1 or 2° C in temperature, and 0·001 in the mol fraction of ammonia, and were within the errors of measurement. In the calculation of k_2, except for conditions near equilibrium, an error of 2° C in temperature will cause an error of about 9% in k_2, whilst an error of 0·001 in the mol fraction of ammonia will affect the magnitude of k_2 by less than 10%. As the errors act in opposite directions, the final inaccuracy of k_2 should not be more than 10%. Errors of measurement may easily cause an additional error of the same order in the k_2 values.

The reaction velocity constant has not been calculated for conditions very near equilibrium, for the errors produced by errors of measurement are then very large.

Using the approximation to apply the kinetic equation to the data of the multi-bed reactor may involve greater errors, because of the more scanty information on catalyst temperatures. It is estimated that in the majority of the examples, the error incurred in the k_2 value should not be greater than 16%.

With regard to the poor accuracy, it is pointed out that the purpose of this work was to find out how much use could be made of the plant data as measured, without introducing more elaborate instrumentation to improve the accuracy and frequency of measurement.

Table 1. Experimental data for the determination of k_2

Pressure: 245 atm. *Temperature range:* 404–555° C. *Efficiency range:* 0·09 to 0·96.

Representative initial gas composition:

	mol fraction
NH_3	0·021
H_2	0·674
N_2	0·225
CH_4	0·048
A	0·032
	1·000

Temp. °C	z mol frac.	Effic. z/z_{eq}	$\Delta z/\Delta w$	Gas rate kM^3/hr	k_2
404	0·0321	0·09	0·096	34·4	17·0
404	0·0263	0·07	0·095	34·2	13·1
414	0·0286	0·08	0·105	23·8	15·2
414	0·0339	0·10	0·093	28·9	19·7
415	0·0247	0·07	0·093	31·1	15·6
420	0·0358	0·11	0·066	33·8	20·4
423	0·0439	0·13	0·105	34·0	43·7
432	0·0354	0·12	0·133	30·9	52·8
433	0·0408	0·13	0·203	23·5	75·2
437	0·0476	0·16	0·138	28·6	99·8
444	0·0590	0·21	0·152	33·6	161
448	0·0522	0·19	0·209	33·5	209
452	0·0484	0·18	0·175	30·4	166
453	0·0536	0·20	0·230	23·2	191
469	0·0665	0·28	0·182	28·2	358
472	0·0761	0·32	0·137	33·0	417
475	0·0631	0·27	0·163	30·1	381
476	0·0687	0·30	0·281	22·9	562
484	0·0743	0·35	0·164	32·2	614
496	0·0922	0·47	0·136	32·5	983
498	0·0833	0·43	0·214	22·6	955
502	0·0876	0·46	0·176	27·6	1112
506	0·0842	0·46	0·194	29·6	1410
512	0·0919	0·52	0·134	31·7	1360
518	0·1088	0·64	0·146	32·1	2460
528	0·0993	0·62	0·125	29·0	2140
529	0·1050	0·67	0·174	22·3	2625
530	0·1054	0·68	0·125	27·1	2481
538	0·1067	0·73	0·125	28·8	3630
547	0·1164	0·85	0·060	26·7	3360
550	0·1149	0·86	0·076	28·6	5440
555	0·1234	0·96	0·052	21·7	11760

RESULTS

Tables 1 and *2* give the values of k_2 determined by the above methods. The values of $\log_e k_2$ are plotted with reciprocal temperature in Figs. 1 and 2.

Table 2. Experimental data for the determination of k_2

Pressure: 300 atm. *Temperature range:* 374–499° C. *Efficiency range:* 0·19 to 0·75.

Representative initial gas composition:

	mol fraction
NH_3	0·060
H_2	0·578
N_2	0·192
CH_4	0·045
A	0·125
	1·000

Temp. °C	*z mol frac.*	*Effic.* z/z_{eq}	$\Delta z/\Delta w$	*Gas rate* kM^3/hr	k_2
374	0·075	0·19	0·008	46·2	1·55
376	0·131	0·34	0·008	54·1	4·46
379	0·120	0·31	0·011	51·0	5·68
385	0·081	0·22	0·015	46·0	5·07
387	0·078	0·21	0·016	42·2	4·82
391	0·145	0·40	0·007	54·5	7·84
395	0·088	0·25	0·016	45·7	7·30
395	0·075	0·21	0·013	50·4	6·10
396	0·107	0·30	0·016	45·1	9·08
396	0·087	0·25	0·015	51·8	8·48
397	0·074	0·21	0·021	32·2	5·62
403	0·152	0·45	0·008	67·4	16·1
404	0·074	0·22	0·017	33·4	5·97
405	0·157	0·47	0·006	66·6	13·1
410	0·082	0·25	0·049	32·0	22·0
412	0·079	0·25	0·049	33·3	23·8
413	0·100	0·31	0·014	51·9	15·4
415	0·148	0·47	0·014	61·6	36·7
420	0·113	0·37	0·015	52·7	26·0
421	0·090	0·30	0·054	31·7	38·2
422	0·143	0·47	0·015	60·1	43·4
425	0·123	0·41	0·021	54·9	49·1
430	0·134	0·46	0·015	55·1	47·3
432	0·097	0·34	0·054	31·6	59·0
436	0·164	0·59	0·010	66·5	67·1
446	0·161	0·62	0·010	65·3	87·6
448	0·099	0·38	0·034	33·2	60·7
451	0·109	0·43	0·082	31·3	174
463	0·147	0·63	0·027	58·1	292
471	0·124	0·56	0·071	30·8	332
487	0·131	0·65	0·072	31·8	603
496	0·142	0·74	0·083	30·5	1120
499	0·140	0·75	0·062	31·6	893

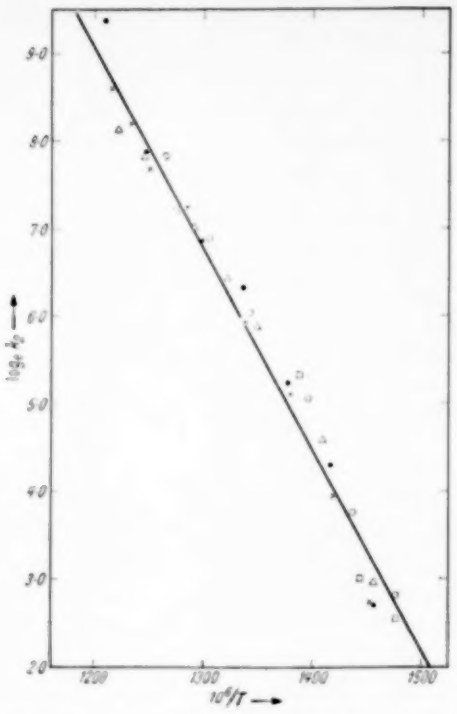

Fig. 1. $\text{Log}_e\ k_2$ versus $1/T$ for five batches of new catalyst. Different symbols denote different batches of catalyst.

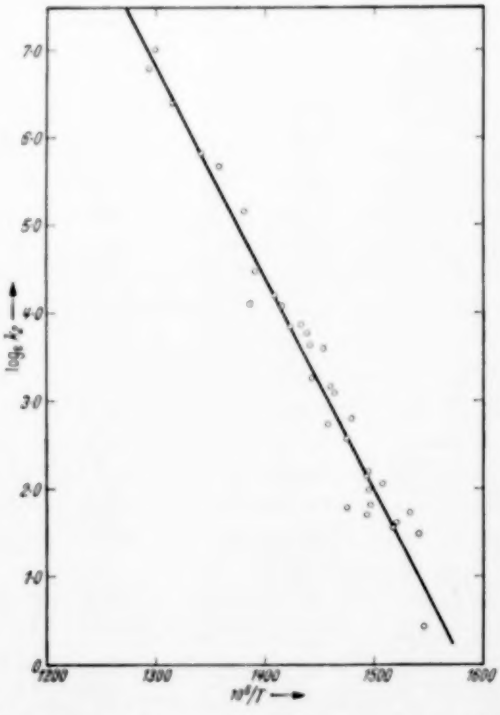

Fig. 2. $\text{Log}_e\ k_2$ versus $1/T$ for one batch of catalyst operating at various temperatures and efficiencies.

VOL. 1 1952

All the data applied to new catalyst, which was multi-promoted iron oxide. Poisons (oxygen containing compounds and sulphur) were probably present in very small quantities in every example. Measurements of them were not undertaken, but their concentration is regarded as being fairly steady between the experimental runs. The actual small variations which occurred will increase the so-called experimental error.

Table 1 and Fig. 1 include data at 245 atm from five charges of catalyst. Initial gas composition was very similar from one run to another, and as there was not much variation in initial reaction temperature, the adiabatic nature of the reaction has resulted in some interdependence of temperature and efficiency, where efficiency $= z/z_{eq}$.

Fig. 2 and *Table 2* present the data at 300 atm pressure from a single batch of catalyst spread between the series of adiabatic beds. Although initial gas composition was again fairly constant, it was possible to obtain some variation of temperature which was independent from the variation in efficiency, thus providing a more comprehensive test of the Temkin equation.

In *Table 3* are summarised values of k_2 and E_{dec} obtained from the two sets of data by calculating the best straight line for the relation $\log_e k_2$ versus $1/T$.

Table 3

Data	*Press atm*	k_2 *at*		E_{dec}
		420° C	*470° C*	
Table 1	245	33·9	318	45800
Table 2	300	30·1	312	47900

Discussion of Results

Fig. 2 and *Table 2* show that, over the experimental range of ammonia concentrations, efficiencies and total rates of flow, the Temkin equation gave values of the reaction velocity constant, k_2, which conformed well with the Arrhenius equation.

Fig. 1 and *Table 1* prove that reproducible results could be obtained with different batches of catalyst, and show that the Arrhenius equation was obeyed under different sets of reaction conditions and wider ranges of efficiencies than in the case of *Table 2*.

The values of E_{dec} obtained at 245 atm and 300 atm are similar. The small difference between the k_2 values is approximately that expected, if the empirical relation between the reaction velocity constant and pressure, mentioned in the subsequent section, is correct, and the concentration of poisons in the reaction gas is similar for the two sets of measurements.

The experimental scatter in the data is considerable, amounting to a coefficient of variation in k_2 of 29% for the first set of data, and 31% for the second.

Nevertheless, the results are good enough to demonstrate that the Temkin equation in conjunction with the Arrhenius equation give a good interpretation of the ammonia synthesis reaction in the plant reactors, making possible the measurement of catalyst activity in terms of the reaction velocity constant k_2, and the apparent activation energy for ammonia decomposition: E_{dec}.

The large experimental scatter will make impossible the detection of real small differences in the reaction velocity constant, and will render approximate any calculations on reactor operation.

Agreement of k_2 and E_{dec} with other Published Results

The values for E_{dec}, the apparent activation energy for ammonia decomposition, accord well with estimates found by other workers (see *Table 4*).

As the reaction velocity constant varies with pressure, it is difficult to compare our results at 245 and 300 atm with others at pressures of 100 atm and less, (see *Table 5*). Moreover, as k_2 is very sensitive to the concentration of poisons in the reaction gas, it is not justifiable to compare different estimates without a knowledge of the gas purity.

Nevertheless it is interesting to note that our results can be correlated fairly well with those of EMMETT and

Table 4. Comparison of values for E_{dec} from various sources

Source of data	*Pressure atm*	E_{dec}	*References*
TEMKIN and PYZHEV . .	1	40000	[1]
TEMKIN and PYZHEVS calculations on WINTERS results	1	46500	[1] and [3]
LARSON and TOUR	10	43500	[1] and [5]
LARSON and TOUR	31·6	46600	[1] and [5]
EMMETT	33·3	45000	[4]
EMMETT	66·6	46500	[4]
EMMETT	100	48900	[4]
EMMETT	100	53000	[4]
I.C.I.	245	45800	
I.C.I.	300	47900	

Table 5. Comparison of k_2 values from various sources

Temp. °C	Source of data	Pressure (atm)						
		300	245	100	66·6	33·3	31·6	10
450	I.C.I.	127	135					
	LARSON and TOUR			424–513			781–915	714–915
	EMMETT			196–212	237–292	346–417		
420	I.C.I.	30·1	33·9					
	LARSON and TOUR						223–268	246
400	I.C.I.	10·7	12·5					
	EMMETT			15·2–21·6	24·1–30·8	37·2–47·4		
370	I.C.I.	2·02	—					
	EMMETT			1·27–2·91	3·19–4·95	7·33–8·95		

LARSON and TOUR, by an empirical relationship $k_2 \propto P^{-0.63}$, which is very similar to that found by EMMETT: $k_2 \propto P^{-0.5}$ (see Fig. 3).

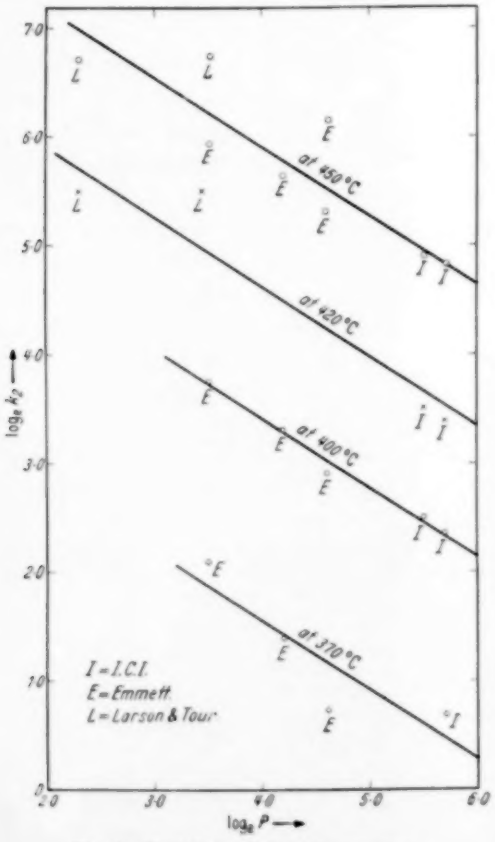

Fig. 3. Variation of k_2 with pressure.

USE OF k_2 AS A MEASURE OF CATALYST ACTIVITY

Two examples are mentioned of this use of the reaction velocity constant. Fig. 4 presents data for five charges of new catalyst which operated in a gas system containing a heavier concentration of poisons than that appertaining to the data for Fig. 1. Although similar catalyst of similar age was used in both cases, the

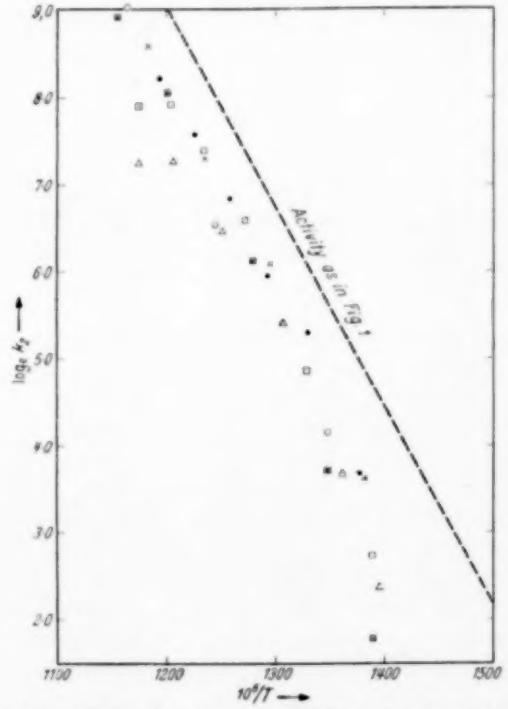

Fig. 4. Effect of poisons on activity of new catalyst. Different symbols denote different batches of catalyst.

activity of the catalyst subject to the greater amount of poisons is only about one third of that operating under the more favourable conditions. This rapid poisoning effect, at least partly due to oxygen-containing compounds, is to be expected from the experimental results of ALMQUIST and BLACK [6], on the poisoning of ammonia catalyst by carbon monoxide and water-vapour.

VOL. 1 1952

The change in activation energy due to the increased poisoning is obscured by the fact that the slope of the line correlating $\log_e k_2$ with $1/T$ is influenced by the greater poisoning of those layers of the catalyst bed which operate at the lower temperatures.

Fig. 5 demonstrates the difference in activity which was observed for two catalysts of different manufacture operating under similar conditions.

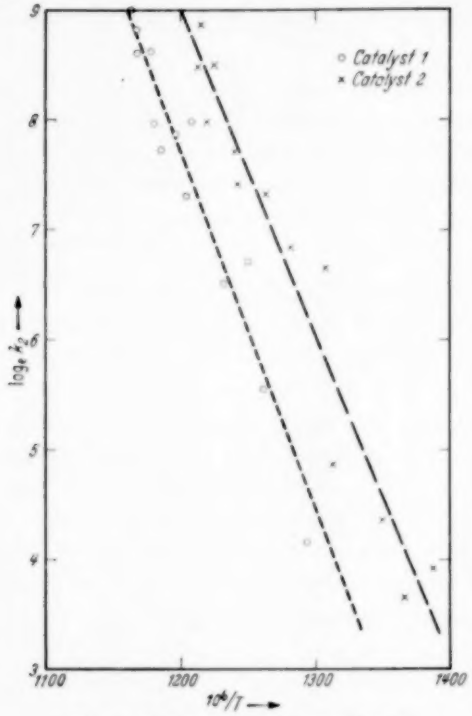

Fig. 5. Comparison of two catalysts.

Calculation of Optimum Conditions

The most useful application of the Temkin equation is to calculate optimum reaction conditions, and then to find how nearly these may be achieved in a plant reactor.

The determination of optimum reaction conditions is a wide problem, but in the example given below, the variables of catalyst activity, total pressure and initial gas composition were fixed.

Maximum reaction velocity for a given gas composition, is attained at a temperature where the differential coefficient of reaction velocity with respect to temperature is zero.

Differentiating eq. (2), under optimum conditions:

$$0 = \frac{\partial}{\partial T}\left(\frac{dA}{dw}\right) = 2\left[\frac{E_{syn}}{RT^2} \cdot k_1 \cdot \frac{P_{N_2} P_{H_2}^{1.5}}{P_{NH_3}} - \frac{E_{dec}}{RT^2} \cdot k_2 \cdot \frac{P_{NH_3}}{P_{H_2}^{1.5}}\right]$$

where E_{syn} = apparent activation energy for ammonia synthesis in cal/mol N_2 reacting.

The above expression gives

$$\frac{k_1}{k_2} = \frac{E_{dec}}{E_{syn}} \cdot \frac{P_{NH_3}}{P_{H_2}^3 P_{N_2}}$$

which reduces to

$$L = \left[\frac{E_{dec}}{E_{syn}}\right]^{\frac{1}{2}} \frac{z}{(1-bz)^2} \cdot \qquad (4)$$

This equation gives L, for any z.

L, being related to the equilibrium constant, is an accurately known function of pressure, temperature

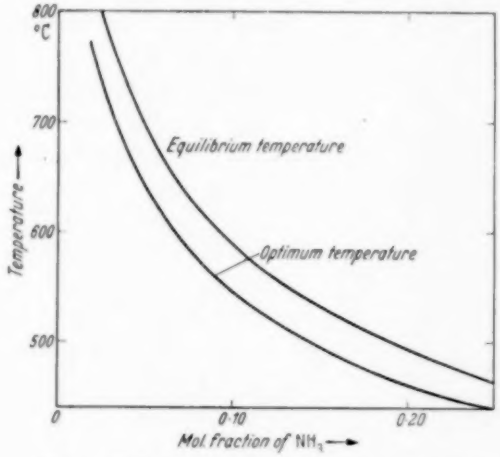

Fig. 6. Relation between optimum temperature and ammonia concentration.

and gas composition. Hence the optimum temperature T, corresponding to z, can be deduced. For the example quoted, a pressure of 245 atm was chosen, with an initial gas composition:

	mol fraction
NH_3	0·016
H_2	0·686
N_2	0·228
CH_4	0·036
A	0·034
Total	1·000

E_{dec} was taken as 47 400, and the function k_2 such that its value at 470° C was 325. A value of 20 800 was taken for E_{syn}, as determined from the relation $E_{syn} - E_{dec} = Q$, the heat of reaction per mol N_2 reacting. With this information, the optimum temperature corresponding to any mol fraction of NH_3 could be calculated. Fig. 6 gives the relation obtained between these two quantities, and Fig. 7 the corresponding

maximum reaction velocities. It is of interest that the reaction velocities, whilst they are high and decrease rapidly at low ammonia concentrations, are low and relatively constant for high ammonia concentrations.

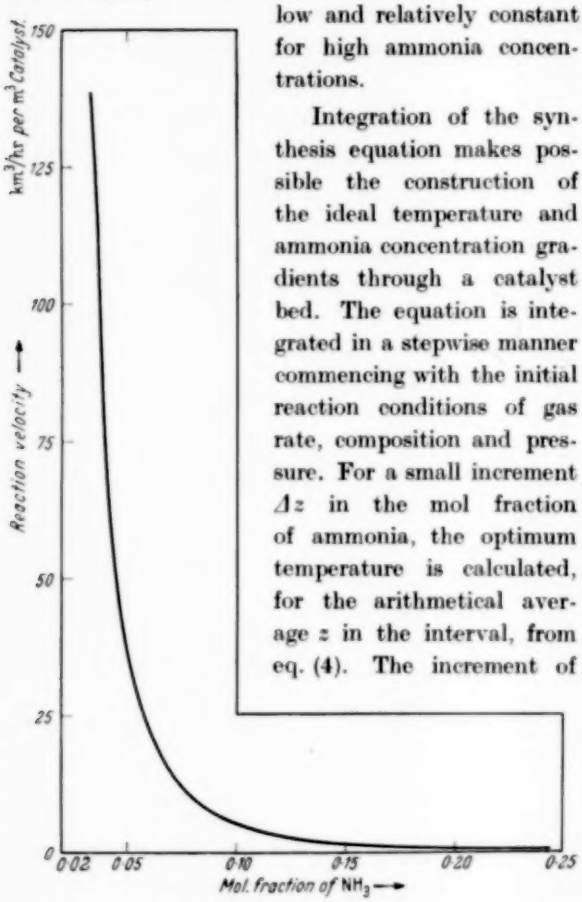

Fig. 7. Maximum reaction velocities at optimum conditions.

Integration of the synthesis equation makes possible the construction of the ideal temperature and ammonia concentration gradients through a catalyst bed. The equation is integrated in a stepwise manner commencing with the initial reaction conditions of gas rate, composition and pressure. For a small increment Δz in the mol fraction of ammonia, the optimum temperature is calculated, for the arithmetical average z in the interval, from eq. (4). The increment of catalyst volume Δw is then found by substituting the average values of V, z, and T in eq. (3) *viz.*:

$$dw = \frac{P^{0.5} a^{1.5} V}{48} \frac{z(1-bz)^{1.5}}{(1+z)[L^2(1-bz)^4 - z^2]} dz.$$

Δz is originally chosen small enough for the approximation to be applied $\frac{\Delta z}{\Delta w} = \frac{dz}{dw}$ at the average conditions. Subsequent increments Δw are calculated in a similar manner until the whole catalyst bed has been taken into account.

The resulting ideal gradients of ammonia concentration and temperature are given in Fig. 8. The unit of the abcissae is: volume of catalyst traversed/initial reaction gas rate, chosen so that results can be easily computed for various gas rates.

THE BEST OPERATING CONDITIONS IN A PLANT REACTOR

Attainment of ideal conditions in a plant reactor would be a complex practical problem involving removal of the heat of reaction from the catalyst bed at a rate decreasing with catalyst age, and varying through the bed from a high figure at the beginning of the reaction to a low figure at the end of the reaction. Moreover, the first part of the bed would be operated at such a high temperature that the activity of the catalyst there would probably be quickly impaired.

A reactor had been designed, however, to give a partial approach to the ideal conditions, by transferring some of the heat of reaction to partially heated gas which flowed in a counter-current direction to the reaction gas, through vertical tubes inserted in the catalyst bed. The rate of removal of the heat of reaction could be varied by altering the rate of flow of the cooling gas, or its initial temperature, but the cooling of particular sections of catalyst could not be varied independently from one another.

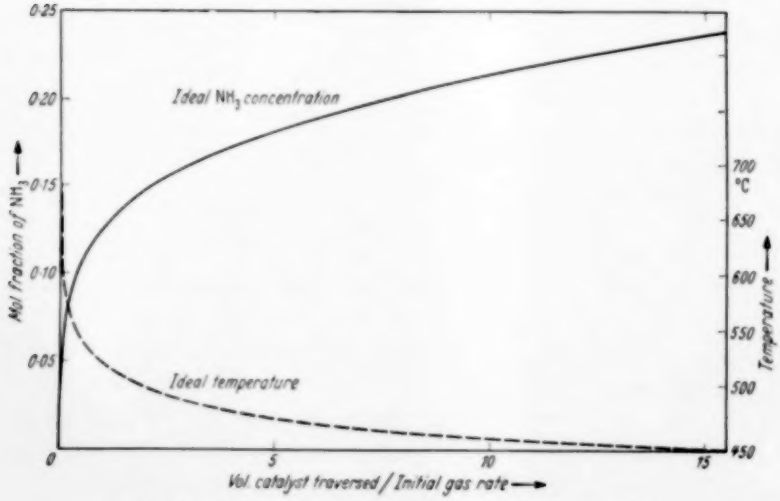

Fig. 8. Ideal temperature and NH_3 concentration gradients.

The kinetic data and methods described above were applied to forecast the output and the best operating conditions of this reactor, by calculating the optimum initial synthesis temperature and the optimum degree of cooling. The same catalyst activity and initial gas composition were assumed as in the calculation of the ideal gradients.

The catalyst bed was considered in small sections, and the kinetic equation was used to give, for each section, the maximum possible reaction which was consistent with a heat balance between the heat of reaction, the change in heat content of the reaction gas, and the heat transferred to the cooling medium.

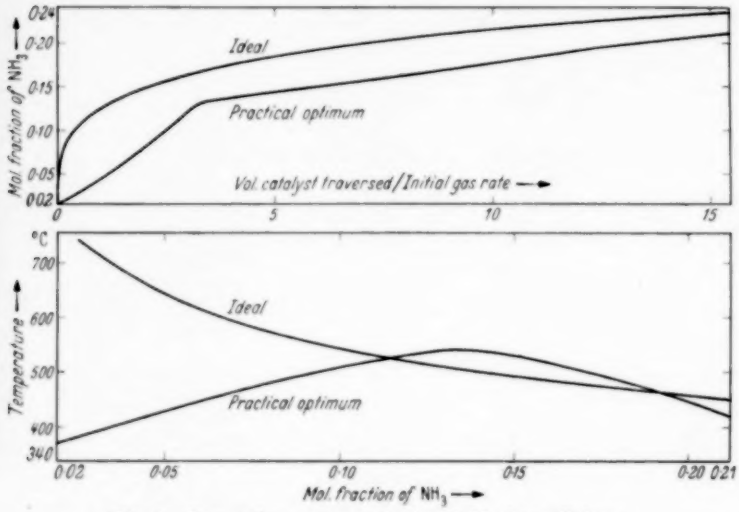

Fig. 9. Comparison of practical and ideal conditions.

The best operating conditions, calculated by the above method, gave an output of ammonia from the reactor, equivalent to an exit mol fraction of 0·21, or a conversion:

(exit mol fraction—inlet mol fraction) × 100, of 19·4% (see Fig. 9).

This compared with a maximum ammonia conversion of 22·0%, calculated for the ideal operating conditions, and a figure of 19·0% which was the maximum conversion actually achieved in the running of the plant reactor.

The agreement between the calculated and achieved practical conditions is good, considering the large coefficient of variation (30%) in the original k_2 values, from which the k_2 function was determined. The actual catalyst temperature gradient was quite close to that calculated, as was the amount of heat transfer from the bed.

The best practical conditions also represent quite a reasonable approach to the ideal. The maximum further improvement in the design and operation of the catalyst bed would only increase the output by less than 14%, although with the present arrangement, the rate of heat removal is least instead of greatest at the commencement of the reaction, and the cooling of one section of catalyst cannot be adjusted independently from another. These limitations still, however, permit of a fair correspondence between the practical and ideal conditions over the last 80% of the catalyst bed (see Fig. 9). The divergence occurs where the optimum temperatures are higher than 550° C so that operation at the lower temperatures has the compensation of preserving the life of the catalyst. This feature, together with Fig. 9 demonstrate that in future developments of the design of reactor, the aim should be to improve still further the correspondence between practical and ideal conditions in the region of the peak temperature and subsequently.

ACKNOWLEDGEMENT

The author wishes to thank the staff of *Ammonia Works* for providing most of the experimental data, and the staff of *Technical Department and Research Department* for helpful advice.

NOTATION

a = mol fraction of H_2 in the reaction gas, corresponding to zero NH_3 content

A = kg mols/hr NH_3

b = constant, such that a $(1-bz)$ is the mol fraction of H_2 in the reaction gas corresponding to a mol fraction z of NH_3

b_2 = frequency factor in the Arrhenius' equation for k_2, the reaction velocity constant for ammonia decomposition

E_{dec} = apparent activation energy for ammonia decomposition

E_{syn} = apparent activation energy for ammonia synthesis

k_1 = reaction velocity constant for ammonia synthesis

k_2 = reaction velocity constant for ammonia decomposition

K_p = equilibrium constant for ammonia synthesis

$L = \dfrac{z_{eq}}{(1-bz_{eq})^2}$

N = number of kilo mols of ammonia

P = total pressure: atm

P_{NH_3}, P_{N_2}, P_{H_2} = partial pressures in atm of NH_3, N_2, and H_2 respectively

Q = heat of reaction, cals/gm mol N_2 reacting

R = gas constant cals/deg., gm mol

t = time, hr
T = temperature, °K
V = rate of reaction gas, M³/hr measured at 1 atm and 20° C
w = volume of catalyst: M³
z = mol fraction of NH_3
z_{eq} = equilibrium mol fraction of NH_3

REFERENCES

[1] TEMKIN, M. I. and PYZHEV, V; Acta Physicochim. 1940 **12** 327–356. [2] GILLESPIE, L. T. and BEATTIE, J. A.; Physic. Rev. 1930 **36** 743. [3] WINTER, E.; Z. physik. Chem. 1931 **13** 401. [4] EMMETT, P. H. and KUMMER, J. T.; Ind. Eng. Chem. 1943 **35** 677. [5] LARSON, A. T. and TOUR, R. S.; Chem. and Met. Eng. 1922 **26** 647. [6] ALMQUIST, J. A. and BLACK, C. A.; J. Amer. Chem. Soc. 1926 **48** 2814.

Hydroextraction IV: Radial distribution of permeability in cakes

M. M. HARUNI and J. ANDERSON STORROW

Chemical Engineering Laboratory, College of Technology, Manchester, England.

(Received 21 March 1952)

Summary—Tests have been made on a 9 in. diameter hydroextractor running at 1050 and 1400 r.p.m. using maize starch, precipitated chalk and kieselguhr.

Résumé—L'étude d'un hydroextracteur tournant à 1050 t/m ou à 1400 t/m a été faite en utilisant de l'amidon de maïs, du carbonate de chaux précipité et du kieselguhr.

It has been shown [1], [2], [3], [4], [5], [6] that observed flow rates, q, of wash water through hydroextractor cakes follow closely the relationship

$$q = \frac{4\pi^3 \cdot n^2 \cdot K_c X}{\mu \cdot g} \left[\frac{r_0^2 - r_L^2}{\log_e \frac{r_0}{r_c}} \right] \qquad (1)$$

and the small whirling cell (Fig. 2) showed hydroextraction permeabilities within ±15% of filtration permeabilities, but there remained variation within this 15% which appeared systematic [4]. The variations of hydroextraction permeability with cake thickness, or cake weight, was not of the form expected

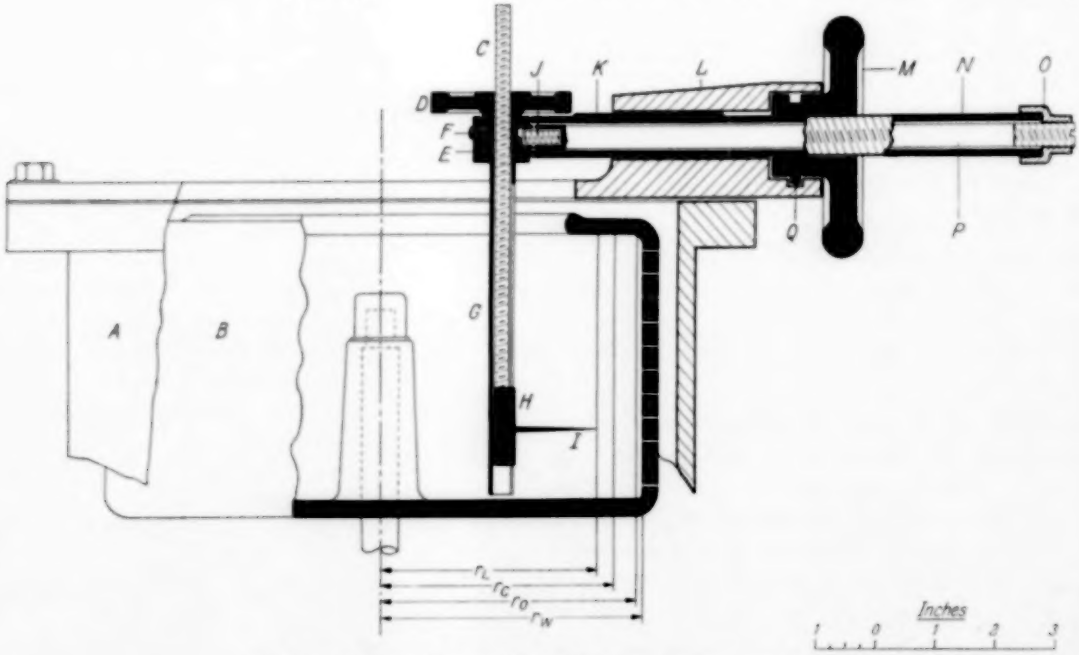

Fig. 1. The centrifuge basket with the probe arrangement.

for streamline flow with a liquid layer of thickness $(r_c - r_L)$ within a cake of thickness $(r_0 - r_c)$, as shown in Fig. 1. The results of tests on maize starch and chalk in both the 9 in. dia. hydroextractor (Fig. 1) as a result of the varying compressive stresses in the centrifugal field. There may be a significant resistance associated with the interface between packed material and the cloth retaining the cake.

APPARATUS

The 9 in. dia. hydroextractor was fitted with a probe mechanism which allowed of the measurement of either r_L, or r_c, at any vertical or radial position within the experimental range. The mechanism shown in Fig. 1 incorporates a probe *I* on the end of rod *C*, which was moved vertically by the rotation of wheel *D*. The head *E* carried a slotted tube *G*, the retention of the probe-holder *H* in this slot allowing

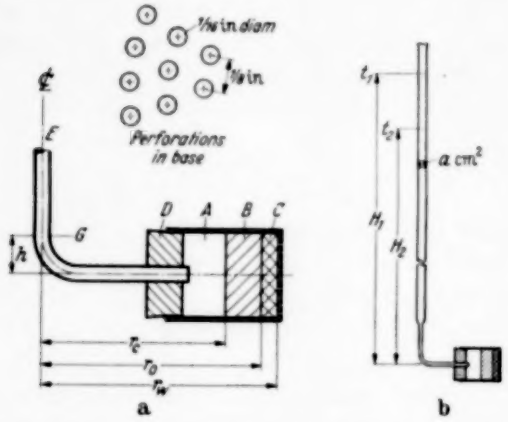

Fig. 2. The small cell: (a) in position for spinning, (b) in position for filtration tests.

vertical movement but no rotation of *C*. Horizontal movement of the probe was caused by rotating wheel *M*, which moved the screwed tube *N* and rod *P* through the head *L*. The rotation of *N* was prevented by a slotted guide. From scales on the moving components it was possible to measure the position of the probe point to a reproducibility of 0·01 mm. This accuracy is particularly desirable in the measurement of radii as a variation of 0·1 mm therein is important, perhaps affecting the estimation of permeability K_c by 1%.

The small cell in Fig. 2 is the complement of the hydroextractor in that cakes may be formed therein by various methods and tested in both filtration and hydroextraction without disturbance [4]. The tests on this cell were always carried out with $r_L = 0$, the liquid level being maintained at level *G* in the transparent feed tube lying on the vertical axis of rotation *E* [Fig. 2(a)]. The arrangement of the cell for filtration permeability measurements is shown in Fig. 2(b). The cell was carried in the 9 in. dia. hydroextractor by an appropriately rigid and balanced fitting which is not shown in the diagram.

CAKE MATERIALS

Various samples of chalk, maize starch and kieselguhr were tested, the results being exemplified by the data in *Tables 1, 2,* and showing the differences encountered. The starch was of the type already used in earlier work in this laboratory. The chalk samples were all precipitated materials, nominally "pure," from various commercial sources. The kieselguhr samples were proprietary "filter-aid" materials.

Table 1. Thickness of cake in 9 in. dia. hydroextractor

(a) *Starch* (alone): $r_0 = 10{\cdot}8$ cm

W g	r_c cm	$r_0^2 - r_c^2$ cm²
200	10·42	7·7
300	10·24	11·5
400	10·06	15·3
500	9·87	19·2
600	9·66	23·2
700	9·45	27·3
800	9·25	31·0
900	9·03	35·0
1000	8·80	39·0
1100	8·60	42·6

(b) *Starch* (under kieselguhr and starch layers: $r_0 = 10{\cdot}8$ cm)

W g	r_c cm	$r_0^2 - r_c^2$ cm²	*Inner layers** g
350	10·15	13·5	100 K + 350 S
350	10·15	13·5	200 K + 350 S
350	10·15	13·5	300 K + 350 S
700	9·46	27·1	300 K

(c) *Starch* (on kieselguhr)

W g	r_0 cm	r_c cm	$r_0^2 - r_c^2$ cm²
350	9·83	9·12	13·6
350	9·26	8·51	13·6
350	9·56	8·82	13·6
500	9·87	8·82	19·4
700	10·26	8·82	27·3

* The "inner layer" is that within the radius of, and thus exerting compression upon, the layer of material under consideration. In (g) above, the cakes were formed from three layers, the kieselguhr being in the middle. The mass of an inner layer is specified as "100 K" for 100 g kieselguhr, or "300 S" for 300 g starch.

(d) *Kieselguhr* (alone): $r_0 = 10{\cdot}74$ cm

W g	r_c cm	$r_0^2 - r_c^2$ cm²
200	10·13	13·0
300	9·82	19·3
400	9·51	25·2
500	9·18	31·5
600	8·82	37·9
700	8·47	43·9

(e) *Kieselguhr* (under starch): $r_0 = 10{\cdot}8$ cm

W g	r_c cm	$r_0^2 - r_c^2$ cm²	*Inner layer* g
200	10·26	11·6	700 S

(f) *Kieselguhr* (on starch):

W g	r_0 cm	r_c cm	$r_0^2 - r_c^2$ cm²
100	9·45	9·1	6·4
200	9·45	8·74	12·8
300	9·45	8·38	19·1

(g) *Kieselguhr* (in between starch layers):

W g	r_0 cm	r_c cm	$r_0^2 - r_c^2$ cm²	*Inner layer* g
100	10·15	9·83	6·1	350 S
200	10·15	9·56	11·3	350 S
300	10·15	9·26	17·0	350 S
200	10·42	9·87	11·4	500 S

Table 2. Effective mean packing densities (g dry solid/cc. cake)

Material	*Sample*	*Packing density*	
In 9 in. dia. hydroextractor basket:			
Starch	1	0·75	
Starch	2	0·74	
Chalk	1	0·57	
Chalk	2	0·64	
Chalk	3	0·67	
Kieselguhr alone	1	0·46	ratio 1·11 : 1
Kieselguhr of sample 1 under starch	—	0·51	
In small cell:			
Starch	1	0·75	
Chalk	1	0·57	
Kieselguhr alone	2	0·37	ratio 1·11 : 1
Kieselguhr of sample 2 under chalk	—	0·41	

Experimental Technique

The methods used in this laboratory for the measurement of hydroextraction permeability have already been described in detail and assessed as comparative techniques [3]. In the present tests, the permeabilities in the 9 in. dia. hydroextractor were obtained from a measurement of the time, t, required for the water layer within the cake radius r_c to move from r_{L_1} to r_{L_2}, where at all times $r_{L_1} < r_{L_2} < r_c$. The probe mechanism is a very sensitive detector of the liquid surface radius r_L and the above is the preferred technique, measuring the movement of r_L when the liquid layer is draining through the cake without any feed to the basket. The equation appropriate to this case is

$$t = \left[\frac{\mu \cdot g \cdot \log_e \frac{r_0}{r_c}}{4\pi^2 n^2 K_c}\right] \cdot \log_e \left\{\frac{r_0^2 - r_{L_1}^2}{r_0^2 - r_{L_2}^2}\right\}. \qquad (2)$$

Series of cakes were tested at various speeds of revolution of the basket, and data for representative experiments are quoted in *Tables 3, 4*. In all the hydroextractor tests the cakes were formed on two layers of twill cloth supported by one layer of duck weave.

The dimensions of the cake were found by using the probe to trace the form of the cake and cloth faces. The cakes in the hydroextractor were produced with faces vertical to within 1 mm by disturbing and lightly re-moulding the face during the formation period. This treatment has no effect on the cake permeability when the operation is carried out with a submerged cake and suitably delicate touch. Cakes formed in this way are also reproducible for any specific quantity of material.

The radii of the cakes were measured "in situ" by the probe mechanism as well as by measurements of samples cut from the cake. This gave a comparison with the earlier technique [1], [2] wherein cakes were formed in layers by successive additions of material, the layer interfaces being dyed and the layer thicknesses obtained from sections of the final cake.

The cakes in the small cell were produced using a "star gauze" during the formation period and were tested with a loosely packed glass wool pad on the inner face of the cake. These precautions did not affect the measured permeabilities of the cakes and were essential in forming and maintaining a uniform cake in the cell by disrupting the helical motion of the fluid adjacent to the inner face of the packed material [4].

In the present tests the cakes were formed on four layers of duck weave cloth.

VOL. 1 1952

Table 3. Starch in 9 in. dia. hydroextractor

$r_0 = 10{\cdot}8$ cm; $r_{L_1} = 7{\cdot}64$ cm; $r_{L_2} = 8{\cdot}31$ cm; $W_0 = 160$ g

W g	r_c cm	$\log_e \frac{r_0}{r_c}$	t_{1050}* sec	t_{1400}* sec	K_{1050}** g/sec²	K_{1400}** g/sec²	K_{mean}** g/sec²	$K(W+W_0)$** g²/sec²
300	10·24	0·0515	40	24	2·39	2·36	2·375	1090
400	10·05	0·07225	49	29	2·745	2·74	2·742	1535
500	9·85	0·0925	57·5	34	2·99	2·99	2·99	1980
600	9·65	0·1126	66	39·5	3·17	3·14	3·15	2400
700	9·45	0·1338	75	45	3·31	3·27	3·29	2830
800	9·24	0·1559	83	50	3·49	3·44	3·47	3300
900	9·03	0·1791	92	55	3·62	3·59	3·6	3820
1000	8·815	0·2035	101	59·5	3·74	3·77	3·75	4350
1100	8·60	0·2281	110	65	3·85	3·87	3·86	4860

* Subscripts 1050, 1400 refer to n' r.p.m. used in the test. ** Values in these columns have been multiplied by 10^7.

Cakes formed in the small cell were tested for filtration permeability, after the centrifuging tests, by using the arrangement of Fig. 2(b) and measuring the time of fall, t, of the liquid level from H_1 to H_2 in the vertical tube of cross sectional area "a." The flow rates used were such that the flow was laminar in all tests. The equation for the analysis of the filtration data is

$$\log_e \frac{H_1}{H_2} = \frac{K_F \,.\, A\, t}{a \,.\, \mu \,.\, L} \qquad (3)$$

where the filter bed is of depth L and cross sectional area A.

Table 4. Kieselguhr in 9 in. dia. hydroextractor

$r_0 = 10{\cdot}74$ cm; $r_{L_1} = 7{\cdot}64$ cm; $r_{L_2} = 8{\cdot}31$ cm; $W_0 = 450$ g

W g	r_c cm	$\log_e \frac{r_0}{r_c}$	$t_{10\,0}$* sec	K** g/sec²	$K(W+W_0)$** g²/sec²
200	10·14	0·0570	9·0	1·18	768
300	9·83	0·0888	10·2	1·64	1230
400	9·51	0·1222	11·7	1·98	1680
500	9·18	0·1571	13·0	2·27	2150
600	8·835	0·1959	14·6	2·53	2650
700	8·465	0·2385	15·9	2·83	3260

* $n' = 1050$ r.p.m. used in all tests.
** Values in these columns have been multiplied by 10^6.

Cakes were made in both forms of apparatus by building cakes from layers of different materials as well as homogeneous cakes, in order to cover the possibility of variation of compressible effects for each material in all cake positions.

Experimental Results

Table 1, contains the dimensions of the cakes used in the hydroextractor, the measurements including starch and kieselguhr layers in various positions in a laminated cake. The data show the variations of radii in the apparatus and the reproducibility obtained. The data are plotted in Fig. 3 and show that to the accuracy of the measurements the packing density of each material was constant. The line A shows kieselguhr data *If*, *Id*, which are independent of compression by kieselguhr alone. The line B shows that the kieselguhr is subject to an apparent compressive effect when below a starch cake, as in data *Ie*, *Ig*. The precise reason for the difference between data B and

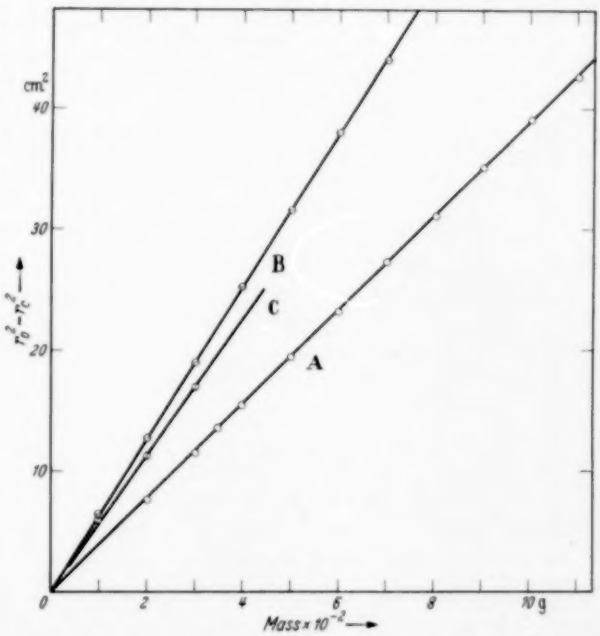

Fig. 3. Relation between volume of cake in hydroextractor and dry weight of material in it: A Starch alone, or starch on or under kieselguhr. B Kieselguhr alone, or on starch. C Kieselguhr under starch.

data *A* is not clear. Kieselguhr beneath a thick bed of kieselguhr (line *A*) does not show the compressed form given by a similar mass of starch (line *B*). This may be due to a great difference in the lateral support against centrifugal stress afforded in the two packed materials. Starch data on line *C* show no change in packing density whatever form the laminated or homogeneous cake may be given.

The linearity of each plot shows that changes in packing density and hence in permeability distribution

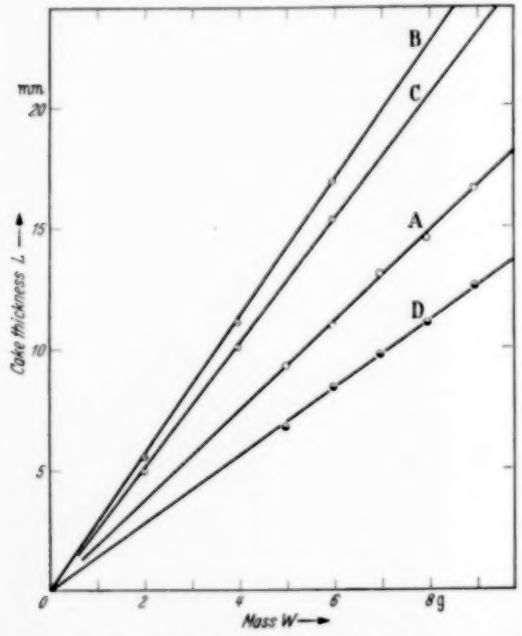

Fig. 4. Relation between thickness of cake in small cell and dry weight of material in it: *A* Chalk alone. *B* Kieselguhr alone. *C* Kieselguhr under chalk. *D* Starch alone.

in cakes cannot be found by thickness measurements, even though the mean thicknesses measured here were probably of a higher accuracy than the means obtained earlier by dyeing and sectioning cakes.

Similar data were obtained for starch, chalk and kieselguhr in the small cell. In these cases the final sample was carefully extruded from the cell by a low air pressure applied to the perforated cell base. The sample was then sectioned for measurement of the layers therein. The results are shown in Fig. 4. Each material alone gave a straight line indicating constant packing density. The kieselguhr again had the peculiarity of apparently closer packing when beneath a less permeable material. In this case the inner material was chalk. The results in *Table 2* include data showing that the packing in the hydroextractor and the small cell was the same for a given material to the accuracy of these measurements. Though this agreement of packing density appears to confirm the agreement found between hydroextraction permeabilities found in the two forms of apparatus, the confirmation is of minor value as the permeability tests are bound to be more sensitive to porosity changes than linear measurements of cake dimensions. The kieselguhr compression caused by loading with an inner layer of less permeable material was the same for either chalk or starch inner layers, although these materials differed considerably in permeability and hence stress transmitted to the kieselguhr. The apparent compression of the kieselguhr beneath starch was not due to the infiltration of the starch giving an apparently thinner layer of kieselguhr. The layers in such cakes were quite easily separated, showing no macroscopic mixing at the interfaces.

The results of the permeability tests are exemplified in *Tables 3, 4* for cakes of starch and kieselguhr in the hydroextractor. The data are consistent in showing large increases in permeability with increasing mass of material in the basket, when tested at constant speed of revolution. This is not the expected result when considering that increasing the charge by adding another layer of cake must increase the centrifugal compressive stress on all layers in the initial cake. If the effect is only a phenomenon due to compressive stress in the cake, it means that the increased packing density and decreased permeability produced in the initial cake is more than offset by the higher porosity and permeability of the new inner layer at smaller radius, thus leading to an increase in mean permeability of the whole cake. This hypothesis requires in the cake a sensitivity to compressive stress, particularly at low stresses, which is not demonstrated by previous comparisons of the compressive effect in the hydroextractor with loads applied directly in a compression cell [2], or by the insensitivity to speed of revolution shown in *Table 3*. The increase of speed from 1050 to 1400 r.p.m., increasing the centrifugal stress by $(1400/1050)^2$, produced very small decreases in the cake permeabilities. The above effects of radial position on compressive stress must influence the permeabilities but it seems unlikely that the major cause of the large effect of charge mass can be in this field.

A more likely cause of the phenomenon is the presence of a significant resistance at the cloth-cake interface, which is a common conjecture in filtration studies. Such a resistance force could arise from an

VOL. 1 1952

approximately constant effective permeability around the interface and thus the mean cake permeability would fall with increasing mass of cake, the interface resistance becoming less important. The dirty cloth on which cakes have been formed is itself of flow resistance only of the order 1% of the cake resistance [1], [2]. Previous tests of the effect of the cloth on drainage from the cake to the holes in the hydroextractor basket wall were consistent in showing that the flow through the cloth was unimportant, either in hydroextraction or in filtration under directly applied load [2], though it should be noted that the investigation at that time was concerned with the source of large changes in permeability and the hydroextraction data were probably in error due to the visual detection technique used for the critical wetting rate [1]. The present data was considered far more reliable for an investigation of the cloth phenomenon by studying the functions of permeability and cake mass.

Consider the hydroextraction permeabilities found by measuring the drainage time t for liquid within a cake to move from r_{L_1} to r_{L_2}. The eq. (2) suggests the use of a plot of t against $\log_e r_0/r_c$, when using the same r_0, r_{L_2} and r_{L_1}, in order to show the effect of cake thickness. The plot should be linear, since C_1 would be constant, if the permeability K_c were also constant in the equation

$$t = \frac{C_1}{K_c} \cdot \log_e \frac{r_0}{r_c} \qquad (4)$$

where

$$C_1 = \frac{\mu \cdot g}{4\pi^2 \cdot n^2} \cdot \log_e \left\{ \frac{r_0^2 - r_{L_1}^2}{r_0^2 - r_{L_2}^2} \right\}.$$

In many tests the lines on such plots are shallow curves within the maximum experimental range imposed by the speed and geometry of the machine used. Fig. 5 includes examples of such plots for cakes of maize starch, and cakes of kieselguhr. If we presume C_1 to be defined correctly, and its value to be constant, the curvature of the lines in Fig. 5 is attributed to changes in K_c. This assumption leads to the values in *Table 3, 4*, with K_c increasing as W increases. If the changes in permeability were continuous with increasing cake mass, the resistance to flow residing completely in the cake itself, the curves in Fig. 5 should pass through the origin of coordinates, as shown by the dotted line for the region wherein no experimental data have been obtained. The possibility of using thin cakes in the hydroextractor is limited by the tendency to crack when supported on a flexible cloth. It appears likely that the curved full lines on Fig. 5 would extrapolate to the broken lines rather than to the dotted line. The former are equivalent to systems containing resistances to flow indicated by the intercepts on the time axis when the cake thickness has been reduced to zero and $r_0 = r_c$, the dotted lines would represent systems without a resistance when $r_0 = r_c$ but with a rapidly increasing mean permeability as cake thickness increases, *e.g.* the permeability of the starch cakes at $n' = 1050$ would have to change four-fold, mainly at

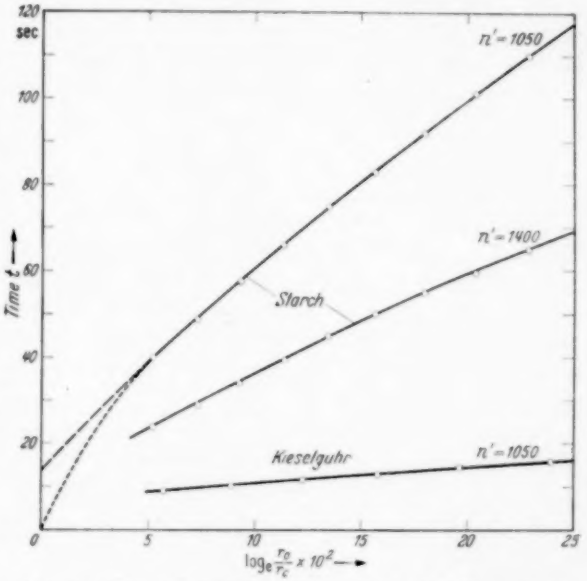

Fig. 5. Plot of drainage time and cake dimensions representing eq. (4).

very low cake thicknesses, to provide the gradient reduction on the dotted curves. There seems less likelihood that this rapid change will occur than that the broken lines represent a condition nearer the truth. The gradient probably suffers an approximately constant rate of change, the curve decreasing to an intercept on the time axis. If the resistance to flow appropriate to this intercept be postulated, the question arises whether the resistance varies with the cake thickness, e.g. due to varying compressive stress, and, if so, whether its variation can be detected or analysed. The analysis of such a case is of perhaps small moment in practice but may be of value in recognising the cause of the phenomenon. The smooth fall in gradient as K_c increases with increasing cake thickness is reasonable on the basis of previous knowledge of the dependence of permeability on compressive stress [2].

Without exception the data for the present experimental materials gave straight line plots for time t

against either cake mass W or $(r_0^2 - r_c^2)$, *e.g.* Fig. 6, 7 include the data derived from *Table 1, 3, 4*. This relationship should not obtain for cakes of constant permeability, for which the appropriate equation is

$$t = \frac{\mu g}{4\pi^2 n^2 K_c} \cdot \log_e \left[\frac{r_0^2 - r_{L_1}^2}{r_0^2 - r_{L_2}^2} \right] \cdot \log_e \sqrt{\frac{\pi X \sigma r_0^2}{\pi X \sigma r_0^2 - W}} \quad (5a)$$

$$= \frac{C_1}{K_c} \log_e \sqrt{\frac{\pi X \sigma r_0^2}{\pi X \sigma r_0^2 - W}} \quad (5b)$$

$$= \frac{C_1}{K_c} \log_e \sqrt{\frac{W_1}{W_1 - W}} \quad (5c)$$

where $W_1 = \pi X \sigma r_0^2$, the mass of cake material to fill the whole cylindrical volume of the basket of

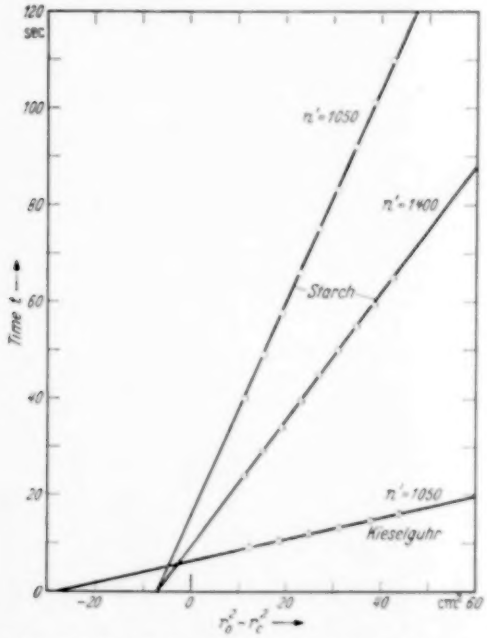

Fig. 6. Relation between drainage time and volume of hydroextractor cake [eq. (6)].

radius r_0. The broken curves on Fig. 7 are hypothetical, being obtained from eq. (5) for selected constant permeabilities. The curves A, B, C pass through the origin of coordinates and in contrast to the experimental data show an appreciable curvature.

Also the plot of $K_c(W + W_0)$ against $\log_e r_0/r_c$ is a straight line (Fig. 8) where "$-W_0$" is the intercept at $t = 0$ in Fig. 7. This is derived from eq. (4) and the forms from Fig. 7.

$$t = C_2(W + W_0) \quad (6)$$

where C_2 is a constant for a series of cakes of one material at one speed of revolution. Thus

$$t = C_2(W + W_0) = \frac{C_1}{K_c} \cdot \log_e \frac{r_0}{r_c}$$

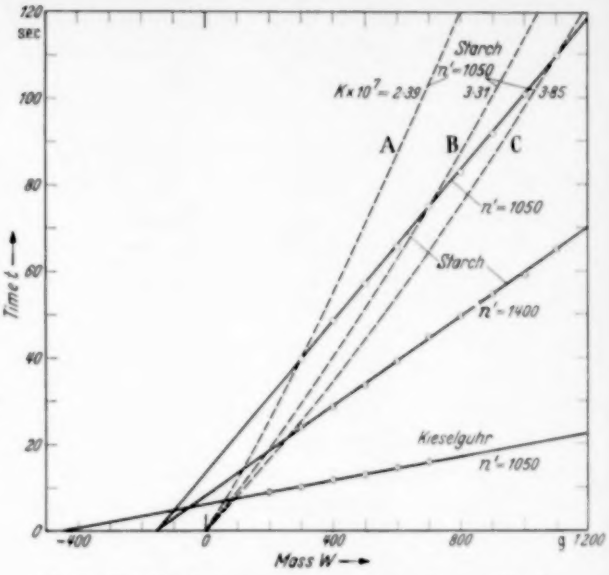

Fig. 7. Relation between drainage time and mass of hydroextractor cake [eq. (6)]; A, B and C are hypothetical lines for constant permeability, obtained from eq. (5).

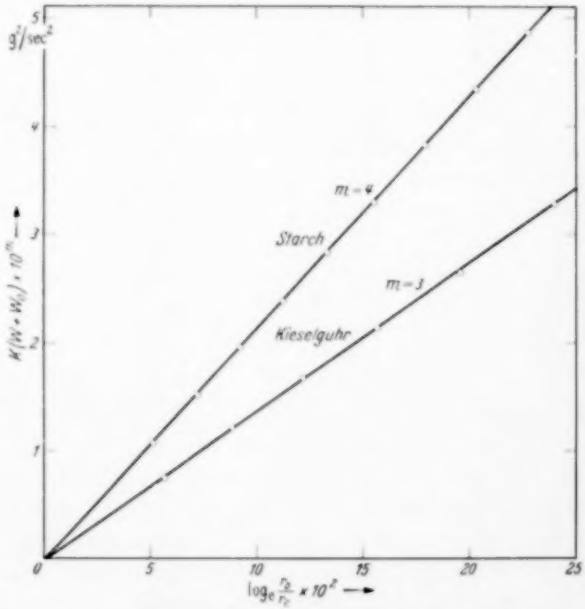

Fig. 8. Plot representing eq. (7).

whence:

$$K_c(W + W_0) = \frac{C_1}{C_2} \cdot \log_e \frac{r_0}{r_c} \cdot \quad (7)$$

The proper relationship for constant K_c is as follows for any value W_0

$$K_c(W + W_0) = \left[\pi X \sigma (r_0^2 - r_c^2) + W_0\right] \cdot \frac{C_1}{t} \cdot \log_e \frac{r_0}{r_c} \cdot \quad (8)$$

The experimental fact of eq. (6), incorporating an appropriate value W_0, reduces this form to eq. (7).

VOL. 1 1952

Table 5. Permeability of innermost layers in hydroextractor

Starch:

	Layer No.*								
	1	2	3	4	5	6	7	8	9
W^{**}(g)	300	400	500	600	700	800	900	1000	1100
Layer $K \times 10^7$ (g/sec²) . .	2·39	4·07	4·3	4·3	4·05	4·95	4·45	4·55	5·1

Mean K for layers 2–9 is $4{\cdot}6 \times 10^{-7}$ g/sec²

Kieselguhr:

	Layer No.*					
	1	2	3	4	5	6
W^{**}(g)	200	300	400	500	600	700
Layer $K \times 10^7$ (g/sec²) . .	11·8	51·7	42·07	44·6	47	57

Mean K for layers 2–5 is 50×10^{-7} g/sec²

* Layers built in their numerical order. ** W is the total mass of material in the cake (g).

The plot in Fig. 8 has apparently removed the time t, though leaving the permeability in terms of all the other test conditions.

The permeability of the cakes has been analysed into permeabilities for the layers added in the building of a cake. With the usual assumptions as to flow conditions [1], [3] the centrifugal head developed by the layer of liquid from r_L to r_0 must be balanced by the sum of the frictional energy requirements for the flow rate q appropriate to each layer of the cake whence this head may be expressed in terms of either mean or layer permeabilities as follows

$$\left.\begin{aligned} &\frac{1}{2}(2\pi n)^2 (r_0^2 - r_L^2) \\ &= \frac{q \cdot g}{2\pi X K_m} \cdot \log_e \frac{r_0}{r_c} \\ &= \frac{q \cdot g}{2\pi X} \left[\frac{\log_e \frac{r_0}{r_1}}{K_1} + \frac{\log_e \frac{r_1}{r_2}}{K_2} + \cdots \frac{\log_e \frac{r_{n-1}}{r_n}}{K_n} \right]. \end{aligned}\right\} \quad (9)$$

Then the inner radius of the nth layer, r_n, is the inner radius r_c for the cake. Whence the relationship between the mean permeability K_m and the layer values, K_1, K_2, . . . , K_n, is

$$\frac{\log_e \frac{r_0}{r_c}}{K_m} = \frac{\log_e \frac{r_0}{r_1}}{K_1} + \frac{\log_e \frac{r_1}{r_2}}{K_2} + \cdots \frac{\log_e \frac{r_{n-1}}{r_c}}{K_n}. \quad (10)$$

The permeability of a layer added to a cake was found from the change in mean permeability of the cake caused by the layer, assuming that the compressive effect of the thin layer was negligible. Thus eq. (10) was used for two layers, the initial cake providing the outer layer.

The data in *Table 5* were obtained for series of tests on starch and kieselguhr in the hydroextractor. The initial cake layer was always of considerably lower permeability than the added layers. This suggests the presence of a high resistance in the outer layer of the cake.

The data in *Table 6* however for cakes of chalk and starch in the small cell (Fig. 2) are expressed as the mean hydroextraction permeabilities for a given mass of material in a complete cake thickness and do not show the low value in the first layer as given by starch in the hydroextractor. The data are similar for three methods of formation of the cake, whether the cakes were formed individually or in layers in the spinning cell, or whether they were formed by filtration in the cell and then spun. The three types of cake only show

Table 6. Hydroextraction permeabilities in small cell

Expressed as $K \times 10^7$ g/sec², the mean value for each cake

Chalk:

W(g)	5	6	7	8	9
Cakes formed in centrifuge . .	4·5	4·2	4·0	4·5	4·8
Cakes formed by successive addition	4·5	4·7	4·5	4·0	4·3
Cakes preformed by suction . .	4·8	4·6	4·4	4·3	4·3

Starch:

W(g)	5	7	9
Cakes preformed by suction . .	3·9	4·4	3·9

minor differences in the variation of K_c with W, including data for K_c decreasing with increasing W. The data in *Table 6* were obtained from cakes maintained under test for a considerably longer time than the cakes in the hydroextractor. The tests represented in *Table 4, 5* were of about an hour in duration for a whole series of W. The tests in the small cell were much slower due to difficulty in cake formation and the production of q, s curves for each cake [3], which thus entailed a total cake life of 4–6 hrs. In view of observations in this laboratory on the variation of permeability with time, the data in *Table 6* are considered less reliable than those in *Table 4, 5* for the present detailed study of permeability distribution.

The kieselguhr cakes formed by spinning in the small cell showed the low permeability in the first layer formed. The data in *Table 7* include the mean permeabilities for each cake and the layer values

Table 7. Kieselguhr in the small cell

W(g)	2	4	6	10
Hydroextraction permeability:				
Mean $K \times 10^6$	3·2	5·27	6·7	8·7
Layer* $K \times 10^6$ . . .	3·2	13·9	14·7	15·8
Filtration permeability:				
Mean $K \times 10^6$	2·74	4·5	5·9	7·52
Layer* $K \times 10^6$ . . .	2·74	12·8	13·4	12·7

* The layer permeability is for the innermost layer, *e.g.* that given for hydroextraction under mass 6 g in the table ($14{\cdot}7 \times 10^{-6}$) is the permeability of the 2 g layer, which changed the mean permeability $5{\cdot}27 \times 10^{-6}$ for the 4 g cake to the mean value $6{\cdot}7 \times 10^{-6}$ for the 6 g cake.

deduced from the two-layer form of the equation based on the summation of the frictional energy requirements for the multi-layer cake:

$$\frac{r_0 - r_c}{K_m} = \frac{r_0 - r_1}{K_1} + \frac{r_1 - r_2}{K_2} + \ldots \frac{r_{n-1} - r_c}{K_n} . \quad (10a)$$

The same cakes were also tested under filtration conditions using the arrangement in Fig. 2 and the technique appropriate to eq. (3). The values obtained for K_F are very near those obtained by the hydroextraction equations and also show the less permeable first layer.

From earlier tests [2] it seemed unlikely that the rapid decrease of permeability with increasing radius as positions near the basket wall was due to compressive effects. As possible confirmatory evidence of this the porosity distribution has been measured in cakes of chalk and of starch. Samples were cut from specified positions in cakes which were submerged throughout their life in the hydroextractor, *i.e.* the cakes were not spun dry before removal from the basket. The water content in each specimen was determined gravimetrically and was used to derive porosities. For starch the mean porosity at the front of the cake, *i.e.* at r_c, was 1·035 times the mean porosity at the back of the cake, *i.e.* near r_0. The dry starch packed in a Lea and Nurse [7] apparatus for the measurement

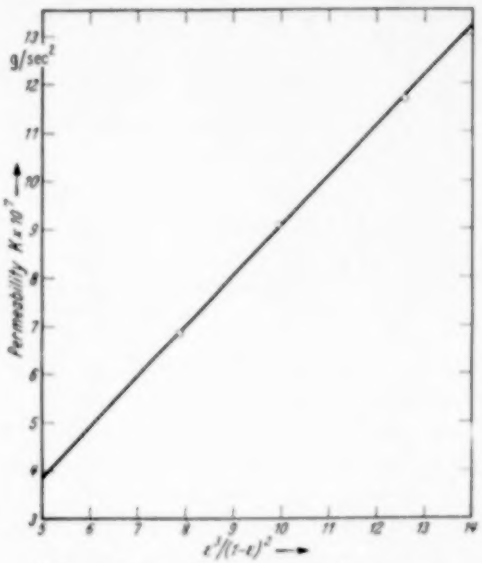

Fig. 9. Permeability from air flow tests.

of specific surface showed a linear relationship between permeability to air and the porosity function $\{\varepsilon^3/(1-\varepsilon)^2\}$, as shown in Fig. 9. Assuming that a similar linear function holds for the flow of water through the packed material, the above porosity distribution would cause a ratio of permeabilities of 1·22:1 from inside to outside of the cake. This change of K_c is insufficient to explain the high curvature at low cake thicknesses assumed with the dotted lines on Fig. 5, the latter needing the permeability distribution of curve B on Fig. 10.

The even gradual change of K_c seems more likely and thus the broken lines on Fig. 5 have been accepted as nearer the truth. The full distribution of permeability with radial position is thus postulated to be that in curve A on Fig. 10 rather than that of curve B. The curve A is based on an interface resistance defined as R in the centrifugal force balance

$$\frac{1}{2}(2\pi n)^2 . (r_0^2 - r_L^2) = \left[\frac{\mu g}{2\pi X K_c} . q . \log_e \frac{r_0}{r_c} \right] + R . \quad (11)$$

In a system with r_L maintained constant, the resistances are both functions of flow rate, q. If it be supposed

VOL. 1 1952

that the cake of thickness $(r_0 - r_c)$ could be maintained under the same centrifugal head without the resistance R, then the higher flow rate q^1 produced would be related to R by

$$R = \frac{\mu g}{2\pi X K_c} \cdot (q^1 - q) \cdot \log_e \frac{r_0}{r_c} . \qquad (12)$$

The ratio of R to the total head expended is thus $\left(\frac{q^1 - q}{q^1}\right)$. If the times for the flow of a volume V be

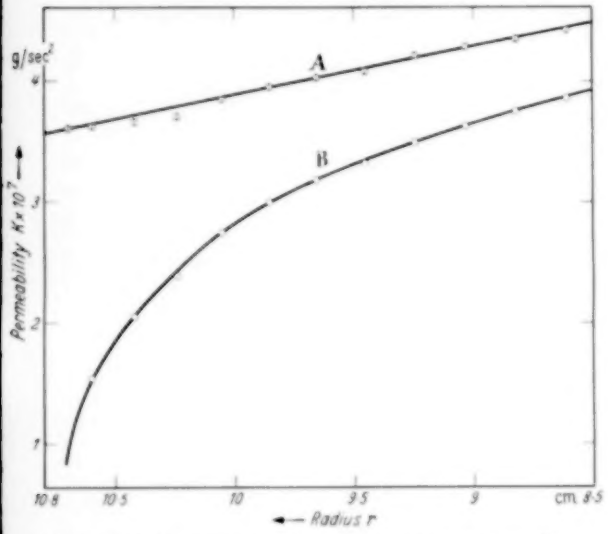

Fig. 10. Mean permeability changes with radial position.
A Assuming the existence of cloth cake interface resistance.
B Assuming no interface resistance.

considered as $t = \frac{V}{q}$ and $t^1 = \frac{V}{q^1}$; then the above force ratio is $\left(\frac{t - t^1}{t}\right)$ or $\frac{t_0}{t}$, where $t_0 = (t - t^1)$. This time difference t_0 can be shown to be equal to the intercept on the t axis in the plot of t against $\log_e r_0/r_c$ (Fig. 5).

From eq. (1), (2) the flow rate q when the liquid radius is maintained at r_L is specified in terms of the time t for the liquid layer to move from inner radius r_{L_2} to r_{L_1} in the variable r_L drainage test described above

$$\frac{q}{\pi X \cdot (r_0^2 - r_L^2)} = \frac{1}{t} \cdot \log_e \cdot \left(\frac{r_0^2 - r_{L_1}^2}{r_0^2 - r_{L_2}^2}\right)$$

$$q = \frac{\pi X}{t} (r_0^2 - r_L^2) \cdot \log_e \left(\frac{r_0^2 - r_{L_1}^2}{r_0^2 - r_{L_2}^2}\right). \qquad (13)$$

Consider a mean flow rate q_m such that the volume of liquid $\pi X (r_{L_2}^2 - r_{L_1}^2)$ is discharged in time t

$$q_m = \frac{\pi X (r_{L_2}^2 - r_{L_1}^2)}{t} . \qquad (14)$$

The rate q is equal to q_m when r_L is given by

$$r_L^2 = r_0^2 - (r_{L_2}^2 - r_{L_1}^2) / \log_e \left(\frac{r_0^2 - r_{L_1}^2}{r_0^2 - r_{L_2}^2}\right). \qquad (15)$$

Thus $(r_0^2 - r_L^2)$ is the logarithmic mean of $(r_0^2 - r_{L_1}^2)$ and $(r_0^2 - r_{L_2}^2)$. The ratio $(r_0^2 - r_{L_1}^2)/(r_0^2 - r_{L_2}^2)$ was about 1·2 and thus as a good approximation

$$(r_0^2 - r_L^2) = \frac{(r_0^2 - r_{L_1}^2) + (r_0^2 - r_{L_2}^2)}{2}$$

$$r_L^2 = \frac{r_{L_1}^2 + r_{L_2}^2}{2} \qquad (16)$$

and with r_{L_1} normally near r_{L_2}

$$r_L = \frac{r_{L_1} + r_{L_2}}{2} . \qquad (17)$$

The agreement between the approximate value from eq. (17) and the true value from eq. (15) is well within the experimental accuracy, *e.g.* with $r_{L_2} = 8{\cdot}31$ and $r_{L_1} = 7{\cdot}64$ cm in this work (*Table 3*), both the values of r_L were 7·98 cm. The above relationships show that the time t for the experimental movement of the liquid surface from r_{L_1} to r_{L_2} may be regarded as the outflow time for the volume between these radii for a system at r_L maintained at the mean of r_{L_1} and r_{L_2}. The experimental drainage time t may thus be considered as the time to be used in the relationships derived above from eq. (13), if the quantities V and q therein be considered as the values $\pi X (r_{L_2}^2 - r_L^2)$ and $\pi X (r_{L_1}^2 - r_{L_2}^2)/t$ respectively.

Thus the intercept t_0 on the time axis when $r_0 = r_c$ in Fig. 5 is assumed to give the interface resistance as the fraction t_0/t of the total head dissipated in the hydroextractor. The data for the dotted line for starch at $n' = 1050$ on Fig. 5, giving curve B on Fig. 10, have been reassessed by calculating the permeabilities from eq. (2) appropriate to time $(t - t_0)$ rather than t. The curve A is obtained which shows a gradual change in permeability in keeping with the measured porosity changes. The range of K_c on curve A is 1·24/1 as against 4·2/1 for curve B and 1·22/1 from the porosity distribution.

Conclusions

No variation in the porosity of the layers of hydroextractor cakes or the cakes in the small cell could be detected by measuring the thicknesses or internal and external radii of such cakes. The packing density was found to be constant throughout the cake with fine materials and was the same for cakes formed in the hydroextractor basket or in the small cell.

The kieselguhr layers were apparently compressed by either starch or chalk layers on them, while outer layers of kieselguhr were not compressed by further added layers of the same material. This may be due to differences in lateral support exerted by the materials or to the lower permeability of the starch

and chalk leading to higher compressive stress due to frictional drag.

Drainage tests showed gradual decrease in permeability with position of increasing radius in the hydroextractor cakes. The permeability of the innermost layer was always higher than that of the rest of the cake and was nearly constant regardless of its radial position. Near the outer surface, the decrease in permeability was large; the value for the innermost layer of a thick cake being four times that of the outermost layer.

Analysis of the experimental results was based on an assumed interface resistance dependent on the flow rate at the cloth-cake contact. This assessment gave a permeability variation within the cake of the order of 1·24:1 from the inner to the outer layer which agreed with permeability distribution estimated from gravimetric determinations of the porosity. The data for kieselguhr in the small cell *(Table 7)* show the same permeability distribution for both filtration and hydroextraction. The phenomenon is not therefore a characteristic of either hydroextraction mechanism or of the proposed flow equations.

NOMENCLATURE

A = cross-sectional area of filter bed (cm²)
a = cross-sectional area of filter tube in filtration tests (cm²)
C, C_1, C_2 = constants
g = gravitational acceleration (cm/sec²)
H = hydrostatic head in filtration tests (cm)
K = permeability (g/sec²), K_1, K_2, K_n for different layers; K_c for hydroextraction; K_F for filtration; K_m for mean value
L = length of filter bed in filtration tests (cm) inner
n = speed of revolution (rev./sec), n' (rev./min)
q = drainage rate through cake (cc/sec)
r = radius from basket axis (cm); r_w for basket surface; r_0 for cake outer surface; r_c for cake inner surface; r_L for liquid inner surface; $r_1, r_2, \ldots, r_n$ for interfaces between cake layers
t = time (seconds)
V = volume (cc)
W = mass of dry solid in cake (g)
X = height of centrifuge basket (cm)
ε = porosity
μ = viscosity of liquid (poise)
σ = packing density of solids in the tested cake; (g solid/cc cake volume)

REFERENCES

[1] BURAK, N. and STORROW, J. A.; J. Soc. chem. Ind. 1950 **69** 8. [2] GUPTA, O. P.; M. Sc. Tech. thesis. Manchester 1948. [3] HARUNI, M. M. and STORROW, J. A.; Hydroextraction—Part I, submitted to Industrial and Engineering Chemistry. [4] HARUNI, M. M. and STORROW, J. A.; Hydroextraction—Part II, *ibid.* [5] HARUNI, M. M. and STORROW, J. A.; Hydroextraction—Part III, *ibid.* [6] INGLESENT, H. and STORROW, J. A.; Ind. Chem. 1951 **27** 76. [7] LEA, F. M. and NURSE, R. W.; Symposium on Particle Size Determination, Institution of Chemical Engineers, London 1947.

VOL. 1 1952

Vacuum distillation I

Test mixtures for evaluation of low pressure columns

F. J. ZUIDERWEG

Koninklijke/Shell-Laboratorium, Amsterdam

(Received 6 September 1951)

Summary—The liquid vapour equilibria of two test mixtures, *viz.* *n*-decane—*trans*-decalin and *n*-hexadecane—*n*-heptylbenzoate, were examined at low pressures; the results were checked for thermodynamic consistency. It was found that the *n*-decane—*trans*-decalin system obeys RAOULTS law, relative volatility values varying from 1·185 at 1·33 kN/m² (10 mm Hg) to 1·36 at 101·5 kN/m² (760 mm Hg). The *n*-hexadecane—*n*-heptylbenzoate system contains an azeotrope at about 90% *n*-hexadecane (pressure range 0·13–2·0 kN/m², 1–15 mm Hg) which limits its applicability as a test mixture to evaluation of columns with not more than 16–18 theoretical plates.

Zusammenfassung—Die Flüssigkeit-Dampfgleichgewichte der binären Gemische *n*-dekan—*trans*-dekalin und *n*-hexadekan—*n*-heptylbenzoat, wurden bei niedrigen Drucken bestimmt; es wurde nachgeprüft ob die Ergebnisse thermodynamisch in Übereinstimmung waren.

Es zeigte sich, daß das *n*-dekan—*trans*-dekalin-System dem RAOULTschen Gesetz entspricht und daß die relativen Flüchtigkeitswerte von 1·185 bei 1·33 kN/m² (10 mm Hg) bis zu 1·36 bei 101·5 kN/m² (760 mm Hg) variieren. Das *n*-hexadekan—*n*-heptylbenzoat-System enthält ein Azeotrop bei ungefähr 90% *n*-hexadekan (Druckgebiet 0·13–2·0 kN/m² (1–15 mm Hg), das die Verwendbarkeit dieses Gemisches beschränkt auf die Beurteilung von Kolonnen mit nicht mehr als 16–18 theoretischen Boden.

The increasing importance of rectification at low pressures makes the availability of test mixtures for calibration and testing of low pressure distillation columns interesting. WILLIAMS [19] summarized the requirements which should be met by such test mixtures as follows:

a) The boiling points of the components should be close together and should be in the range 100–200° C at the operating pressure;

b) the mixtures should not deviate too much from ideality;

c) any mixture of the components should be accurately analyzable, preferably by a simple and rapid method which requires only a small sample;

d) the components should remain liquid at temperatures well below the operating temperature, preferably even at room temperature;

e) the components should be thermally and chemically stable at the operating temperature;

f) the components should be readily available and easy to purify.

However, apart from the above requirements relating to the nature of the components to be selected, a further demand as to the vapour-liquid equilibrium of the test mixture should be added, *e.g.* the data should be accessible to control on thermodynamic consistency. In general, the technique of determination of liquid vapour equilibria is rather difficult, and this may be said particularly of the measurements of low pressure equilibria. Thermodynamic control is here a powerful expedient in estimating possible errors made during the determination.

Unfortunately, most test mixtures proposed [7], [11], [19] are not accessible to control on thermodynamic consistency, mostly owing to lack of accurately measured vapour pressures of the components.

On the other hand, in the few cases where thermodynamic control of low pressure vapour liquid equilibria is possible, large systematic errors can be shown [3], [4], [9], [16].

In the present study the vapour-liquid equilibria of two binary mixtures have been reported*. The first mixture, *n*-decane—*trans*-decalin, may be used for testing columns in the pressure range from 10 to 760 mm Hg. For pressures lower than 10 mm Hg the *n*-decane—*trans*-decalin mixture is unsuitable in view of its low boiling point at these pressures. The second mixture, *n*-hexadecane—*n*-heptylbenzoate was examined in order to have a more representative test mixture as regards molecular weight for vacuum distillation. The *n*-hexadecane—*n*-heptylbenzoate system may be used for calibration of columns in the pressure range 1–15 mm Hg.

Both mixtures fulfil well the requirements a) to f) mentioned above: the components may be obtained by purification and/or synthesis from commercially available base materials; analysis may be performed quickly and accurately by means of refractive index measurement; the components are liquid at room temperature and stable at distillation temperatures. The *n*-hexadecane—*n*-heptylbenzoate mixture, however, contains an azeotrope and deviates rather much from ideality; not more than 16–18 theoretical plates can be accurately measured with it.

In the second paper in this series, the results of testing a Vigreux column and a rotating-band column with the binary mixtures mentioned over a wide range of pressures will be described.

Check of Thermodynamic Consistency

In recent literature on the checking of vapour-liquid equilibria for thermodynamic consistency several methods of correlation have been given [5], [10], [18], [20], frequently based on special integrations of the Duhem-equation. A more general method, which is very simple in application too, is described by Redlich and Kister [12] and by Coulson and Herington [6].

The method consists in calculating the ratio of activity coefficients from the α-values and vapour pressure ratio by

$$\frac{\gamma_1}{\gamma_2} = \alpha \frac{P_2}{P_1} \tag{1}$$

after which the $\log \gamma_1/\gamma_2$ values obtained are plotted against the mol fraction of volatile component in the liquid phase. In the case of thermodynamic consistent results the following condition should be met:

$$\int_0^1 \log \frac{\gamma_1}{\gamma_2} \, dx = 0, \tag{2}$$

so the net area between the curve obtained ("exchange function") and the abscissa should be zero.

For accurate work, activity coefficients should be corrected for gas law deviations and pressure effects on the liquid. These corrections may be incorporated in the vapour pressures of the pure components according to Benedict *et al.* [2] by:

$$\log \frac{P_1}{p_1^0} = \frac{1}{2{\cdot}303\,RT} \left[(V_1 - B_1)(P - p_1^0) \right]. \tag{3}$$

* In the present study the dimensions of the various magnitudes are expressed in the metre—kilogram—second units system.

In this system the unit of force is called Newton (N); it has the dimensions kg m/sec². One Newton is equivalent to 10^5 dynes.

The second virial coefficient B in this equation is calculated from critical data by Berthelot's equation:

$$B = \frac{9}{128}\frac{RT_c}{P_c}\left[1 - 6\left(\frac{T_c}{T}\right)^2\right]. \qquad (4)$$

Vapour Liquid Equilibria

Base materials

n-Decane was obtained by dehydratation of a commercial decanol-1 and subsequent hydrogenation of the resultant *n*-decene. The base material, the olefinic intermediate product and the final product were distilled in a 60-plate Oldershaw column. Only the fractions differing less than 0·1° C in Cottrell boiling point were combined.

Trans-decalin was obtained from commercial decalin by fractional distillation.

In order to make the yield as high as possible, the cis-decalin present was first converted to *trans*-decalin by isomerisation with about 20% $AlCl_3$ catalyst at 50° C according to Seyer and Yip [15]. The reaction product was sharply fractionated in a 60-plate Oldershaw column; again, only the fractions differing less than 0·1° C in Cottrell boiling point were combined.

n-Hexadecane was a commercial product, purified by repeated recrystallization from a mixture of benzene-methylethyl ketone; the recrystallized product was then distilled under reduced pressure.

n-Heptylbenzoate was synthesised by heating an excess of *n*-heptanol with benzoylchloride; both materials were previously purified by distillation. The reaction product was subjected to vacuum rectification in a Vigreux column (equivalent to about 15 theoretical plates). Only the fractions differing less than 0·0001 in refractive index were combined.

Physical properties of the materials obtained are given in Table 1. The large difference in refractive index between the components of each of the two test mixtures offers the possibility of analysis by this magnitude. To this end refractive index determinations of a number of mixtures of the components were made; the data obtained are given in Tables 2 and 3.

Table 1. Physical properties of materials used

	n_D^{20}	*Boiling point* °C	*Melting point* °C
n-decane	1·4118	174·15	—
Litt. [1]. . . .	1·41189	174·12	
t-decalin	1·4696	187·7	—
Litt. [14] . . .	1·46968	187·5	
Litt. [16] . . .	1·4692	187·30	
n-hexadecane . .	1·4347		17·95
Litt. [1]. . . .	1·43448		18·15
n-heptylbenzoate	1·4917	—	—

Table 2. Relation between refractive index and composition in the system n-decane—t-decalin

n_D^{20}	*Mol. fr. n-decane*	n_D^{20}	*Mol. fr. n-decane*
1·4118	1·000	1·4510	0·284
1·4322	0·607	1·4639	0·083
1·4416	0·436	1·4696	0·000

Table 3. Relation between refractive index and composition in the system n-hexadecane—n-heptylbenzoate

n_D^{20}	*Mol. fr. n.* C_{16}	n_D^{20}	*Mol. fr. n.* C_{16}
1·4347	1·000	1·4714	0·294
1·4429	0·818	1·4767	0·210
1·4486	0·701	1·4826	0·125
1·4542	0·592	1·4917	0·000
1·4653	0·394		

Apparatus

Most of the vapour-liquid equilibrium determinations were performed with the Othmer-type still sketched in Fig. 1. To avoid systematic errors by condensation or overheating of the vapours, the heater for compensation of heat losses was assembled around a jacket through which the vapours from the equilibrium chamber were passed off.

In order to avoid bumping of the liquid at lower pressures, the liquid chamber was filled with Ni-chromium Fenske helices.

This apparatus is, however, not suitable for use at pressures of about 1 mm Hg as then the pressure drop in the vapour line is too large. Therefore an apparatus as described by Williams [19] was used for this pressure range. It proved necessary to modify the apparatus slightly as it appeared from measurement of the boiling point of *n*-hexadecane at 1 mm Hg that there was still a considerable pressure gradient in the vapour line. The upper part was arranged like a reflux condenser, with a separate pressure exchange tube to the receiver part (Fig. 2).

VOL. 1 1952

Vapour pressure determinations of *n*-decane and *trans*-decalin were made in a Cottrell boiling point apparatus (liquid capacity about 20 ml) (Table 4); the data on *n*-hexadecane and *n*-heptylbenzoate were obtained by distilling the pure materials in the equilibrium still of Fig. 2 at various pressures (Table 7).

At the lowest pressures the pressure in the apparatus was kept constant by a manostat as described by WILLIAMS [19]; at higher pressures a pressure regulator of the design given by TODD [17] was used.

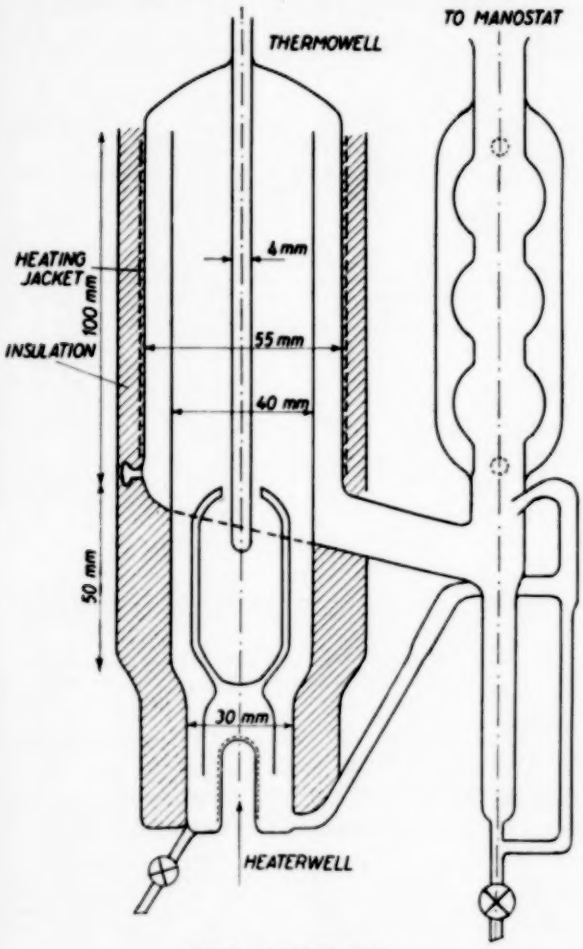

Fig. 1. Othmer Still.

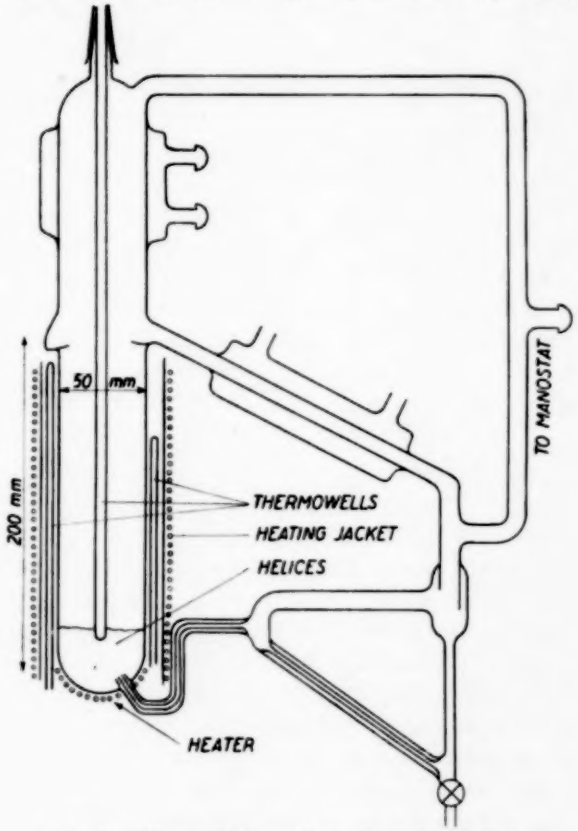

Fig. 2. Othmer Still, used at about 0·13 kN/m².

Table 4. Vapour pressures of n-decane and trans-decalin

n-decane				*trans-decalin*			
t °C	*P* kN/m²	*t* °C	*P* kN/m²	*t* °C	*P* kN/m²	*t* °C	*P* kN/m²
56·7	1·41	184·1	129·7	60·1	1·41	179·1	82·9
64·65	2·10	186·9	138·3	68·55	2·10	175·6	76·25
76·15	3·56	188·4	143·0	80·9	3·56	171·9	69·6
86·25	5·45	187·1	139·0	91·75	5·45	173·5	72·2
93·9	7·45	185·0	132·3	100·0	7·45	177·1	78·9
99·85	9·45	182·9	125·7	106·45	9·45	180·6	85·5
107·15	12·60	180·6	119·0	114·4	12·60	183·7	92·2
82·4	4·64	178·2	112·3	87·6	4·64	186·7	98.9
174·7	102·9	175·8	105·7	188·4	102·9	188·4	102·9
179·7	116·4	174·7	102·9	185·5	96·3		
181·9	123·0			182·4	89·5		

n-Decane—trans-decalin binary system

The data obtained at atmospheric pressure with the equilibrium still of Fig. 1 are collected in Table 5. In checking these data for thermodynamic consistency, the following values were used in the calculation of the correction for gas law deviations etc. according to eq. (3) and (4).

	Crit. temp. °C	*Crit. press.* MN/m²	*Molal vol.* m³/k mol
n-decane	344	2·09	0·234
t-decalin	410	2·88	0·183

Table 5. Vapour-liquid equilibrium n-decane—trans-decalin atmospheric pressure

Composition, mol. fraction n-decane		log α	log $\frac{P_1}{P_2}$	log $\frac{\gamma_1}{\gamma_2}$
Liquid	*Vapour*			
0·241	0·305	0·140	0·134	0·006
0·354	0·432	0·143	0·134	0·009
0·351	0·427	0·140	0·134	0·006
0·338	0·405	0·130	0·134	−0·004
0·312	0·387	0·143	0·134	0·009
0·315	0·382	0·127	0·134	−0·007
0·305	0·370	0·127	0·134	−0·007
0·300	0·370	0·137	0·134	0·003
0·362	0·441	0·137	0·134	0·003
0·391	0·460	0·124	0·134	−0·010
0·445	0·527	0·143	0·134	0·009
0·565	0·641	0·137	0·133	0·004
0·612	0·676	0·121	0·133	−0·012
0·694	0·754	0·127	0·133	−0·006
0·717	0·776	0·137	0·133	0·004
0·810	0·855	0·140	0·133	0·007
0·825	0·862	0·124	0·133	−0·009
0·691	0·750	0·127	0·133	−0·006
0·065	0·087	0·140	0·134	0·006
0·218	0·276	0·137	0·134	0·003
0·199	0·245	0·114	0·134	−0·020
0·195	0·245	0·127	0·134	−0·007
0·165	0·210	0·130	0·134	−0·004
0·105	0·137	0·134	0·134	0·000

By applying this correction the log of vapour pressure ratio of the components calculated from the data in Table 4 (ranging from 0·140 to 0·143) is reduced by about 5%.

The ^{10}log of the corrected vapour pressure ratio and the ^{10}log of the ratio of activity coefficients calculated are given in Table 5 too.

From the plot of the atmospheric data in Fig. 3 it may be concluded that the results obtained are thermodynamically consistent; the system behaves ideally at least within the limits of experimental error.

As the vapour-liquid equilibrium at atmospheric pressure proved to be ideal, only a few check determinations were carried out at reduced pressures, *viz.* by measuring boiling point differences at various pressures between pure *n*-decane and two mixtures of *n*-decane and *trans*-decalin. These measurements were carried out in two Cottrell boiling point apparatuses already mentioned above. Temperature differences were determined with the aid of a differential thermocouple and a sensitive galvanometer (enabling readings within 0·01–0·02° C). The results obtained are collected in Table 6 and shown in Fig. 4.

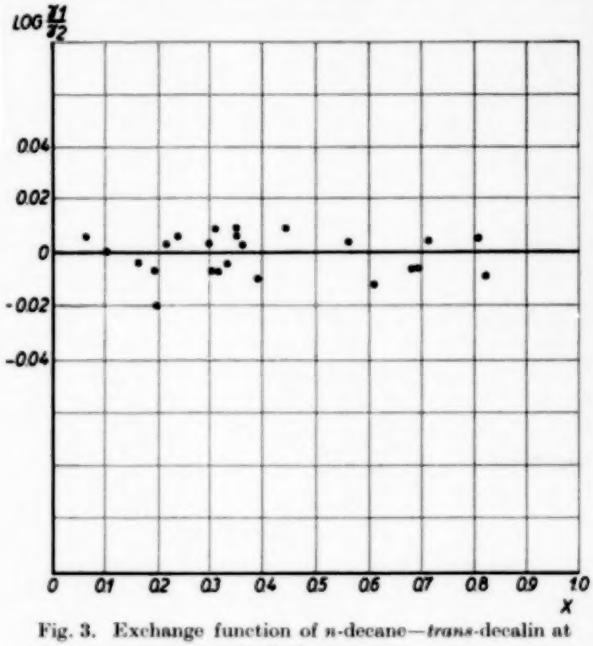

Fig. 3. Exchange function of *n*-decane—*trans*-decalin at atmospheric pressure.

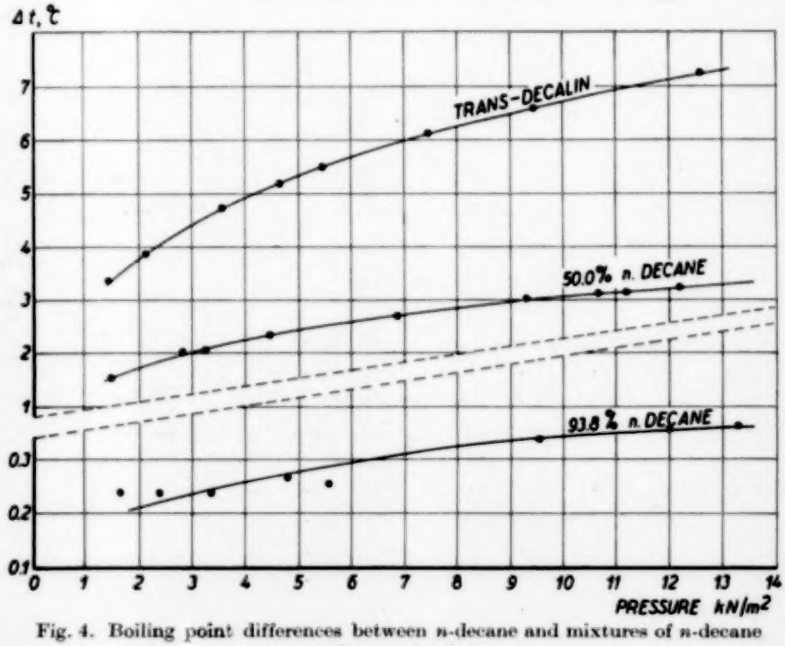

Fig. 4. Boiling point differences between *n*-decane and mixtures of *n*-decane and *trans*-decalin.

VOL. 1 1952

Table 6. Temperature intervals between boiling points of n-decane and n-decane—trans-decalin mixtures

0 mol % n-decane		*50·0 mol % n-decane*		*93·8 mol % n-decane*	
kN/m²	*t, ° C*	*kN/m²*	*t, ° C*	*kN/m²*	*t, ° C*
1·41	3·38	1·49	1·67	1·58	0·24
2·10	3·90	2·81	2·04	3·36	0·24
3·56	4·74	4·45	2·36	5·58	0·26
5·45	5·50	6·86	2·70	7·36	0·32
7·45	6·12	9·30	3·01	9·55	0·34
9·45	6·60	11·20	3·14	12·00	0·36
12·60	7·25	12·2	3·23	4·80	0·27
4·64	5·19	32·1	2·09	2·40	0·24

From the data with the mixture containing 93·8 mol% of *n*-decane, dt/dx values at $x = 1$ in the $t - x$ diagram may be calculated. REDLICH and KISTER [12] have shown how to calculate α values from these data. Taking the values from Fig. 4 at resp. 2·67, 6·66 and 13·33 kN/m² (20, 50 and 100 mm Hg), the following results are obtained:

P, kN/m²	2·67	6·67	13·33
mm Hg	20	50	100
dt/dx (Fig. 4)	−3·7	−5·0	−5·8
$d \log P_1/dt$ (derived from Table 4)	0·0202	0·0178	0·0162
α	1·21	1·26	1·28
ideal α from vapour pressures*	1·205	1·25	1·30

* Corrections for divergence from ideal gas laws may be ignored in view of low total pressure.

The above calculations show that the system *n*-decane—*trans*-decalin behaves ideally at lower pressures too.

This can also be demonstrated by comparing the measured total pressure of the mixture containing 50 mol % *n*-decane with the calculated pressure according to RAOULTS law.

The calculations yielded the following results:

This test [13] which is highly sensitive to divergence from the ideal, shows that the differences between calculated and experimental total pressure are very small and within the error of experimental observation (about 0·02 kN/m²).

The system *n*-decane—*trans*-decalin being ideal, plate numbers of columns distilling under total reflux may be calculated with FENSKE's formula [8]. As the α-value does not vary much with concentration, an average value may be used at every specified pressure, as follows:

Pressure		*α-value*
kN/m²	*mm Hg*	
1·33	10	1·185
2·67	20	1·205
6·67	50	1·255
13·33	100	1·305
101·5	760	1·36

Recently, STRUCK and KINNEY [16] and FENSKE, MYERS and QUIGGLE [7] published data on the vapour-liquid equilibrium *n*-decane—*trans*-decalin over a wide range of pressures. They found α-values differing greatly from the values presently reported, *viz.* at 10 mm Hg, $\alpha = 1{\cdot}11$, at 100 mm Hg, $\alpha = 1{\cdot}22$, at 760 mm Hg, $\alpha = 1{\cdot}30$. The authors did not test their data for thermodynamic consistency, however, so that large systematic errors in the data given remained unobserved. Applying the criterion of REDLICH etc. to some of their data, the result presented in Fig. 5 is obtained. It is seen that the $\log \gamma_1/\gamma_2$-function can be represented by a straight line, running parallel to the abcissa at a distance of about $\log \gamma_1/\gamma_2 = -0{\cdot}02$. This shows that systematic errors are present in the determinations made; the result, however, suggests too that the *n*-decane—*trans*-decalin system behaves ideally. This may also be shown by calculating total pressures according to RAOULT's law from

Pressure observed		*Boiling pt. n. C_{10}*	*Δt for mixture 50·0 mol % n. C_{10} (Fig. 4)*	*Boiling pt. mixture 50·0 mol % n. C_{10}*	*Vapour pressure*		*Calculated pressure*	*Difference calc—obs.*
					n. C_{10}	*tr.-dec.*		
kN/m²	*mm Hg*	*° C*	*° C*	*° C*	*kN/m²*	*kN/m²*	*kN/m²*	*kN/m²*
2·67	20	69·8	1·95	71·75	2·92	2·42	2·67	0·00
6·67	50	91·2	2·70	93·90	7·44	5·92	6·68	+0·01
10·66	80	102·9	3·10	106·0	12·03	9·31	10·67	+0·01
13·33	100	108·6	3·30	111·9	15·10	11·52	13·31	−0·02

boiling points and compositions of the binary systems given by STRUCK and KINNEY. As appears from the ratio between calculated and experimental pressures—also represented in Fig. 5 as a function of liquid composition—the system is actually almost ideal. The deviations found between actual and calculated pressures are invariably smaller than the

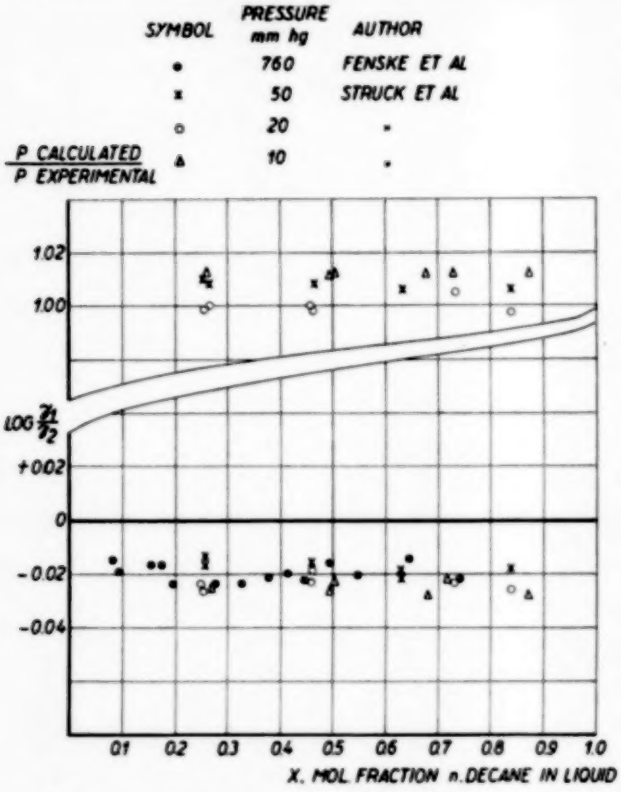

Fig. 5. Correlation of literature data on the *n*-decane—*trans*-decalin equilibrium ([9], [16]).

limits within which the pressure on the system was kept constant during the determinations (about 0·5 mm Hg).

n-Hexadecane—n-heptylbenzoate binary system

The vapour-liquid equilibrium of the *n*-hexadecane—*n*-heptylbenzoate system was measured at three pressures: 0·13, 0·49 and 2·0 kN/m² (1, 3·7 and 15 mm Hg, respectively). For determinations at 0·49 and 2·0 kN/m² the Othmer apparatus of Fig. 1 was used; the measurements at 0·13 kN/m² were carried out in the equilibrium still of Fig. 2. The data on the vapour pressures of the components and the vapour-liquid relations obtained are collected in Tables 7–10.

Table 7. Vapour pressures of n-hexadecane and n-heptylbenzoate

n-hexadecane				*n-heptylbenzoate*			
t °C	*P* N/m²	*t* °C	*P* N/m²	*t* °C	*P* N/m²	*t* °C	*P* N/m²
111·1	180	130·2	550	110·8	113	107·2	96
109·8	163	125·9	430	101·2	59	106·3	92
107·8	144	134·9	730	115·6	162	104·8	82
105·7	128	131·9	615	112·1	133	103·0	74
116·0	256	137·8	860	131·7	395	123·9	266
113·1	208	140·1	905	128·1	318	139·5	640
110·7	179	136·9	800	121·9	236	148·0	933
107·0	139	152·0	1640	117·9	180	156·8	1440
103·5	115	158·7	2080	127·8	320	170·5	2390
100·6	92	190·4	7250	122·3	251	176·5	2970
98·8	80	158·0	2080	142·1	730	182·0	3670
97·4	73	149·8	1450	135·9	545		
131·5	585	142·2	1010	131·3	400		
122·3	368	170·9	3620	103·0	68		
120·1	328			101·0	62		
133·9	695	125·8	420	111·4	127		

Table 8. Vapour-liquid equilibrium n-hexadecane—n-heptylbenzoate. Experimental data at 133 N/m²

Composition mol. fraction n-hexadecane		*Temperature*	log α	$\log \frac{P_1}{P_2}$	$\log \frac{\gamma_1}{\gamma_2}$
Liquid	*Vapour*	°C*			
0·822	0·828	105·1	0·018	0·181	−0·163
0·760	0·782	105·1	0·054	0·181	−0·127
0·719	0·744	105·1	0·055	0·181	−0·126
0·712	0·742	105·1	0·065	0·181	−0·116
0·640	0·686	105·3	0·090	0·180	−0·090
0·500	0·603	105·9	0·182	0·180	+0·002
0·477	0·587	106·0	0·192	0·179	+0·013
0·417	0·533	106·4	0·203	0·179	0·024
0·230	0·403	108·2	0·354	0·177	0·177
0·212	0·391	108·5	0·377	0·177	0·200
0·186	0·351	108·8	0·374	0·176	0·198
0·170	0·320	109·1	0·361	0·176	0·185
0·163	0·302	109·2	0·346	0·176	0·170
0·135	0·268	109·6	0·370	0·175	0·195
0·082	0·209	110·6	0·471	0·174	0·297
0·096	0·188	110·3	0·340	0·174	0·166
0·086	0·183	110·5	0·376	0·174	0·202
0·073	0·153	110·8	0·360	0·174	0·186
0·057	0·127	111·1	0·382	0·174	0·208
0·794	0·808	105·1	0·038	0·181	−0·143
0·812	0·813	105·1	0·003	0·181	−0·178
0·842	0·850	105·1	0·026	0·181	−0·155

* Smoothed from experimental data.

VOL. 1 1952

Table 8. (Continued)

Composition mol. fraction n-hexadecane		Temperature	log α	$\log \frac{P_1}{P_2}$	$\log \frac{\gamma_1}{\gamma_2}$
Liquid	Vapour	°C*			
0·888	0·886	105·2	−0·009	0·180	−0·189
0·925	0·925	105·4	0·000	0·180	−0·180
0·847	0·847	105·1	0·000	0·181	−0·181
0·847	0·847	105·1	0·000	0·181	−0·181
0·784	0·790	105·1	0·014	0·181	−0·167
0·767	0·779	105·1	0·029	0·181	−0·152
0·909	0·896	105·3	−0·065	0·180	−0·245
0·886	0·900	105·2	0·064	0·181	−0·171
0·900	0·900	105·2	0·000	0·181	−0·181
0·903	0·900	105·2	−0·015	0·181	−0·196
0·327	0·492	107·1	0·300	0·178	0·122
0·312	0·491	107·2	0·328	0·178	0·150
0·271	0·439	107·7	0·323	0·177	0·146
0·586	0·662	105·5	0·140	0·180	−0·040
0·133	0·293	109·6	0·431	0·175	−0·256
0·073	0·189	110·8	0·472	0·174	−0·298
0·065	0·158	111·0	0·431	0·174	−0·257
0·068	0·152	110·9	0·390	0·174	−0·216
0·057	0·133	111·1	0·404	0·174	−0·230

Table 9. Vapour-liquid equilibrium n-hexadecane—n-heptylbenzoate. Experimental data at 490 N/m²

Composition mol. fraction n-hexadecane		Temp.	log α	$\log \frac{P_1}{P_2}$	$\log \frac{\gamma_1}{\gamma_2}$
Liquid	Vapour	°C*			
0·136	0·225	132·6	0·267	0·157	0·110
0·136	0·229	132·6	0·277	0·157	0·120
0·134	0·234	132·6	0·297	0·157	0·140
0·137	0·214	132·6	0·233	0·157	0·076
0·132	0·238	132·6	0·312	0·157	0·155
0·133	0·245	132·6	0·326	0·157	0·169
0·167	0·275	132·2	0·277	0·157	0·120
0·176	0·305	132·1	0·312	0·157	0·155
0·244	0·373	131·2	0·267	0·158	0·109
0·250	0·377	131·2	0·258	0·158	0·100
0·303	0·411	130·5	0·207	0·158	0·049
0·434	0·526	129·3	0·161	0·159	0·002
0·424	0·514	129·4	0·158	0·159	−0·001
0·301	0·416	130·5	0·220	0·158	0·062
0·290	0·416	130·7	0·241	0·158	0·083
0·418	0·518	129·5	0·176	0·159	0·017
0·335	0·450	130·3	0·212	0·158	0·054
0·286	0·408	130·8	0·236	0·158	0·078
0·341	0·461	130·2	0·218	0·158	0·060

* Smoothed from experimental data.

Table 9. (Continued)

Composition mol. fraction n-hexadecane		Temperature	log α	$\log \frac{P_1}{P_2}$	$\log \frac{\gamma_1}{\gamma_2}$
Liquid	Vapour	°C*			
0·140	0·253	132·5	0·318	0·157	0·161
0·093	0·169	133·2	0·298	0·156	0·142
0·038	0·083	134·1	0·360	0·156	0·204
0·039	0·081	134·1	0·339	0·156	0·183
0·631	0·694	128·0	0·123	0·159	−0·036
0·631	0·694	128·0	0·123	0·159	−0·036
0·473	0·571	129·0	0·171	0·159	0·012
0·760	0·779	127·5	0·046	0·160	−0·114
0·750	0·778	127·5	0·067	0·160	−0·093
0·798	0·807	127·4	0·025	0·160	−0·135
0·821	0·828	127·4	0·021	0·160	−0·139
0·842	0·846	127·4	0·012	0·160	−0·148
0·873	0·871	127·4	−0·008	0·160	−0·152
0·896	0·896	127·4	0·000	0·160	−0·160
0·973	0·973	127·6	0·000	0·160	−0·160
0·968	0·972	127·6	0·059	0·160	−0·101
0·936	0·936	127·5	0·000	0·160	−0·160
0·134	0·228	132·6	0·281	0·157	0·124

Table 10. Vapour-liquid equilibrium n-hexadecane—n-heptylbenzoate. Experimental data at 2·0 kN/m²

Composition mol. fraction n-hexadecane		Temp.	log α	$\log \frac{P_1}{P_2}$	$\log \frac{\gamma_1}{\gamma_2}$
Liquid	Vapour	°C*			
0·076	0·140	164·6	0·297	0·146	0·151
0·116	0·197	163·9	0·272	0·146	0·126
0·181	0·287	163·0	0·260	0·146	0·114
0·196	0·301	162·8	0·248	0·146	0·102
0·205	0·322	162·7	0·267	0·146	0·121
0·186	0·293	162·9	0·258	0·146	0·112
0·282	0·383	161·5	0·199	0·146	0·053
0·385	0·480	160·4	0·170	0·146	0·024
0·440	0·533	159·8	0·161	0·147	0·014
0·470	0·556	159·5	0·149	0·147	0·002
0·486	0·577	159·3	0·158	0·147	0·011
0·404	0·493	160·2	0·158	0·146	0·012
0·565	0·633	158·4	0·124	0·147	−0·023
0·418	0·491	160·0	0·130	0·146	−0·016
0·383	0·484	160·4	0·179	0·146	0·013
0·222	0·335	162·4	0·246	0·146	0·100
0·095	0·163	164·3	0·267	0·146	0·121
0·886	0·888	156·5	0·008	0·148	−0·140
0·809	0·823	156·5	0·040	0·148	−0·108
0·760	0·784	156·7	0·059	0·148	−0·089
0·619	0·680	158·0	0·116	0·147	−0·031
0·565	0·638	158·4	0·132	0·147	−0·015

* Smoothed from experimental data.

The ratios of the activity coefficients calculated from these experimental data are plotted in Fig. 6–8. It is seen that there is considerable spreading in the results obtained. In drawing the curves through the points the position of the azeotrope in the system

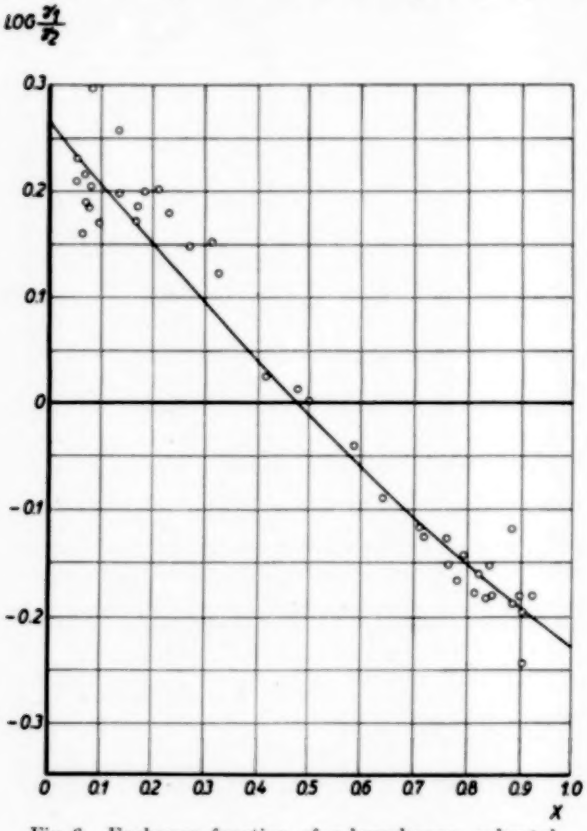

Fig. 6. Exchange function of *n*-hexadecane—*n*-heptylbenzoate at 0·13 kN/m².

should be exactly known. This cannot accurately be determined from the equilibrium measurements themselves, however; therefore distillation tests were carried out on a mixture with about 86·5 mol % *n*-hexadecane in a Vigreux column (about 10 theoretical plates).

Under total reflux the top composition was determined as a function of the pressure (Table 11).

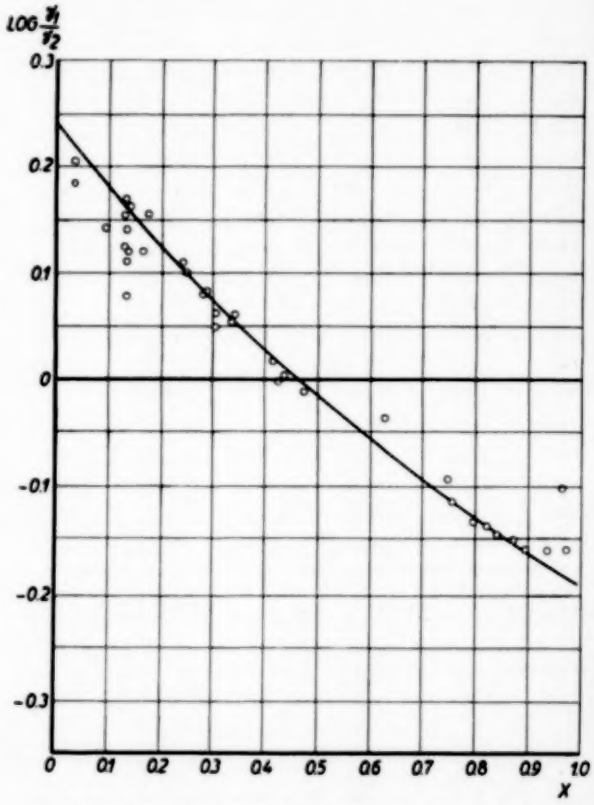

Fig. 7. Exchange function of *n*-hexadecane—*n*-heptylbenzoate at 0·49 kN/m².

Table 11. Determination of azeotropic composition in the system n-hexadecane–n-heptylbenzoate by means of distillation in a 10-plate Vigreux column

Pressure kN/m²		*Composition mol. % n.C₁₆*	
Top	*Bottom*	*Top*	*Bottom*
1·45	1·60	89·1	86·8
0·57	1·00	88·7	86·8
0·40	0·80	88·3	86·7
0·80	0·85	88·8	86·7
1·35	1·45	89·3	86·6
1·05	1·20	89·0	86·5
0·27	0·65	88·1	86·5

Extrapolation and interpolation of these data gives the following azeotropic compositions:

Pressure kN/m²	*Azeotropic comp. mol % n.C₁₆*
0·13	87·5
0·49	88·5
2·0	89·5

The "exchange function" was then laid through these azeotropic points so that the area condition is complied with. It appears that the experimental values, especially at low concentrations of *n*-hexadecane, exhibit relatively great deviations from the curve drawn; if, however, the nature of the measurements is taken into account, (low pressures,

VOL. 1 1952

irregular boiling), the general result is not unsatisfactory.

In order to calculate plate-numbers at total reflux, smoothed values of α were derived from the lines drawn in Fig. 6–8 and the vapour pressure ratio of the components. From these α-values, recorded in Table 12, curves were calculated from which the number of plates between top and bottom (differential plate number) can be directly derived from the refractive indices of top and bottom products found (Fig. 9). This figure shows that, owing to the existence of the azeotropic point, not more than 16–18 theoretical plates can be measured with the *n*-hexadecane—*n*-heptylbenzoate system.

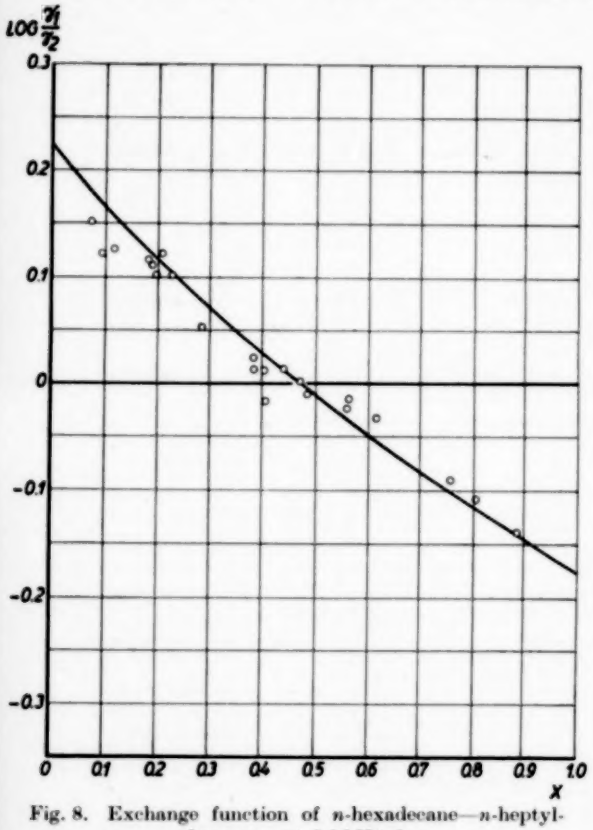

Fig. 8. Exchange function of *n*-hexadecane—*n*-heptylbenzoate at 2·0 kN/m².

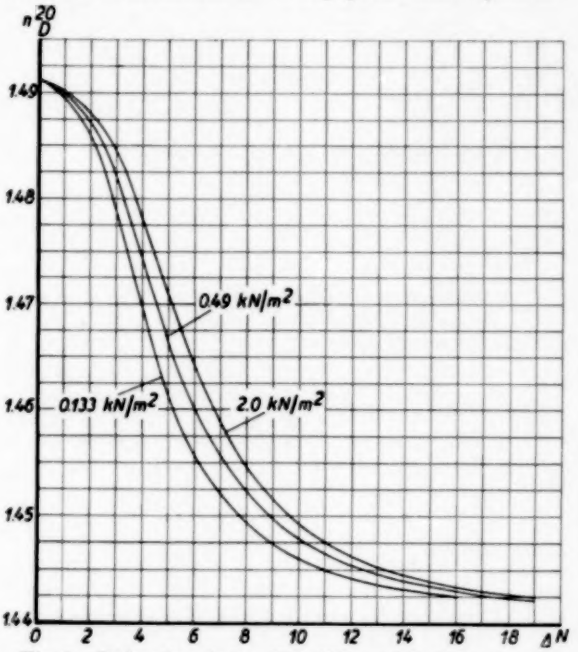

Fig. 9. Refractive index *VS* differential plates in the system *n*-hexadecane—*n*-heptylbenzoate at various pressures.

Table 12. Vapour-liquid equilibrium data of n-hexadecane—n-heptylbenzoate smoothed values at various pressures

x	0·13 kN/m²		0·49 kN/m²		2·0 kN/m²	
	α	y	α	y	α	y
0·0	2·73	0·000	2·48	0·000	2·31	0·000
0·1	2·37	0·209	2·17	0·195	2·05	0·186
0·2	2·08	0·342	1·92	0·324	1·82	0·313
0·3	1·85	0·443	1·71	0·423	1·64	0·413
0·4	1·64	0·523	1·53	0·505	1·49	0·498
0·5	1·47	0·595	1·39	0·582	1·37	0·579
0·6	1·31	0·662	1·27	0·656	1·26	0·655
0·7	1·19	0·735	1·16	0·730	1·16	0·730
0·8	1·07	0·810	1·07	0·810	1·07	0·810
0·9	0·975	0·898	0·99	0·899	0·995	0·899
1·0	0·89	1·000	0·92	1·000	0·93	1·000

NOTATION

B	= second virial coefficient	m³/k mol
N	= (see footnote on page 165)	
P	= total pressure	N/m²
P_1, P_2	= corrected vapour pressures [eq. (3)]	N/m²
p°	= vapour pressure	N/m²
R	= gas constant	Nm/k mol °K
T	= abs. temperature	° K
V	= molal volume	m³/k mol
x	= mol fraction volatile component in liquid	
y	= mol fraction volatile component in vapour	
α	= relative volatility	
γ	= activity coefficient	

Indices:

^{1} = volatile component
^{2} = heavy component

REFERENCES

[1] A.P.I. project 44 Natl. Bur. Standards, Washington.
[2] BENEDICT, M., JOHNSON, C. A., SOLOMON, E., RUBIN, L. C.; Trans. Amer. Inst. Chem. Engrs 1945 **41** 371–392.
[3] BERG, L., POPOVAC, D. O.; Chem. Eng. Progr. 1949 **45**

683–691. [4] BRAGG, L. B., RICHARDS, A. R.; Ind. Eng. Chem. 1942 **34** 1088–1091. [5] CARLSON, H. C., COLBURN, A. P.; Ind. Eng. Chem. 1942 **34** 581–589. [6] COULSON, E. A., HERINGTON, E. F. G.; Trans. Faraday Soc. 1948 **44** 636–644. [7] FELDMAN, F., MYLES, M., WENDER, I., ORCHIN, O.; Ind. Eng. Chem. 1949 **41** 1032–1036. [8] FENSKE, M. R.; Ind. Eng. Chem. 1932 **24** 482–485. [9] FENSKE, M. R., MYERS, H. S., QUIGGLE, D.; Ind. Eng. Chem. 1950 **42** 649–653. [10] GILMONT, R., WEINMANN, E. A., KRAMER, F., MILLER, E., HASHMALL, F., OTHMER, D. F.; Ind. Eng. Chem. 1950 **42** 120–126. [11] PERRY, E. S., FUGUITT, R. T.; Ind. Eng. Chem. 1947 **39** 782–786. [12] REDLICH, O., KISTER, A. T.; Ind. Eng. Chem. 1948 **40** 341–348. [13] REDLICH, O., KISTER, A. T.; J. Amer. Chem. Soc. 1949 **71** 505–507. [14] SEYER, W. F., WALKER, R. D.; J. Amer. Chem. Soc. 1938 **60** 2125–2128. [15] SEYER, W. F., YIP, C. W.; Ind. Eng. Chem. 1949 **41** 378–380. [16] STRUCK, R. T., KINNEY, C. R.; Ind. Eng. Chem. 1950 **42** 77–82. [17] TODD, F.; Anal. Chem. 1948 **20** 1248. [18] WHITE, R. R.; Trans. Amer. Inst. Chem. Engrs 1945 **51** 539–554. [19] WILLIAMS, F. E.; Ind. Eng. Chem. 1947 **39** 779–782. [20] WOHL, K.; Trans. Amer. Inst. Chem. Engrs 1946 **52** 215–249.

Vacuum distillation II

Performance of a Vigreux column and a spinning band column over a wide range of pressures

F. J. ZUIDERWEG

Koninklijke/Shell-Laboratorium, Amsterdam

(Received 6 September 1951)

Summary—Performance figures referring to a 11 mm diameter Vigreux column and a 6 mm diameter spinning band column over a pressure range of about 0·13 kN/m²–101·5 kN/m² (about 1–760 mm Hg) are presented.

In order to gain an insight into the mechanisms of material transfer involved, analyses of separate vapour and liquid phase resistances were made.

In the case of the Vigreux column it was found that liquid phase resistance was about half the total resistance at atmospheric pressure. A reduction in pressure causes the liquid phase resistance to be increased by increasing liquid viscosity on the one hand and to be decreased by the higher vapour rates on the other hand. These two compensating factors cause a total efficiency loss of the Vigreux column of about 25% when the pressure is reduced from atmospheric value to about 0·13 kN/m² (1 mm Hg). At this top pressure the maximum pressure drop along the Vigreux section is about 0·3 kN/m² (3–4 mm Hg) per metre.

In a spinning band column the main resistance to material transfer is offered by the vapour phase. This resistance is reduced by creating turbulence through rotation of the spinning band. The present study disclosed the existance of two limiting values of rotational speed: a lower limit below which rotation does not yet cause turbulence, and a higher limit above which back mixing in the liquid phase causes the separating power to be independent of—or to decrease with—speed of rotation.

Due to the fact that the extent to which turbulence can be effected in the vapour phase proves to depend on rotational speed and vapour density to the same degree, the sensitiveness to pressure variations of the spinning band column is rather great. Reduction of the pressure from atmospheric value to about 1·3 kN/m² (10 mm Hg) causes an efficiency loss of about 70%; in fact at this pressure the separating power of the spinning band column was not better than that of a wetted wall column of the same dimensions.

Zusammenfassung—Es werden die Leistungszahlen einer Vigreux-Kolonne, Durchmesser 11 mm, und einer Drehbandkolonne, Durchmesser 6 mm, über einen Druckbereich von ungefähr 0,13 kN/m²—101,5 kN/m² (1—760 mm Hg) gegeben.

Um eine Einsicht in den Mechanismus des Stoffaustausches zu bekommen, wurden die Widerstände der Dampf- und der Flüssigkeitsphase separat analysiert.

In der Vigreux-Kolonne ergab sich der Widerstand der Flüssigkeitsphase zu ungefähr der Hälfte des totalen Widerstandes bei atmosphärischem Druck. Druckverminderung veranlaßt einerseits eine Zunahme des Widerstandes der Flüssigkeitsphase infolge erhöhter Flüssigkeitsviskosität und andererseits eine Abnahme infolge höherer Dampfgeschwindigkeiten. Diese zwei einander kompensierenden Faktoren verursachen einen totalen Leistungsverlust der Kolonne von ungefähr 25%, wenn der Druck vom atmosphärischen Wert bis zu ungefähr 0,13 kN/m² (1 mm Hg) erniedrigt wird. Bei diesem Druck am Kopf der Kolonne ist der maximale Druckverlust entlang der Kolonne ungefähr 0,3 kN/m² (3—4 mm Hg) pro Meter.

In einer Drehbandkolonne wird der Hauptwiderstand gegen den Stoffaustausch durch die Dampfphase geleistet. Dieser Widerstand wird mittels einer durch Drehung des Drehbandes verursachten Wirbelbewegung herabgesetzt. Die Untersuchung ergab die Existenz von zwei beschränkenden Umdrehungsgeschwindigkeitswerten: einen niedrigen Grenzwert unter welchem die Drehung noch keine Wirbelbewegung verursacht und einen höheren Grenzwert über welchem Rückmischung in die Flüssigkeitsphase die Ursache ist, daß die Trennungsfähigkeit von der Umdrehungsgeschwindigkeit unabhängig ist oder damit abnimmt.

Da das Maß, in welchem eine Wirbelbewegung in der Dampfphase erreicht werden kann, im gleichen Maße von der Umdrehungsgeschwindigkeit und Dampfdichte abhängig ist, ist die Druckänderungsempfindlichkeit der Drehbandkolonne ziemlich groß. Herabsetzung des Druckes von atmosphärischem Wert bis zu ungefähr 1,3 kN/m² (10 mm Hg) verursacht einen Nutzeffektverlust von ungefähr 70%; tatsächlich ist die Trennungsfähigkeit der Drehbandkolonne bei diesem Druck nicht besser als die eines leeren zylindrischen Rohrs von gleichen Abmessungen.

VOL. 1 1952

INTRODUCTION

Though fractionation at subatmospheric pressures may be employed as a means of obtaining a sharper separation (*e.g.* by increasing the relative volatility of the components), vacuum distillation is generally used in order to lower the boiling points of the components when heat-sensitive materials are to be distilled. The maximum effect to be obtained from the decrease in pressure applied depends, however, upon the pressure drop occurring between top and bottom of the fractionating column used. This largely governs the selection of types of fractionating column in vacuum distillation.

When the pressure in the reboiler should be below 13·3 kN/m²* (100 mm Hg), bubble plate columns cannot well be used unless the number of plates is very low; some type of packed column must then be resorted to. When the pressure in the reboiler must be still lower (*e.g.* below 1·33 kN/m² [10 mm Hg]), the pressure drop of this type of column is too large too [28], so that in this pressure region use should be made of open tube columns.

If the thermal hazard of the material distilled is still too high when using these columns, molecular or semi-molecular distillation may be applied; the procedure to obtain a sharp separation with this type of apparatus is, however, not simple.

Thus far, published information on the performance of low-pressure fractionating columns has been scarce. Moreover, practically no efforts have been made to give an interpretation of the pressure effects found. Perhaps the best study in this respect was made by SCHAFFNER, BOWMAN and COULL [26] on their empty tube column with alternating hot and cold sections.

Discussion of published results is further hampered by the fact that sometimes separating power data have been calculated with thermo-dynamically inconsistent equilibrium data [2], [28].

In general it may be concluded, however, that packed columns lose distinctly in separating efficiency when the pressure is reduced. FELDMAN [16] *et al.* showed a Podbielniak Heligrid column to have a 50% lower separating power at 6·7 kN/m² (50 mm Hg) than at atmospheric pressure.

On the other hand, open tube columns seem to retain their separating power fairly well. Measurements by WILLIAMS [34] at atmospheric pressure and at 0·13 kN/m² (1 mm Hg) show only a small efficiency loss. BREIWISCH [4] determined the separating effect of a number of wetted wall columns of different diameters under laminar flow in the vapour phase. At pressures of 1·3 kN/m²—4·0 kN/m² the results correlated well with the theoretical separating power, as is the case at atmospheric pressure [23], [32].

Sometimes columns with rotating elements are recommended for use in vacuum fractionation. BIRCH, NATHAN and GRIPP [3] describe a rotating band column of large diameter and give test data at atmospheric pressure. Low-pressure separating power data were not determined; distillation curves obtained at low pressures, however, suggest a reasonable separating power.

In this study the performance of two types of open tube column frequently used in vacuum distillation was investigated. Performance figures for a Vigreux column and a rotating band column over a wide range of pressure are given. They were determined with the low-pressure test mixtures *n*.decane-*trans*decalin and *n*.hexadecane-*n*.heptylbenzoate described in the companion paper [36].

An interpretation of the pressure effects found has been given. In order to facilitate the discussion of the experimental results, a comprehensive survey of the principles that govern material transfer in the columns tested will be given in the following paragraph.

THEORETICAL

In the evaluation of laboratory distillation apparatus the separating power is generally expressed in the theoretical plate number. The influence of operating variables on the overall performance of the apparatus is thus easily recognized and, moreover, the plate number found may be used in simple approximate calculations to investigate the utility of the apparatus in actual distillations. In the present work the same criterion will therefore be applied too.

In the open tube type of column, however, concentrations vary gradually through the length of the apparatus and not stepwise as is the case in an ideal plate column. When, therefore, the data obtained require a more fundamental interpretation, recourse should be had to the principles underlying the material transfer in the gradual countercurrent vapour-liquid exchange process.

* In the present study the dimensions of the various magnitudes are expressed in the metre—kilogram—second units system.

In this system the unit of force is called Newton (N); it has the dimensions kg m/sec². One Newton is equivalent to 10^5 dynes.

In a recent study, BYRON, BOWMAN and COULL [7] gave a qualitative evaluation of pressure effects on the efficiency in the normal rectification process ("contact rectification"). According to their point of view, in the pressure region below 1·3 kN/m² (10 mm Hg)† two detrimental influences of pressure are becoming noticeable:

a) relative increase in vertical back-diffusion over transverse diffusion owing to increase in diffusion coefficient,

b) non-equilibrium between liquid and vapour at the vapour-liquid interface owing to the relatively low vaporization rate.

Both these factors would invalidate the theoretical approach to the vapour-liquid exchange process along lines customary in the case of processes at normal pressures.

However, in their deductions with respect to point a) BYRON *et al.* disregarded the convection factor in the exchange process, which counteracts the vertical back-diffusion. In the analysis of rectification efficiency of wetted wall columns by WESTHAVER [32] and by KUHN [23] it is shown that the back-diffusion effect is controlled by the ratio of diffusivity to linear vapour velocity. Since pressure reductions affect both factors to about the same extent it is seen that at low pressure back-diffusion cannot be more detrimental than at high pressures.

In discussing point b) indicated by BYRON *et al.* it should be noted that the approach to equilibrium at the vapour-liquid interface depends on the ratio of the total vaporization-condensation rate to the rate of material transfer. In cases where the second rate is large compared with the first, equilibrium cannot be obtained.

Calculation according to the well-known LANGMUIR formula shows that at a partial pressure of 0·067 kN/m² (0·5 mm Hg) the vaporization rate at 100° C of a substance with molecular weight about 200 equals about 0·2 kg/m² sec.

The transfer rate in a column as tested in the present investigation, though depending on relative volatility, may be estimated at about 0·0025 kg/m² sec. The transfer rate therefore equals about 1% of the vaporization-condensation rate and equilibrium between vapour and liquid may be assumed, even at the low pressure quoted.

† In this region the mean free path of the molecules is still small with respect to the dimensions of the apparatus.

Therefore there seem to be no objections to a theoretical approach based on principles which also form the starting point of considerations on the normal pressure exchange processes.

Generally, there will be diffusional resistance to the transfer process both in vapour and in liquid phase. Using the "height of a transfer unit" concept introduced by CHILTON and COLBURN [9], [11], the following relations may be given for the material transfer in the vapour phase and the liquid phase respectively, neglecting mutual influences of vapour and liquid flow:

$$\frac{(\text{H.T.U.})_V}{d} = a_V \, Re_V^{p_V} \, . \, Sc_V^{q_V}, \tag{1}$$

$$\frac{(\text{H.T.U.})_L}{w} = a_L \, Re_L^{p_L} \, . \, Sc_L^{q_L} \tag{2}$$

in which for the case of distillation

$$(\text{H.T.U.})_V = z \Big/ \int_{y_1}^{y_2} \frac{dy}{y_i - y}, \tag{3}$$

$$(\text{H.T.U.})_L = z \Big/ \int_{x_1}^{x_2} \frac{dx}{x - x_i}. \tag{4}$$

Generally, the liquid and vapour transfer factors $(\text{H.T.U.})_L$ and $(\text{H.T.U.})_V$ cannot directly be measured, the interfacial concentrations x_i and y_i being unknown. The overall effect found may be interpreted in terms of an overall vapour transfer factor, $(\text{H.T.U.})_{OV}$, defined as

$$(\text{H.T.U.})_{OV} = z \Big/ \int_{y_1}^{y_2} \frac{dy}{y^* - y} \tag{5}$$

and which is related with the separate phase (H.T.U.) values by

$$(\text{H.T.U.})_{OV} = (\text{H.T.U.})_V + \overline{m} \, \frac{V}{L} \, (\text{H.T.U.})_L. \tag{6}$$

The average value of the slope of the equilibrium line, $\overline{m}$ may be found from

$$\overline{m} = \frac{L}{V} \, \frac{(\text{H.T.U.})_{OV}}{(\text{H.T.U.})_{OL}} \tag{7}$$

in which $(\text{H.T.U.})_{OL}$ in analogy with (4) is given by

$$(\text{H.T.U.})_{OL} = z \Big/ \int_{x_1}^{x_2} \frac{dx}{x - x^*}. \tag{8}$$

The coefficients a, p and q in eq. (1) and (2) being known, it will in principle be possible to predict the variations in separating power when varying the total

VOL. 1 1952

pressure on the distillation apparatus. This may be done by inserting the appropriate values of the physical constants at each pressure.

Considering the case of constant vapour and liquid mass flow, the influence of pressure upon $(\text{H.T.U.})_V$ will not be very great. The SCHMIDT numbers of gases are nearly constant over a wide range of pressures and temperatures*, and therefore variations in $(\text{H.T.U.})_V$ originate only from variations in the vapour REYNOLDS number. In distillation, pressure variations always being accompanied with temperature variations, the effect on $(\text{H.T.U.})_V$ found will only be due to the temperature influence on the vapour viscosity. This influence is only small (μ_V being approximately proportional to $\sqrt{T}$). In accordance with these considerations, GILLILAND and SHERWOOD [18] found in vaporization experiments in a wetted wall column that under wide variation of the pressure (abt 13 kN/m²—260 kN/m²) $(\text{H.T.U.})_V$ remained essentially constant at constant vapour mass flow.

On the other hand, the temperature variations cause large variations in the liquid viscosity and diffusivity. Using the relation

$$\frac{D_L \mu_L}{T} = \text{constant},$$

it is found that the liquid SCHMIDT number is proportional to $\mu_L^2/T\varrho_L$, while the liquid REYNOLDS number varies proportionally with μ_L^{-1}. Though depending upon the numerical values of the power coefficients p_L and q_L in eq. (2), in general the result will be that a reduction in pressure causes an increase in the $(\text{H.T.U.})_L$ value.

Therefore, if the liquid phase resistance cannot be neglected, it is seen from eq. (6) that the overall separating power of a distillation column will decrease with decreasing total pressure ($\overline{m}$ and L/V remaining constant).

In order to arrive at a more quantitative interpretation of the effects described above the coefficients a, p and q in eq. (1) and (2) should be evaluated. Though this has to be done at least partly by experiment, some general remarks can be made.

When the vapour flow is laminar, the distilling column being a cylindrical tube, eq. (1) becomes [32].

$$\frac{(\text{H.T.U.})_V}{d} = 0{\cdot}0573\, Re_V\, Sc_V. \qquad (9)$$

Under turbulent flow conditions in the vapour, as will generally be the case in a Vigreux column, the exponential values p_V and q_V will differ largely from unity. Recent investigations into the influence of REYNOLDS number and SCHMIDT number over wide ranges upon material transfer in open tubes and packed beds suggest that p_V will be equal to about 0·2 [22], [27] and that q_V may be put at 0·6–0·8 [21], [22], [29].

For the liquid phase when flowing in laminar motion along the wall of the distilling column, the following relation holds [35]:

$$\frac{(\text{H.T.U.})_L}{w} = 0{\cdot}0589\, Re_L\, Sc_L. \qquad (10)$$

Practical application of eq. (10) is complicated by the fact that the liquid layer thickness, w, depends on the liquid flow rate. In an open tube column some indication about the magnitude of this variable may be found from hold up measurements.

Generally, in distillation, full turbulent flow does not develop in the liquid phase; very little is known about the values to be assigned to the coefficients p_L and q_L in this case. Recalculation of some values of BRINSMADE and BLISS [6], who measured transfer coefficients in the extraction of acetic acid from methyl isobutyl ketone with water in a wetted wall column, shows a value of about 0·65 for q_L; the value of p_L equalled zero, indicating that the liquid flow rate had no influence.

From the above considerations it may be concluded that unless the liquid and vapour phases are flowing in viscous motion, most of the coefficients in eq. (1) and (2) have to be assessed by experiment. An exception may be made for the power coefficient q_V on the vapour SCHMIDT number. The actual variation in this SCHMIDT number being small, the value to be used for q_V does not matter very much. In this work q_V will be put at 0·67 without further verification.

The evaluation of the remaining constants should be done by calculating $(\text{H.T.U.})_V$ and $(\text{H.T.U})_L$ values from the overall $(\text{H.T.U.})_{OV}$ values. This can be done with the aid of eq. (6) and (7) when data from experiments in which $\overline{m}$ or L/V have been varied are available.

Some final remarks should be made about the influence of mechanical agitation, as is applied in a rotating band column. By this agitation material transfer is increased by creating extra turbulence in the vapour

* These considerations are only valid when the pressure in the distillation apparatus is high enough for the mean free path of the molecules to be small with respect to the dimensions of the apparatus. In the normal countercurrent apparatus this will always be the case.

phase particularly. As a first approximation the influence of vapour velocity and extra turbulence induced by the rotation on $(H.T.U.)_V$ may be visualized as separate independent effects*. Generally, this will show up in a decrease of the coefficient a_V in eq. (1) as a function of the intensity of agitation.

From the studies of Taylor [30] on the stability of a stagnant fluid between two rotating cylinders it is shown that turbulence only sets in when the rotational speed exceeds a certain critical value. The existence of a critical rotational speed in the case of a fluid flowing in axial direction between the cylinders was shown by Cornish [12] by pressure drop measurements on the water flow through narrow annuli with rotation of the inner cylinder.

Fig. 1. Photograph of part of Vigreux column tested.

It should therefore be expected that in the case of rotation of a strip or a cylindrical tube there will also be a critical rotational speed below which rotation does not increase the material transfer effectively. In a first approximation, assuming the width of the strip to be equivalent to the diameter of a rotating cylinder, a relation for the critical Reynolds number of rotation may be derived from the equations given by Fage [14].

$$(Re_R)_{crit.} = \left(\frac{\omega r d \varrho_V}{\mu_V}\right)_{crit.} \sim c\left(\frac{d}{\Lambda}\right)^{1.5}. \qquad (11)$$

It will be clear that eq. (11) cannot be exact for a rotating band column; a distinct influence of the dimensions of the apparatus on the critical rotational speed is to be expected however.

* In this approximation it is assumed that the residence time of the vapour entering the bottom of the rotary column is long enough to ensure the vapour obtaining the flow pattern induced by the rotating element. This will only be the case when a relatively long ("infinite") column is being used.

The above discussions suggest that the reduction in coefficient a_V in eq. (1) under influence of rotation should be correlated against the Reynolds number of rotation, Re_R. As shown by studies on heat and mass transfer in agitated vessels [10], [19], [20], the power coefficients of the Schmidt number may be put at 0·5–0·7 when turbulence has been fully developed; as before, a value of $q_V = 0{\cdot}67$ will be assumed in the present study.

Actually, the effect of agitation will only be great in cases where vapour flow is so small that laminar motion prevails when the stirring device is not actuated. In this case $(H.T.U.)_V$ will increase linearly with Re_V.

The ultimate correlation equation by which the vapour phase transfer factor should be represented will therefore have the following general appearance:

$$\frac{(H.T.U.)_V}{d} = a_R\left(\frac{d}{\Lambda}\right)^n . Re_R^m . Re_V . Sc_V^{0.67}.$$

Apparatus and Experimental Procedure

Vigreux column

The measurements with the Vigreux column may be divided into two parts, *e.g.* measurements of separating power, pressure drop and maximum boil-up rates at pressures from about 0·13 kN/m²–101·5 kN/m² (1 to 760 mm Hg) on the one hand and determination of the separate $(H.T.U.)_V$ and $(H.T.U.)_L$ values at atmospheric pressure on the other hand.

The low pressure performance data were obtained in a Vigreux column with a rectifying section of 1 m in length and 11 mm in diameter. The vertical distance between two rows of horizontal indentions was 24 mm. A photograph of a part of the rectification section used is given in Fig. 1. The column was surrounded by a heating jacket to secure adiabatic operation. Boil-up rate was measured at the bottom end of the column by means of a calibrated measuring tube in the reflux return line. To prevent irregular boiling and bumping, the contents of the boiling flask were heated by means of a bare nichromium wire coil. To measure the pressure drop an oil differential manometer was fitted between the boiling flask and the top of the condenser of the column. Some separate pressure drop measurements were made by recording the temperature drop between top and bottom of the column when distilling a pure liquid (*e.g. n*-hexadecane) at total reflux.

The separating power of the column described was determined at atmospheric pressure (*n*-heptane/methyl-

VOL. 1 1952

cyclohexane, *n*-decane/*trans*decalin, Tables 1 and 2), at 13·3 kN/m² (100 mm Hg) (*n*-decane/*trans*decalin,

Table 1. Separating power of 1 m Vigreux column
Binary system n-heptane-methylcyclohexane
Pressure 101·5 kN/m²

Boil-up rate	n_D^{20}	n_D^{20}	*Theoretical plates*
ml/h	*top*	*bottom*	*n*
740	1·4030	1·4098	10
410	1·4009	1·4089	12
950	1·4020	1·4088	10
220	1·4007	1·4088	12·5
520	1·4018	1·4087	10·5
400	1·4015	1·4087	11
240	1·4021	1·4095	11·5
650	1·4026	1·4094	10
610	1·4018	1·4090	11
870	1·4028	1·4088	9
220	1·4011	1·4091	12
1050 (max)	—	—	—

Table 2. Separating power of 1 m Vigreux column
Binary system n-decane-transdecalin

Pressure	*Boil-up rate*	*Mol. % n-decane*		*Theoretical plates*
kN/m²	*ml/h*	*top*	*bottom*	*n*
101·5	930	70·3	6·7	10·3
	1050 (max)	65·1	6·7	9·5
	340	79·5	5·6	12·5
	280	73·4	5·1	11·8
	700	67·9	4·3	11·5
13·3	380	55·0	6·8	10·1
	250	56·0	6·1	10·8
	140	56·3	6·1	10·7
	240	55·0	5·8	10·7
	450	50·7	5·5	9·6
	370	51·8	5·4	10·5
	500 (max)	—	—	—
1·33	190	29·5	5·8	10·0
	90	28·0	5·5	9·9
	250	27·6	5·5	9·8
	160	27·0	5·5	9·6
	280	36·2	9·2	8·8
	230	36·0	9·2	8·8
	190	37·0	9·2	9·0
	350 (max)	—	—	—

Table 2), at 1·33 kN/m² (10 mm Hg) (*n*-decane/transdecalin, *n*-hexadecane/*n*-heptylbenzoate, Tables 2 and 3), and at 0·16 kN/m² (1·2 mm Hg) (*n*-hexadecane/*n*-heptylbenzoate, Table 3).

Samples were taken at the top and bottom of the column, using special vacuum adapters. An equilibration time of 30 to 60 min was allowed for. Analysis of the products was made by determination of refractive indices with a normal ABBE refractometer, read off to the fourth decimal place. The *n*-heptane-methylcyclohexane data were converted directly into

Table 3. Separating power of 1 m Vigreux column
Binary system n-hexadecane-n-heptylbenzoate

Pressure	*Boil-up rate*	*Pressure drop*	*Mol. % n-C_{16}*		*Theoretical plates*
kN/m²	*ml/h*	*kN/m²*	*top*	*bottom*	*n*
1·33	170	0·09	74·4	1·9	9·9
	280	0·21	74·4	1·9	9·9
	430	0·26	76·0	4·6	9·6
	410	0·30	76·0	4·6	9·6
	380	0·30	75·7	4·6	9·4
	170	0·09	77·8	3·7	10·9
	450 (max)	—	—	—	—
0·16	270	0·43	79·5	12·0	9·1
	200	0·30	79·9	6·0	10·2
	230	0·39	79·0	5·2	9·7
	170	0·26	79·0	4·8	9·8
	120	0·17	79·3	4·8	10·0
	120	0·13	78·5	4·7	9·3
	280 (max)	—	—	—	—

plate numbers with the aid of the alignment chart given by BROOKS, NELSEN and ZAHN [5]; refractive index data from the other binary mixtures were converted into plate numbers using the calibration curves and relative volatility data given in the companion paper [36]. Maximum boil-up rate was recorded when initial flooding was observed visually at some point along the length of the column.

As described in the theoretical part, a more thorough interpretation of the results to be obtained at various pressures may only be given in terms of the separate phase resistances. This may be done by analyzing the overall performance data, expressed as $(\text{H.T.U.})_{OV}$, by means of eq. (6), using data obtained at various $\overline{m}$ and L/V values. In order to reach some accuracy in these evaluations, the variations in $\overline{m}$ or L/V should be as large as possible. This implies that, in the case of distillation, a binary mixture should be used whose components have widely different boiling points. Further, variation in $\overline{m}$ can only be obtained

when the average composition of the contents of the column is varied; this can be done if the separating power of the apparatus is limited.

Some further points should be considered when evaluating the separate phase resistances by this method. The results are reliable only when, under the conditions applied, no channelling of the liquid phase or incomplete wetting of the column area take place. These effects may give rise to discrepancies, which cannot be correlated by eq. (6), as may for instance be shown for data of DUNCAN, KOFFOLT and WITHROW [13] obtained on a RASCHIG ring packed column. Moreover, when varying the L/V ratio, the possibilities of changes in the vapour-liquid interaction should not be overlooked.

In the present work it was found that only very few wide boiling binary systems do not exhibit the channelling effect when distilled in an open tube type of column. For this reason, use was made of the binary mixture of 2,2,4-trimethylpentane-*n*-octane.

The experiments in which $\overline{m}$ was varied (at total reflux) were made in a short (0·22 m) Vigreux column, cut from the 1-*m* column described before. This column was again provided with reboiler, condenser and reflux-measuring device; adiabatic conditions were maintained with a heating jacket, in which the heat applied was controlled by a Tagliabue Celectray, which kept the temperature difference between column surface and heating jacket at zero value.

Variations in L/V ratio were obtained by making experiments at partial reflux. In order to determine the exact liquid-vapour ratio, use was made of an experimental procedure in which two points of the operating lime were determined, *viz.* the distillate composition and the liquid composition in the intersection point of equilibrium line and operating line ("pinch composition"). This was achieved with the experimental lay out, sketched in Fig. 2.

The small length (0·22 m) of Vigreux column was placed upon a 0·50 m section, diameter 16 mm of a packed column, filled with small nichromium wire rings (about 2 mm in diameter). The separating power of this piece of packed column was equivalent to about 20 theoretical plates, so that under conditions of partial reflux, using the 2,2,4-trimethylpentane-*n*-octane system, the concentrations in the lower part might be expected to be constant and to be equal to the "pinch composition". This was checked by taking samples at points at about 0·10 and 0·20 m from the bottom end of the packed section.

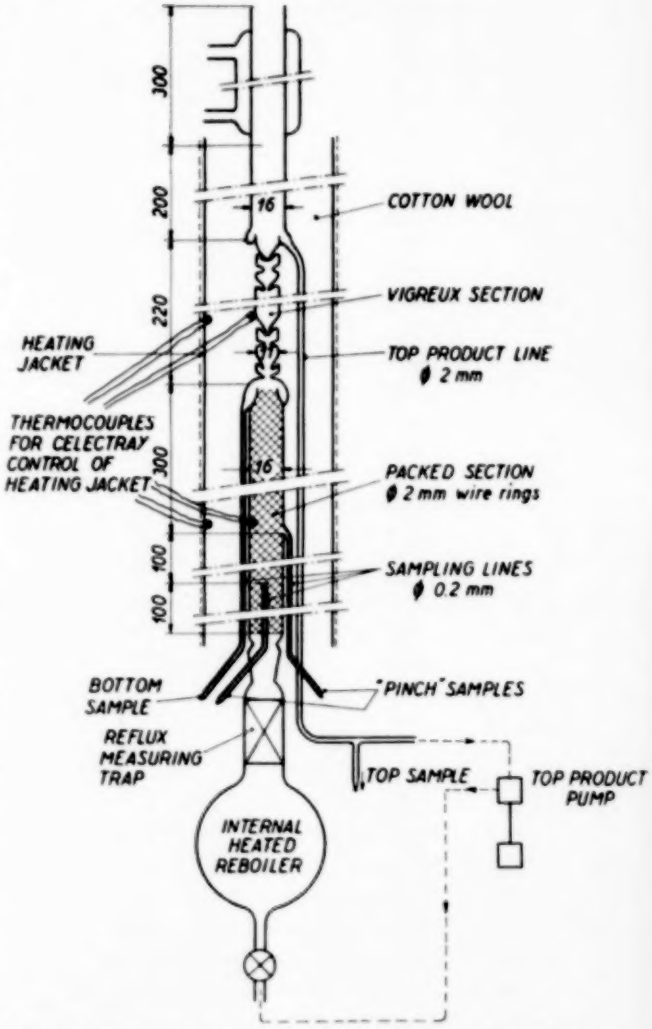

Fig. 2. Diagram of apparatus for experiments at finite reflux ratio with Vigreux column.

The top end of the Vigreux section was fused to a short wetted-wall column (0·20 m) in order to ensure that the reflux entering the Vigreux section was at boiling point. The top product was withdrawn at the top of the Vigreux section by means of a small reciprocating pump with variable stroke. The distillate heated to boiling point, was delivered continuously to the reboiler, thus ensuring a closed system in which the concentrations were becoming stationary.

VOL. 1 1952

Adiabatic operation of the apparatus was again effected by means of automatic control of the heating jacket with the Tagliabue Celectray; two control points and a heating jacket with two separate windings were now used, one at the Vigreux section and one at the packed "pinch" section.

Apart from the samples withdrawn from the pinch section mentioned above, liquid samples were taken at the bottom end of the Vigreux section and of the distillate withdrawn with the pump. All samples were withdrawn continuously by means of small capillaries at rates of 1–2 ml per hour. In each experiment the rate of distillate was determined separately, from which by means of the proper L/V ratio (from top and "pinch" compositions) boil-up rate and reflux rate were calculated. Generally there was good correlation between the calculated reflux rate and the reflux rate measured at the bottom end of the packed section with a reflux measuring trap.

Analysis of the liquid samples was made by determination of the refractive index with a *Bausch and Lomb* precision refractometer, enabling readings in three units in the fifth decimal place. By this means concentrations could be determined with an accuracy of about 0·5 mol % absolute. To ensure utmost precision, the scale of the refractometer was calibrated with pure *n*-octane or 2,2,4-trimethylpentane during each determination.

From the concentration data obtained, the separating power of the Vigreux column was calculated, assuming the 2,2,4-trimethylpentane-*n*-octane system to be ideal; corrections were made for deviations from ideal gas laws [1]. The calculated relative volatility data, based upon vapour pressure data from A.P.I. project 44, National Bureau of Standards, Washington, are given in Table 4. Calculation of the total reflux data was made by using a differential liquid and vapour transfer units *vs* composition curve. The partial reflux experiments were calculated by plotting the top, bottom and pinch concentrations on a large-scale McCABE-THIELE diagram, drawing the operating line through the top and pinch compositions and reading $(y^* - y)$ and $(x - x^*)$ values as functions of y and x, respectively. $(\text{H.T.U.})_{OV}$ and $(\text{H.T.U.})_{OL}$ were found by graphical integration of the results obtained. The average slope of the equilibrium line was calculated from eq. (7), using L/V values read off from the McCABE-THIELE diagrams.

Table 4. Calculated relative volatility 2,2,4-trimethylpentane-n-octane

x	α	x	α
0·10	1·91	0·70	2·03
0·30	1·95	0·90	2·09
0·50	1·99		

Rotating band columns

The rotating band columns were purchased from H. S. MARTIN, Evanston, Ill., U.S.A. The rectifying section of the first column, (a "*Pyros-Glover* microstill"), in which the majority of the experiments were run, consisted of a straight glass tube, 0·60 m in length, 6 mm internal diameter. In this tube a flattened coil of nichrome wire (abt. 0·2 mm thick) through which a nichrome strip is inserted could rotate. The width of the strip was about 4·5 mm, the total width including the nichrome wire about 5 mm. The strip was rotated by means of a variable speed motor, driven via a tungsten shaft, running through the condenser section. The second "*Pyros-Glover* microstill" tested had a rectifying section of 3 mm diameter at a length of 0·40 m. The total width of the rotating band in this column was about 2 mm. The microstills were fitted with a device for partial condensation (the primary condenser cooled with air, the secondary or product condenser with water). The columns were further completely surrounded by a vacuum jacket and heating jacket. In order to avoid bumping in the low pressure determinations, heating of the reboiler contents was again done by means of a bare heating spiral. To minimize effects of draft upon the boil-up rate, reboiler and lower end of the columns were placed in a Dewar flask.

In the low-pressure experiments the inlet of the shaft of the rotating strip should be sealed; this was reached by piercing the shaft through a cylindrical piece of rubber, which was fitted to the top of the condenser by means of a thick vacuum tube, glycerol being used as a lubricant.

In determining the separating power of the microstills, samples of the top product were drawn by reducing the cooling of the primary condenser somewhat after an equilibration time of 1–2 hrs. No samples of the bottom contents were taken during the distillation; the bottom composition was analyzed before and at the end of a distillation and the average value taken. The hold up of the column being small, this method was believed not to introduce serious errors.

The boil-up rate was measured by counting drops from a calibrated dripping tip at the bottom end of the rectification section.

Experiments were run at atmospheric pressure in the 6 mm and 3 mm stills with *n*-heptane-methylcyclohexane, varying boil-up rate and speed of rotation (Table 10). Reduced pressure experiments were made in the 6 mm still with *n*-decane-transdecalin at 10·7 kN/m² and at 2·0 kN/m² (80 and 15 mm Hg) and with *n*-hexadecane-*n*-heptylbenzoate at 0·67 kN/m² (5 mm Hg); the rotational speed was kept constant at 50 rev. p. second (Table 11).

Discussion of Experimental Results

Vigreux column

The results obtained with the 1-*m* Vigreux column at various pressures (Tables 1, 2, 3) are plotted as theoretical plate number *vs* boil-up rate in Fig. 3. It is clear that the separating power of the column is not very much influenced by pressure. Comparing the plate number at maximum boil-up rate, efficiency is nearly constant at 9–10 plates. At constant boil-up rate, however, a distinct pressure influence is shown; decreasing the pressure from atmospheric to 1·3 kN/m² (10 mm Hg) shows a decrease in separating efficiency of about 25%. This effect, as already described in the theoretical part, may perhaps be due to an increase in liquid phase resistance at lower pressures. In order to arrive at a more quantitative interpretation, separate phase resistance determinations were made at atmospheric pressure with the 0·22-*m* Vigreux column already described.

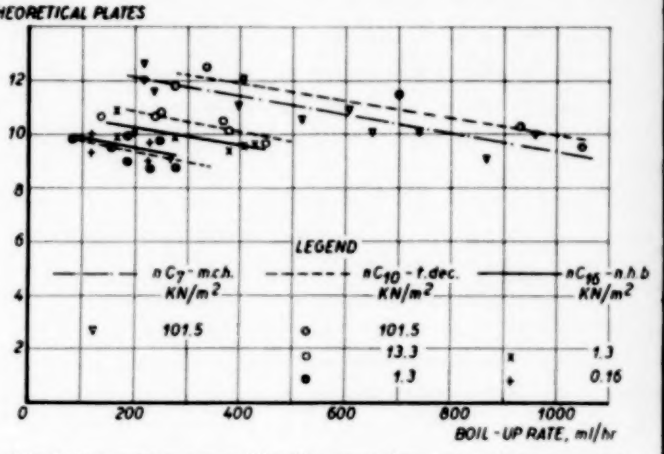

Fig. 3. Separating power of 1 m Vigreux column at various pressures.

Table 5. Separating power of 0·22 m Vigreux column (total reflux)
Binary system 2,2,4-trimethylpentane-n-octane
Pressure 101·5 kN/m²

Boil-up rate ml/h	Composition, mol. fr. top	Composition, mol. fr. bottom	Separating power $(H.T.U.)_{OV}$	$\bar{m}$
1000	47·0	22·0	0·141	1·26
420	52·0	19·5	0·106	1·24
630	50·5	20·0	0·115	1·26
1000	46·0	19·0	0·127	1·29
840	45·5	18·0	0·122	1·30
420	52·0	17·5	0·097	1·25
690	47·0	17·0	0·111	1·29
1100	41·0	17·0	0·135	1·34
1100	66·5	35·5	0·112	0·97
750	68·5	32·0	0·095	0·98
420	71·5	33·0	0·087	0·95
1100	64·0	33·0	0·113	1·00
420	68·5	29·0	0·088	1·00
1000	80·5	51·5	0·097	0·77
1100	79·5	52·0	0·103	0·77
420	82·5	48·0	0·080	0·78
1050	77·5	47·5	0·100	0·82
420	84·5	51·5	0·080	0·74
420	84·5	51·0	0·082	0·76
720	79·5	47·5	0·091	0·81

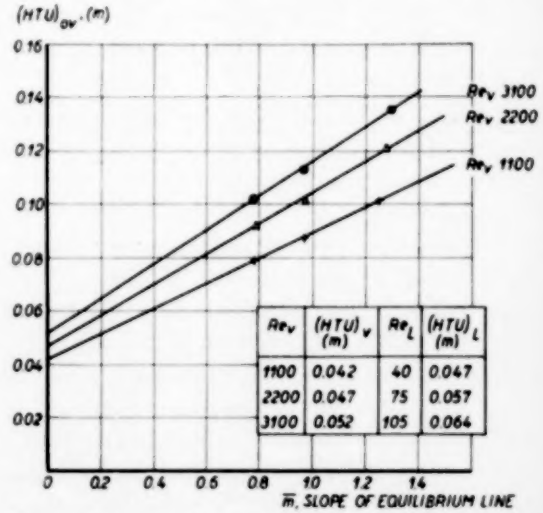

Fig. 4. Determination separate phase resistances of Vigreux column.

Results at total reflux, in which the average concentration in the column and thus $\bar{m}$ was varied, are listed in Table 5. From these data a plot of $(H.T.U.)_{OV}$ *vs* boil-up rate was made; at three distinct values of

VOL. 1 1952

the boil-up rate (*e.g.* at 400, 800 and 1100 ml/hr) $(H.T.U.)_{OV}$ data were read off and plotted in Fig. 4 as a function of the average slope of equilibrium line, $\bar{m}$. In this plot, the intersection points on the ordinate indicate—according to eq. (6)—the $(H.T.U.)_V$ values, the slope of the lines representing the $(H.T.U.)_L$ values. From the data obtained (recorded in Fig. 4 too) it is seen that the vapour and liquid phase resistances are of the same order of magnitude, liquid phase resistance being the largest of the two.

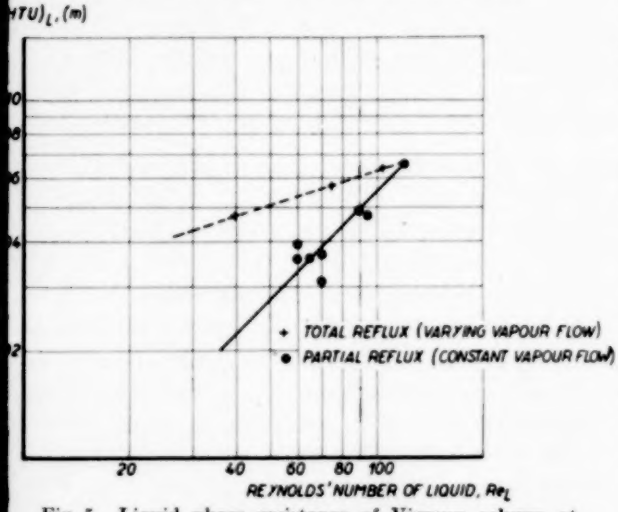

Fig. 5. Liquid phase resistance of Vigreux column at total reflux and partial reflux.

The $(H.T.U.)_V$ data were used to evaluate the coefficients a_V and p_V still unknown in eq. (1).

The following equation was obtained *, the diameter of the column being included in the constant a_V:

$$(H.T.U.)_V = 0{\cdot}0146\, Re_V^{0{\cdot}20}\, Sc_V^{0{\cdot}67}. \qquad (12)$$

Calculated and experimental $(H.T.U.)_V$ data are compared as follows:

Re_V	$(H.T.U.)_V$, (m) eq. (12)	$(H.T.U.)_V$, (m) exp.
1100	0·0421	0·042
2200	0·0482	0·047
3100	0·0519	0·052

* The physical constants at distillation conditions necessary for calculation of the *Re* and *Sc* numbers for the 2,2,4-trimethylpentane-*n*-octane system and the other systems are given in Table 8. Liquid densities and vapour viscosities were taken from current handbooks like International Critical Tables etc.; vapour densities were calculated from ideal gas law, liquid viscosities were estimated from the work of NEDERBRAGT and BOELHOUWER [24]. Finally, liquid diffusivities and vapour diffusivities were calculated by the correlations given by WILKE [33] and GILLILAND [17], respectively.

It may be concluded that full turbulence has developed at REYNOLDS numbers as low as 1100; this is caused by the disturbances induced in the vapour by the indentions in the column surface.

The liquid phase transfer factors $(H.T.U.)_L$ are plotted in Fig. 5 as a function of REYNOLDS number of the liquid. It is seen that $(H.T.U.)_L$ increases with Re_L, raised to a power of about 0·3. This indicates turbulent flow in the liquid phase. However, the REYNOLDS numbers are very low, nearly all below 100, and laminar flow should be expected. In that case, $(H.T.U.)_L$ should increase about linearly with Re_L, as indicated by eq. (10). It was therefore expected that in the measurements under total reflux turbulence was induced in the liquid phase by the vapour flow. Indications of this effect were already found when making the low pressure runs in the 1-*m* column. At boil-up rates much lower than the maximum boil-up rate the liquid phase was visibly agitated by the vapour flow. At higher vapour velocities the turbulence induced in the liquid phase will increase. This effects a simultaneous decrease in the liquid phase resistance, *i.e.* $(H.T.U.)_L$ does not increase so sharply as would be expected on the basis of pure laminar behaviour only.

In order to evaluate this effect further, experiments at partial reflux at nearly constant vapour rate were made. In these experiments, the turbulence effect of the vapour flow on the liquid phase may be assumed to be nearly constant. The data obtained by the method described in the experimental part are assembled in Table 6. In order to evaluate the separate $(H.T.U.)_L$ values from the $(H.T.U.)_{OV}$ values measured, use was made again of eq. (6), in which the vapour phase transfer factor $(H.T.U.)_V$ was calculated with eq. (12). The $(H.T.U.)_L$ values ultimately obtained are plotted against REYDOLDS number in Fig. 5 too.

Though the resulting data are of only moderate accuracy, it is clear that at a constant vapour velocity, $(H.T.U.)_L$ increases about linearly with Re_L, *i.e.* the separating efficiency is proportional to contact time as is the case in pure laminar flow [eq. (10)]. From Fig. 5 and Table 6 it can be deduced that at constant liquid rate doubling of the vapour rate effects a considerable decrease of the liquid phase resistance [compare the $(H.T.U.)_L$ values under total and partial reflux at Re_L about 60].

The results thus far obtained on the short Vigreux column have given the following information: 1) a

Table 6. Separating power of 0·22 m. Vigreux column at partial reflux
Binary system 2,2,4-trimethylpentane-n-octane; pressure 101·5 kN/m²

Boil-up rate	*Liquid rate*	Re_V	Re_L	*Compositions mol. fract.*			$\frac{L}{V}$	$\overline{m}$	$(H.T.U.)_{OV}$	$(H.T.U.)_V$	$(H.T.U.)_L$
ml/h	*ml/h*			*top*	*bottom*	*pinch*			*m*	*m*	*m*
1380	720	3900	70	0·450	0·220	0·195	0·52	1·26	0·144	0·054	0·037
1050	680	2900	65	0·623	0·314	0·230	0·65	1·06	0·110	0·051	0·036
1280	620	3600	60	0·725	0·455	0·400	0·48	0·86	0·118	0·053	0·036
1280	620	3600	60	0·730	0·470	0·405	0·48	0·84	0·123	0·053	0·040
1310	970	3700	95	0·425	0·185	0·110	0·74	1·32	0·139	0·053	0·048
1180	960	3300	90	0·475	0·205	0·095	0·81	1·26	0·129	0·052	0·049
1220	750	3400	70	0·556	0·265	0·215	0·62	1·15	0·110	0·052	0·031
1250	1250	3500	120	—	—	—	1·0	1·00	—	0·053	0·066

relation for calculation of vapour phase transfer factors $(H.T.U.)_V$ [eq. (12)]; 2) liquid phase resistance is of the same order of magnitude as vapour phase resistance at atmospheric pressure; 3) liquid phase transfer resistance is decreased by turbulence, induced in the liquid by the vapour flow.

This information should be used for interpretation of the data found at various pressures with the 1-*m* Vigreux column. However, the effect mentioned under 3) greatly complicates such a further interpretation. No adequate data at the various pressures being available at present, the following approximate reasoning as to the turbulence effects in the liquid phase due to vapour flow may be employed.

The action of the vapour flow will be a result of the impact and shearing forces exerted by the vapour on the liquid phase. The degree to which the liquid phase is being agitated by these forces depends not only upon their magnitudes but also on the liquid flow rate and physical properties of the liquid. These same factors however play a similar role in the flooding phenomenon in which the liquid layer is disrupted and thrown upwards by the forces exerted by the vapour flow. Therefore, as a first approximation, it seems plausible to take the turbulence effects in the liquid phase in the total reflux experiments the same at equal fractional flooding rates. Thus, column efficiencies at various pressures should be compared for instance at maximum boil-up rate or at half the maximum boil-up rate. Under these conditions of constant turbulence effects, $(H.T.U.)_L$ will be assumed to increase linearly with Re_L as found with the octane experiments at atmospheric pressure (Fig. 5).

The above considerations enable the calculation of $(H.T.U.)_L$ data from the overall separating power figures obtained at various pressures in the 1-*m* Vigreux column. In using eq. (6), $(H.T.U.)_V$ values were first calculated with relation (12) from the octanes experiments. According to eq. (2), the results should ultimately be correlated against the liquid SCHMIDT number, using $(H.T.U.)_L/Re_L$ as the proper variable.

Calculations of $(H.T.U.)_L/Re_L$ values at maximum boil-up rates and half maximum boil-up rates are summarized in Table 7. The results are finally plotted in Fig. 6 *vs* the liquid SCHMIDT number. Correlation of the data by this method is fairly good; as might be expected two separate functions are obtained, namely:

At maximum boil-up rate

$$(H.T.U.)_L = 12{\cdot}4 \times 10^{-6}\, Re_L\, Sc_L^{0{\cdot}9}. \qquad (13)$$

At half the maximum boil-up rate

$$(H.T.U.)_L = 11{\cdot}8 \times 10^{-6}\, Re_L\, Sc_L. \qquad (14)$$

Fig. 6 shows that at maximum boil-up rate $(H.T.U.)_L/Re_L$ values are about half the values obtained at half the maximum boil-up rates. This indicates the effect of higher turbulence in the liquid phase at the higher vapour rates, which is reflected in power coefficient of the SCHMIDT number in eq. (13), which differs from unity.

At half the maximum load however this power coefficient equals unity; the turbulence effects of vapour flow are obviously negligible now.

An explanation may be given by the consideration that at half maximum load the shearing forces exerted on the liquid are only about a fourth of the stresses at maximum boil-up rate (taking the friction factor approximately constant).

Assuming eq. (14) as a true expression for the laminar flow condition, the ratio of the constants in

VOL. 1 1952

Table 7. Calculation of $(H.T.U.)_L$ in 1 m Vigreux column at various pressures

System	Pressure	Boil-up rate ml/h		HETP*	$(H.T.U.)_{OV}$	Re_V	$(H.T.U.)_V$**	$\frac{\lambda}{m}(H.T.U.)_L$	$\frac{\lambda}{m}$	$(H.T.U.)_L$	Re_L	$\frac{(H.T.U.)_L}{Re_L}$
	kN/m²	max.	half max.	m	m		m	m		m		m
n-C_7-mch	101·5	1050		0·109	0·110	3200	0·051	0·059	1·01	0·058	82	$0·71 \times 10^{-3}$
			525	0·091	0·092	1600	0·044	0·048	1·01	0·048	41	$1·16 \times 10^{-3}$
n-C_{10}-*t*-dec	101·5	1050		0·102	0·107	3000	0·046	0·061	1·10	0·055	82	$0·68 \times 10^{-3}$
			525	0·087	0·092	1500	0·040	0·052	1·10	0·047	41	$1·15 \times 10^{-3}$
	13·3	500		0·103	0·109	2100	0·044	0·065	1·11	0·059	22	$2·7 \times 10^{-3}$
			250	0·093	0·098	1050	0·038	0·060	1·11	0·054	11	$4·9 \times 10^{-3}$
	1·3	350		0·114	0·120	1700	0·040	0·080	1·13	0·071	9	$7·9 \times 10^{-3}$
			175	0·105	0·111	850	0·035	0·076	1·13	0·067	4·5	15×10^{-3}
n-C_{16}-*n*-h-b	1·3	450		0·107	0·099	2200	0·040	0·059	0·83	0·071	20	$3·5 \times 10^{-3}$
			225	0·098	0·090	1100	0·035	0·055	0·83	0·066	10	$6·6 \times 10^{-3}$
	0·16	280		0·109	0·100	1500††	0·037	0·063	0·83	0·076	9·5††	8×10^{-3}
			140	0·103	0·095	750††	0·032	0·063	0·83	0·076	5††	17×10^{-3}
2,2,4-*t*-m-p-*n*-C_8	101·5									0·064†	105	$0·61 \times 10^{-3}$
										0·051†	52	$0·98 \times 10^{-3}$

* Data taken from Fig. 3.
** Calculated with eq. (12).
† Data from Fig. 5.
†† Calculated on average column pressure and temperature.

eq. (14) and in eq. (10) should give an indication of the average liquid layer thickness. This ratio shows

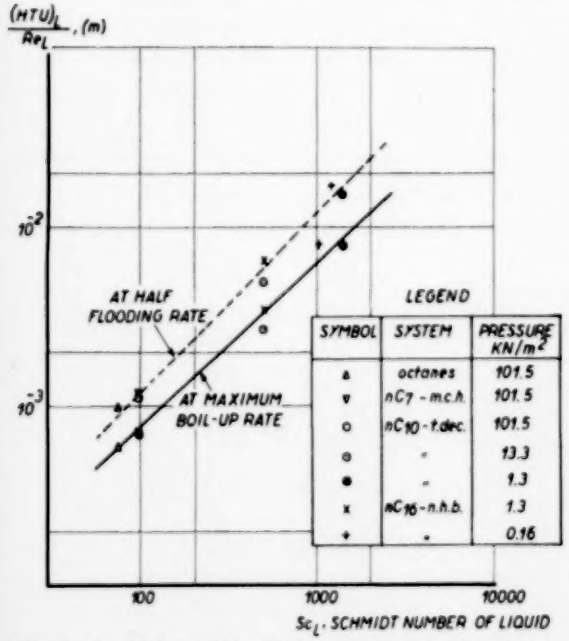

Fig. 6. Correlation of liquid phase resistance data of 1 m Vigreux column.

for w a value of 0·20 mm. Though no special hold up measurements were made with the present column, its value may be estimated at about 6–7 ml [8]; this shows an average liquid layer thickness of 0·17 to 0·20 mm. The agreement between the two w-values thus calculated is quite good and in fact much better than would be expected on the basis of the many assumptions and uncertainties in physical constants involved.

It has been shown that the method of interpretation used leads to quite logical and consistent results. They enable us to formulate the following insight gained with respect to the influence of pressure upon the separative effect of a Vigreux column.

At constant boil-up rate, a decrease in pressure gives rise to a large increase in liquid phase resistance to material transfer because of increasing viscosity. As at atmospheric pressure this liquid phase resistance is already more than half the total resistance, it causes the overall separating power to diminish at a reduction in pressure. However, this effect is partly nullified by a simultaneous increase in turbulence induced in the liquid by the increasing vapour velocity.

The question may be raised how far the present results may be compared with those obtained on other types of column.

In the case of packed columns, the effect of vapour rate in generating turbulence in the liquid may be

much smaller than with the Vigreux column. This will be caused by the distribution of the liquid over more or less capillary spaces in which it cannot well be agitated, in particular when the packing material is fine. Moreover, wetting of the packing may be a function of the liquid rate, complicating the $(H.T.U.)_L$ vs flow rate relation. Both factors suggest that in packed columns a decrease in pressure will cause a greater loss in overall efficiency than in the Vigreux column.

This reasoning is substantiated by available literature data. FELDMAN *et al.* [16] showed a Podbielniak Heligrid column to lose about 50% of its separating power when reducing the pressure from 101·5 kN/m² to 6·7 kN/m² (760 to 50 mm Hg). Approximately the same effect may be shown from data obtained by STRUCK and KINNEY [28] on several types of column packing. It should be kept in mind however that in their work incorrect values of the relative volatility for the *n*-decane-transdecalin system were used. Correction of the STRUCK and KINNEY data using the relative volatilities mentioned in the present paper shows a decrease of about 30% in separating power at the same pressure region mentioned above.

BERG and POPOVAC [2] determined the efficiency of Fenske helices packing at various pressures with the toluene-*n*-octane system. The vapour-liquid equilibrium data used are thermodynamically inconsistent however. Approximate correction of these data shows that at maximum boil-up rate the separating efficiency decreases by 20% when applying a pressure reduction from atmospheric pressure to 6·7 kN/m² (50 mm Hg).

Apart from the study of the pressure effects upon the separating power, some other aspects of a fractionating column should be considered in judging the performance of the apparatus at low pressures.

Pressure drop data obtained with the *n*-hexadecane-*n*-heptylbenzoate system are given in Table 3. It is seen that at the lowest pressure used (0·16 kN/m² or 1·3 mm Hg) pressure drop of the Vigreux column is still moderate though equal to a number of times the top pressure (at max. boil-up rate about 0·4 kN/m² (3 mm Hg). REED and FENSKE [25] suggest that pressure drop data of a packed column obtained at various pressures may be correlated by plotting the product of average vapour density and pressure drop against mass flow rate. As demonstrated in Fig. 7, this correlation also holds fairly well for the Vigreux column.

The pressure drop measurements recorded with the oil manometer being taken between reboiler and top of the column, it was thought that some extra pressure loss occurred in the reboiler section (including the reflux measuring device). Therefore some pressure drop measurements on the Vigreux section proper were made by recording the temperature drop between top and bottom ends of this section when refluxing pure *n*-hexadecane (see Table 9). The temperature drop data were converted into pressure drop data by using the vapour pressure curve of *n*-hexadecane. The results (plotted in Fig. 7 too) show that the actual pressure drop over the Vigreux section is some 30% lower than the pressure drop over the whole column.

Maximum boil-up rate is seen in Fig. 3 to be affected markedly by a reduction in total pressure. As

VOL. 1 1952

Table 8. Constants used in calculations

System	Pressure	Liquid			Vapour			Sc_L	Sc_V
		Density	Viscosity	Diffusivity	Density	Viscosity	Diffusivity		
	kN/m²	kg/m³	N sec/m²	m²/sec	kg/m³	N sec/m²	m²/sec		
n-heptane-*m*-cyclohexane	101·5	660	$0·26 \times 10^{-3}$	4×10^{-9}	3·3	7×10^{-6}	$3·7 \times 10^{-6}$	100	0·57
2,2,4-*t*-*m*-pentane-*n*-octane	101·5	620	$0·21 \times 10^{-3}$	$4·5 \times 10^{-9}$	3·5	7×10^{-6}	$3·3 \times 10^{-6}$	75	0·60
n-decane-transdecalin	101·5	690	$0·27 \times 10^{-3}$	$3·9 \times 10^{-9}$	3·8	7×10^{-6}	$3·6 \times 10^{-6}$	100	0·51
n-decane-transdecalin	13·3	770	$0·56 \times 10^{-3}$	$1·5 \times 10^{-9}$	0·6	6×10^{-6}	19×10^{-6}	500	0·53
n-decane-transdecalin	1·3	820	$0·90 \times 10^{-3}$	$0·8 \times 10^{-9}$	0·07	$5·5 \times 10^{-6}$	$0·16 \times 10^{-3}$	1400	0·49
n-hexadecane-*n*-heptylbenzoate	1·3	760	$0·54 \times 10^{-3}$	$1·4 \times 10^{-9}$	0·085	$5·0 \times 10^{-6}$	$0·13 \times 10^{-3}$	500	0·45
n-hexadecane-*n*-heptylbenzoate	0·16	780	$0·87 \times 10^{-3}$	$0·8 \times 10^{-9}$	0·011	$4·5 \times 10^{-6}$	$0·9 \times 10^{-3}$	1400	0·45

a first approximation it may be concluded that by employing a tenfold reduction in pressure, maximum boil-up rate is reduced to half its original value. This approximate statement is in agreement with the results found by STRUCK and KINNEY [28] on packed columns. A more accurate correlation may be given by plotting

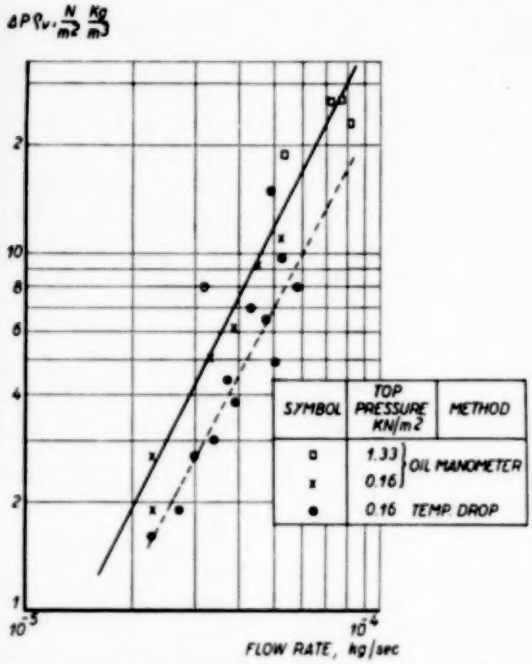

Fig. 7. Correlation of pressure drop data obtained with the *n*-hexadecane *n*-heptylbenzoate system in Vigreux column.

Table 9. Pressure drop measurements on Vigreux column, length 1·0 m, diameter 11 mm, at 0·16 N/m² top pressure by means of temperature drop when refluxing n-hexadecane

Boil-up rate	*Vapour temperatures °C*		*Pressure drop*
ml/h	*top*	*bottom*	*kN/m²*
270	109·5	130·5	0·40
220	110·0	128·0	0·33
190	109·0	124·0	0·24
150	109·0	121·0	0·17
120	109·0	118·0	0·12
160	109·0	120·0	0·15
200	109·0	123·0	0·22
260	109·0	125·0	0·26
300	109·0	129·0	0·36
310	110·0	132·0	0·44
150	110·0	122·5	0·20
120	109·0	115·0	0·07
240	108·0	127·0	0·32
250	109·0	133·0	0·49
140	108·5	118·0	0·13

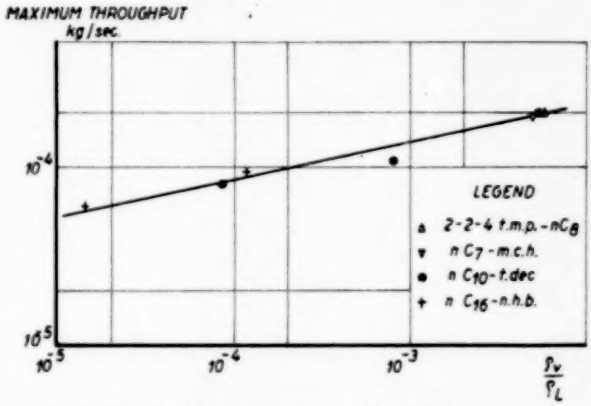

Fig. 8. Correlation maximum throughput data of Vigreux column.

the maximum boil-up rate (expressed as mass flow rate) versus the ratio of vapour and liquid densities [25], as shown in Fig. 8.

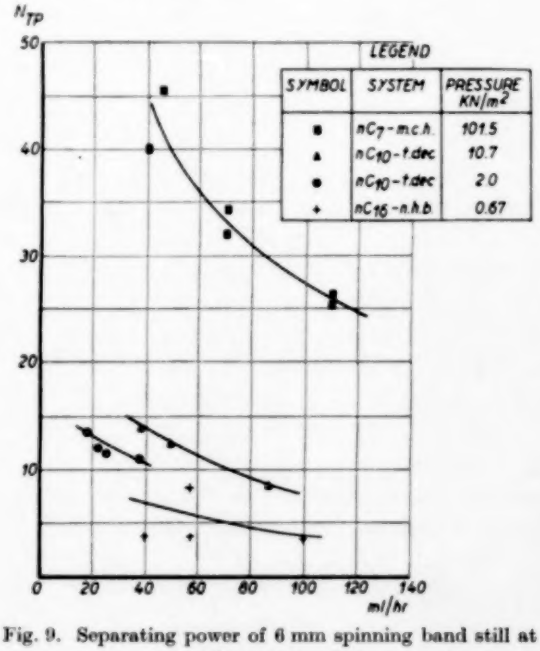

Fig. 9. Separating power of 6 mm spinning band still at various pressures.

No measurements of hold up were made in this study of the Vigreux column. It is believed that its value will not be much influenced by the pressure applied, viscosity and density effects entering the equations for layer thickness of a falling liquid film only by the 1/3 power [15].

From the results obtained in this study it may be stated in conclusion that, though of only moderate separating power, the Vigreux type of fractionating column will be a useful tool in vacuum distillation down to bottom pressures of about 0·67 kN/m² (5 mm Hg).

Rotating band columns

Separating power data measured with the 6 mm rotating band column at constant rotational speed of about 50 rev. per sec under varying pressures are presented in Fig. 9 as a function of boil-up rate. At atmospheric pressures the separating efficiency proves to be fairly high (H.E.T.P. values of 15–25 mm being realized). A tenfold reduction in pressure however has a detrimental effect: a decrease of about 70% in separating power is observed.

Before discussing these phenomena more fundamentally, some attention should be paid to the relative vapour and liquid phase resistances under the conditions of the experiments. Considering the REYNOLDS numbers of vapour flow in Tables 10 and 11 it should be concluded that the flow type is laminar. Neglecting the influence of the rotating element for a moment, the material transfer in the vapour phase should obey eq. (9). At total reflux, the *n*-heptane-methylcyclohexane system liquid REYNOLDS numbers being about 2·7% of Re_V, calculation from eq. (9) and (10) shows that $(H.T.U.)_L$ presents only about 8% of the total resistance to material transfer (assuming liquid layer thickness at about 0·1 mm [31]). From this discussion it may be concluded that at zero speed of rotation the overall efficiency may be adequately described in terms of vapour phase material transfer. Now, at first sight, it might be expected that by increasing the vapour phase material transfer by agitation, liquid phase resistance would become controlling. However, the construction of the rotating band column is such that the spinning band agitates the liquid phase as well. In this study therefore the percentage liquid phase resistance will be assumed not to be influenced very much by agitation. Consequently,

Table 10. Performance of rotating band columns at atmospheric pressure
System n-heptane-m-cyclohexane

Column diam.	*Boil-up rate*		*Rotational speed*		n_D^{20} *products*		*Separating power*	
mm	*ml/h*	Re_V	*rev/sec*	Re_R	*top*	*bottom*	*n*	$\frac{(H.T.U.)_{OV}}{d}$
6	70	380	45	1950	1·3963	1·4155	34·5	2·9
	70	380	47	2000	1·3975	1·4155	32	3·1
	70	380	17	730	1·4000	1·4155	27	3·7
	80	430	18	770	1·4007	1·4155	26	3·9
	70	380	18	770	1·3995	1·4155	28	3·6
	70	380	8·5	370	1·4055	1·4155	18	5·6
	80	430	8·5	370	1·4075	1·4156	15	6·7
	80	430	4·2	180	1·4102	1·4157	11·5	8·9
	70	380	3·3	150	1·4105	1·4158	10	10·2
	70	380	2·0	85	1·4117	1·4158	7·5	13·6
	80	430	40	1700	1·3987	1·4165	32	3·1
6	100	540	67	2900	1·4070	1·4175	21	4·8
	110	590	50	2150	1·4023	1·4168	26·5	3·8
	110	590	50	2150	1·4033	1·4170	25·5	3·9
	110	590	28	1200	1·4045	1·4170	23·5	4·5
	110	590	32	1400	1·4048	1·4171	23·5	4·3
	110	590	15	640	1·4082	1·4172	18	5·6
	110	590	4	170	1·4133	1·4173	8·5	12·0
	110	590	6	260	1·4123	1·4174	11	9·3
6	50	270	67	2900	1·3921	1·4141	43·5	2·3
	45	240	57	2450	1·3935	1·4166	45	2·2
	50	270	60	2600	1·3951	1·4167	40·5	2·5
	35	190	35	1500	1·3933	1·4167	46	2·2
	40	220	8·5	370	1·4008	1·4168	29	3·5
	40	220	4·7	200	1·4048	1·4170	23	4·4
	40	220	50	2150	1·3960	1·4172	40	2·5
	45	240	47	2000	1·3947	1·4180	45·5	2·2
	40	220	60	2600	1·3945	1·4181	46·5	2·1
	35	190	9	390	1·4009	1·4182	33·5	3·0
	45	240	23	1000	1·3975	1·4184	40·5	2·5
	40	220	10	430	1·3965	1·4187	44	2·3
	45	240	11	470	1·4017	1·4192	36	2·8
	45	240	4	170	1·4108	1·4193	20·5	4·9
	40	220	1·7	75	1·4142	1·4194	14·5	6·9
3	39	420	27	230	1·3935	1·4154	42	3·2
	36	390	18	150	1·3952	1·4158	38	3·5
	36	390	11	95	1·4030	1·4152	21	6·3
	36	390	6	50	1·4088	1·4175	18	7·4
	24	260	27	230	1·3893	1·4135	57	2·3
	21	230	27	230	1·3900	1·4148	56	2·4

VOL. 1 1952

Table 11. Performance of 6 mm rotating band column at reduced pressures

Test mixture	Pressure		Boil-up rate		Rotational speed		n_D^{20} products		Separating power	
	kN/m^2	mm Hg	ml/h	Re_V	rev/sec	Re_R	top	bottom	n	$\frac{(H.T.U.)_{OV}}{d}$
n-decane-transdecalin	10·7	80	87	670	50	390	1·4515	1·4672	8·5	12·4
			50	380	50	390	1·4376	1·4672	12·5	8·4
			38	290	50	390	1·4327	1·4672	14	7·5
	2·0	15	38	330	50	90	1·4457	1·4659	11	9·5
			19	160	50	90	1·4383	1·4659	13·5	7·7
			25	220	50	90	1·4437	1·4659	11·5	9·1
			22	190	50	90	1·4396	1·4650	12	8·7
n-hexadecane-n-heptylbenzoate	0·67	5	40	400	50	60	1·4584	1·4880	3·6	26
			57	560	50	60	1·4663	1·4906	3·7	25
			100	990	50	60	1·4644	1·4902	3·7	25
			57	560	50	60	1·4483	1·4903	8·3	11

in the discussions to follow, vapour phase resistance to transfer will be considered controlling throughout.

In order to gain more insight into the mechanism of agitation in connection with the separation process, of this paper, the data obtained should be plotted as $(H.T.U.)_{OV}/d\,Re_V$ *vs* the REYNOLDS number of rotation Re_R. The picture obtained by this method is shown in Fig. 10.

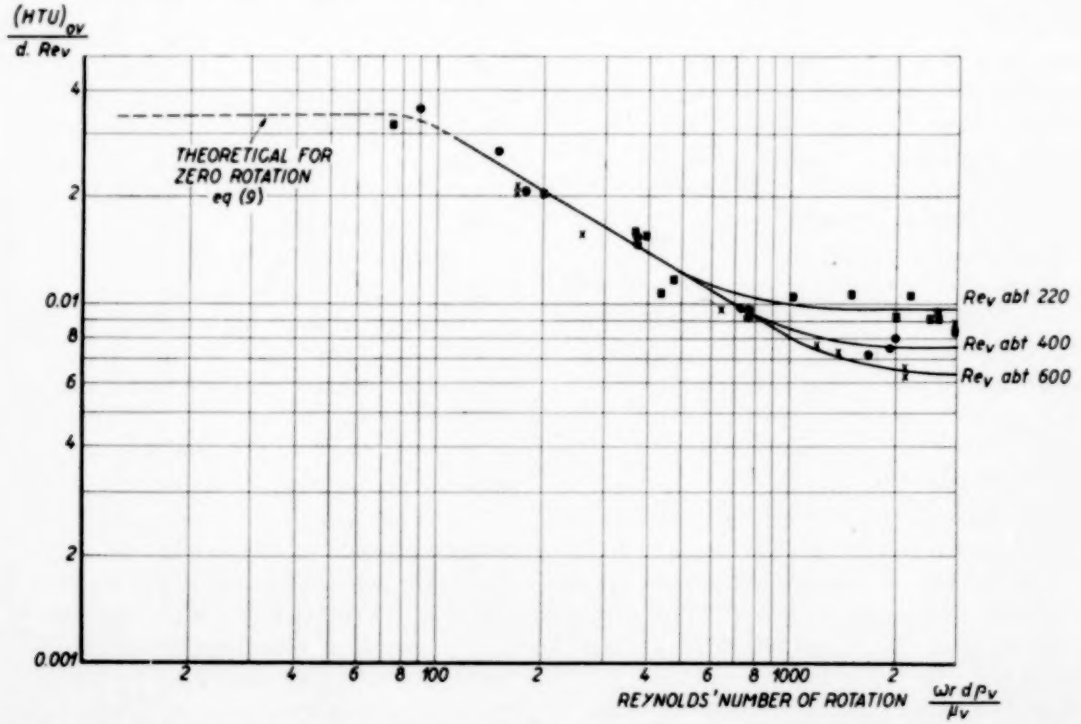

Fig. 10. Influence of rotational speed at atmospheric pressure on overall vapour resistance in 6 mm spinning band column.

a number of experiments were run at atmospheric pressure with n-heptane-methylcyclohexane under wide variation of rotational speed in the 6 mm column (Table 10). As was suggested in the theoretical part

It is seen that at Re_R up to 100 separating power of the column equals approximately the theoretical value calculated with eq. (9). Obviously the effect of rotation is negligible at the rotational speed applied

(about 2 to 3 rev. per sec). Increasing Re_R above 100, a distinct influence of rotation is noted, however; it should be concluded therefore that Re_R about 100 represents the critical value discussed in the theoretical part.

In the region Re_R 100–700 the data obtained at various vapour rates are well correlated by one single straight line. In this region the flowrate-separating power function is not affected by the stirring rate, $(\text{H.T.U.})_{OV}/dRe_V$ being constant at a specified rotational speed in agreement with the suggestion given in the theoretical part.

When the REYNOLDS number of rotation is raised above 700, it has a less pronounced effect on causing a further decrease in the $(\text{H.T.U.})_{OV}$ value. In fact, for a vapour flow of $Re_V = 220$, rotation above $Re_R = 1000$ does not decrease $(\text{H.T.U.})_{OV}$ any further. At higher vapour flow rates this critical Re_R-number has a higher value.

In discussing this phenomenon, the possibility of a limit set by liquid resistance which has so far been neglected should be considered here. From Fig. 10 it is learned that at $Re_R = 1000$, the overall $(\text{H.T.U.})_{OV}$ has been reduced by about 75%. In the discussion on the relative values of phase resistances it was shown that total vapour resistance equalled about 92% when no agitation is applied; therefore when at $Re_R > 1000$ liquid phase resistance should become controlling. a larger decrease than about 75% in $(\text{H.T.U.})_{OV}$ would be expected; moreover, no consideration has yet been given to the fact that liquid phase resistance is reduced too by the agitation. It seems therefore quite possible that liquid phase resistance as such cannot be the cause of the existence of a second critical rotational speed above which no further increase in overall separating power can be effected.

When imagining the action of the rotating band on the separation process, it will be clear that the separating efficiency is particularly enhanced when the agitation increases the velocity of diffusion in the direction perpendicular to the directions of vapour and liquid flow. This effect will in particular be obtained by the centrifugal action of the rotating band. However, agitation will increase diffusion in the direction of vapour and liquid flow as well, causing a counter-diffusional effect. Normally counter-diffusion or back-diffusion plays no important role [23], [32] in a wetted-wall column; at high rotating speeds however the rotating strip becomes twisted and vertical mixing effects in the liquid and vapour phases are becoming very probable.

Generally, back-diffusional effects are counterbalanced by increasing the convection streams in the separation process. Thus it should be expected that with higher liquid and vapour loads vertical mixing causes a smaller decrease in separating power than at lower loads. As already pointed out above, this effect is borne out by the experimental results: at lower loads ($Re_V = 220$) separating efficiency is increased less than at high loads ($Re_V = 600$, Fig. 10).

The criterion whether the rotating band causes marked vertical mixing in vapour or liquid streams may be found in the relative linear velocities in the phase concerned and the circumferential velocity of the stirring mechanism. The higher the linear velocity in the phase, the less the probability that large portions of it will be swung back by the agitating element. Due to large difference in linear velocities, mixing effects in the vapour phase are not likely to be the same at atmospheric and at low pressure. Under both these conditions however in the experiments made liquid velocities are of the same order of magnitude. Therefore, when back-diffusional effects can be shown to be the same in the atmospheric and in the low-pressure experiments, liquid mixing should be regarded responsible.

An indication of the back-diffusional effects is obtained by considering the $(\text{H.T.U.})_{OV}$-Re_V relationship. When no vertical mixing occurs, $(\text{H.T.U.})_{OV}$ is proportional to Re_V. This is the case at low numbers of revolution, as shown in Fig. 11 (4 and 8·5 rev. per sec). At about 50 rev. per sec at atmospheric pressure, mixing causes $(\text{H.T.U.})_{OV}$ to be proportional to $Re_V^{0.55}$. As shown in Fig. 11 too, this relation also holds at lower pressures. Now, recalling the fact that linear velocities in the vapour phase are 10–50 fold the atmospheric vapour velocities, it should be concluded that vertical mixing effects play only an important role in the liquid phase, thus limiting the ultimate separating power to be obtained by agitation.

In connection with the back-diffusional effects found, it will be clear that the experiments at lower pressures can only be correlated with the atmospheric pressure experiments under conditions of corresponding vertical mixing, *i.e.* only experiments at the same rotational speed (50 rev. per sec) may be used in the correlation.

The final correlation of the experiments with the 6 mm column at 50 rev. per sec is presented in Fig. 12

VOL. 1 1952

as curve A, in which the $(H.T.U.)_{OV}$ data, corrected for REYNOLDS number and SCHMIDT numbers involved, are plotted against the REYNOLDS number of rotation. It is seen that the data obtained at various pressures without varying the rotational speed correlate in a like manner as data obtained at atmospheric pressures with variation of rotational speed (see curve B). Obviously correlation of data against the REYNOLDS number of rotation is sound; it shows that an increase in density has the same effect as an increase in rotational speed. At pressures of about 2·0 kN/m² (15 mm Hg) the density of the vapour phase is so low that even agitation at 50 rev. per sec does not have any effect on the overal separating power. As may be calculated from eq. (9), separating power is even 30% too low, owing to vertical mixing effects in the liquid phase at this high number of revolution.

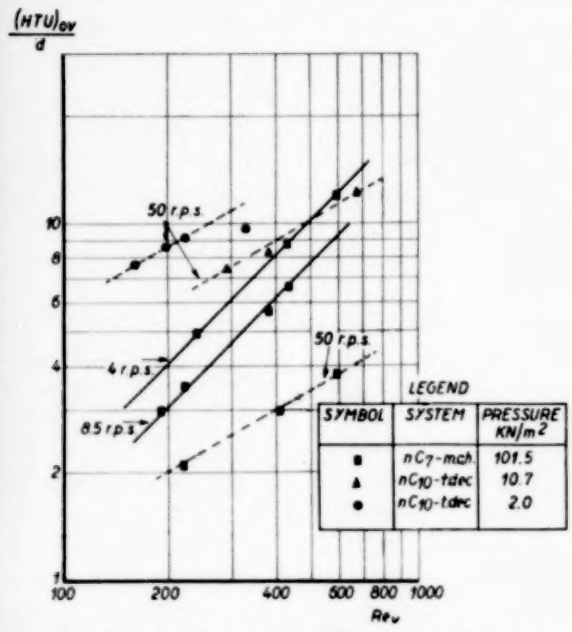

Fig. 11. Relationship between $(H.T.U.)_{OV}$ and REYNOLDS number of vapour flow at various rotational speeds. (6 mm spinning band column)

In Fig. 12 the results obtained with the 3 mm diameter spinning band column are plotted too (curve C). Further data obtained at atmospheric pressure by BIRCH [3] *et al.* on a 36 mm diameter rotating band column are included (curve D). In both cases an influence of REYNOLDS number of rotation on the separating power analogous to that found with the 6 mm diameter column is shown. At rotational speeds of the BIRCH column higher than that corresponding

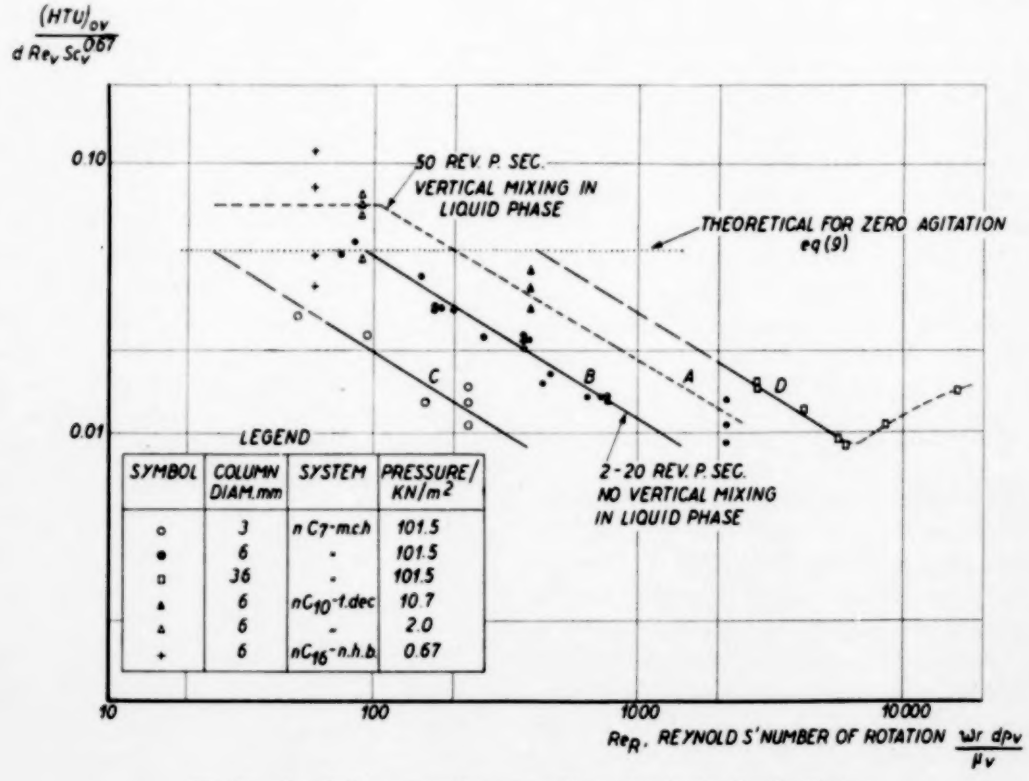

Fig. 12. Correlation separating power data of spinning band columns

with $Re_R \sim 6000$, $(\text{H.T.U.})_{OV}$ is found to increase again, showing the same mixing effects as described with the 6 mm column.

In spite of correlation against Re_R it is seen from Fig. 12 that the data for the three columns do not coincide on a single line, but three separate functions are obtained. This should be ascribed to different $(Re_R)_{\text{crit.}}$ values for each of the three columns, as might be expected on the ground of the theoretical discussions on agitation. As suggested, the critical values for Re_R should be a function of the ratio of diameter to clearance of the columns concerned. The following $(Re_R)_{\text{crit.}}$ values and d/Δ values may be tabulated from Fig. 12 and the dimensional data on the three columns:

Diameter column mm	$(Re_R)_{\text{crit.}}$	d/Δ *(approx.)*	$\dfrac{(Re_R)_{\text{crit.}}}{\left(\frac{d}{\Delta}\right)^{2.5}}$
3	25	3	1·6
6	95	5	1·7
36	400	9	1·7

It is seen that $(Re_R)_{\text{crit.}}$ increases markedly with the d/Δ ratio.

Actually, it may be calculated that Re_R is proportional to d/Δ raised to the 2·5 power. The influence of column dimensions in this respect is thus much more pronounced with spinning band columns than with concentric tube columns [*cf.* eq. (11)]. This quantitative relationship found should be considered with some reserve however; it is only indicative of the trend which various factors involved have on the efficiency of the rotating band column.

Under conditions liquid when mixing effects play no role, the following ultimate relation for $(\text{H.T.U.})_{OV}$ may be derived from Fig. 12.

$$\frac{(\text{H.T.U.})_{OV}}{d} = 0{\cdot}065\left(\frac{d}{\Delta}\right)^{2{\cdot}5} . Re_R^{-0{\cdot}4} . Re_V . Sc_V^{0{\cdot}67}.$$

Though this equation has only an illustrative value, it shows that at constant boil-up rate, Re_V and Sc_V being approximately independent of total pressure, separating power is controlled by Re_R. Thus, at constant speed of rotation, vapour density being proportional to pressure, separating power varies with pressure, raised to approximately 0·6 power.

The results gained with the spinning band columns may be compared with those obtained in other transfer processes influenced by agitation.

WILLINGHAM [35] and co-workers gave data on a rotating concentric tube column. Their results clearly show the existence of a critical rotational speed, above which a transition range follows in which the separating power increases sharply with rotational speed; at higher numbers of revolutions separating power increases less markedly. Though the results do not correlate well when using the method of the present paper, in the higher ranges of rotational speed $(\text{H.T.U.})_{OV}$ seems to decrease $Re_R^{0{\cdot}65}$.

Measurements on material and heat transfer in agitated vessels were made by HIXSON [19], [20] *et al.* and by CHILTON, DREW and JEBENS [10]. Using paddle type stirrers, they found the material and heat transfer coefficients to increase with Re_R raised to 0·62–0·67 power.

In both cases of the rotary concentric tube column and the agitated vessels material and heat transfer are enhanced to about the same degree as found with the spinning band columns. It therefore seems justified to consider the spinning band column as a series of agitated units, in each of which the effect of agitation has the same result as found in separate agitated vessels.

Finally it should be concluded from the present study that vapour-phase agitated columns cannot, as a rule, be regarded as special low-pressure columns. In fact, at pressures of about 1·3 kN/m² (10 mm Hg) and below, the separating efficiency is not better than that found with a wetted-wall column of the same dimensions and length.

Acknowledgement—The author is greatly indebted to Ir. E. SWEEP for his constant interest during this investigation and for the valuable criticism offered in the preparation of this paper. Assistance in the experimental work was given by J. J. DE JONG Jr., P. LEENEN, H. G. WEYLAND and G. P. WIJKER. The Management of the *Koninklijke/Shell-Laboratorium, Amsterdam (N.V. De Bataafsche Petroleum Maatschappij, The Hague)* is gratefully acknowledged for the permission to publish the results obtained.

NOTATION

a	= constant in eq. (1) and (2)	
c	= constant in eq. (11)	
D	= diffusivity	m²/sec
d	= diameter of column	m
H.T.U.	= height of transfer unit	m
L	= liquid flow rate	kmols/sec
$\overline{m}$	= averaged slope of equilibrium line	

VOL. 1 1952

N = (see footnote on page 175)
n = theoretical plate number of column
p = constant in eq. (1) and (2)
q = constant in eq. (1) and (2)
Re_L = REYNOLDS number of liquid flow, $4wu_L\varrho_L/\mu_L$
Re_R = REYNOLDS number of rotation, $\omega r d\varrho_V/\mu_V$
Re_V = REYNOLDS number of vapour flow, $du_V\varrho_V/\mu_V$
r = half width of rotating strip m
Sc = SCHMIDT number, $\mu/D\varrho$
T = temperature °K
u = average linear velocity m/sec
V = vapour flow rate kmols/sec
w = thickness liquid layer m
x = liquid composition, mol fraction
x^* = liquid composition, in equilibrium with vapour
y = vapour composition, mol fraction
y^* = vapour composition, in equilibrium with liquid
z = height of column m
Δ = clearance between two rotating cylinders or between column diameter and spinning band, $(d-2r)$ m
μ = viscosity Nsec/m²
ϱ = density kg/m³
ω = angular velocity rad/sec

Indices

1 = lower end of column
2 = upper end of column
L = liquid phase
V = vapour phase
i = at plane of contact between liquid and vapour phase

REFERENCES

[1] BENEDICT, M., JOHNSON, C. A., SOLOMON, E., RUBIN, L. C.; Trans. Amer. Inst. Chem. Engrs 1945 **41** 371–392. [2] BERG, L., POPOVAC, D. O.; Chem. Eng. Progr. 1949 **45** 683–691. [3] BIRCH, S. F., GRIPP, V., NATHAN, W. S.; J. Soc. Chem. Ind. 1947 **66** 33–40. [4] BREIWISCH; Tom Reel 15 Frame No. 2285–2291. [5] BROOKS, R. R., NELSEN, F. M., ZAHN, V.; Petr. Refiner 1948 **27** 620–621. [6] BRINSMADE, D. S., BLISS, H.; Trans. Amer. Inst. Chem. Engrs 1943 **39** 679–713. [7] BYRON, E. S., BOWMAN, J. R., COULL, J.; Ind. Eng. Chem. 1951 **43** 1002–1010. [8] CARNEY, T. P.; Laboratory Fractional Distillation, p. 94, New York 1949. [9] CHILTON, T. H., COLBURN, A. P.; Ind. Eng. Chem. 1935 **27** 255–260. [10] CHILTON, T. H., DREW, T. B., JEBENS, R. H.; *Ibid.* 1944 **36** 510–516. [11] COLBURN, A. P.; Trans. Amer. Inst. Chem. Engrs 1939 **35** 211–236. [12] CORNISH, R. J.; Proc. Roy. Soc. 1933 **140** 227–240. [13] DUNCAN, D. W., KOFFOLT, J. H., WITHROW, J. R.; Trans. Amer. Inst. Chem. Engrs 1942 **38** 259–280. [14] FAGE, A.; Proc. Roy. Soc. 1938 **165** 501–517. [15] FALLAH, R., HUNTER, T. G., NASH, A. W.; J. Soc. Chem. Ind. 1934 **53** 369–379 T. [16] FELDMAN, F., MYLES, M., WENDER, I., ORCHIN, O.; Ind. Eng. Chem. 1949 **41** 1032–1036. [17] GILLILAND, E. R.; *Ibid.* 1934 **26** 681–685. [18] GILLILAND, E. R., SHERWOOD, T. K.; *Ibid.* 1934 **26** 516–523. [19] HIXSON, A. W., BAUM, S. J.; *Ibid.* 1941 **33** 478–485. [20] HIXSON, A. W., BAUM, S. J.; *Ibid.* 1941 **33** 1433–1439. [21] HOUSTON, R. W., WALKER, C. A.; *Ibid.* 1950 **42** 1105–1112. [22] KREVELEN, D. M. v., HOFTIJZER, P. J.; Chem. Eng. Progr. 1948 **44** 529–536. [23] KUHN, W., RYFFEL, K.; Helv. Chim. Acta 1943 **26** 1693–1721. [24] NEDERBRAGT, G. W., BOELHOUWER, J. W. M.; Physica 1947 **13** 305–318. [25] REED, T. M., FENSKE, M. R.; Ind. Eng. Chem. 1950 **42** 654–660. [26] SCHAFFNER, R. M., BOWMAN, J. R., COULL, J.; Trans. Amer. Inst., Chem. Engrs 1943 **39** 77–92. [27] SHERWOOD, T. K.; Ind. Eng. Chem. 1950 **42** 2077–2084. [28] STRUCK, R. T., KINNEY, C. R.; *Ibid.* 1950 **42** 77–82. [29] SUROSKY, A. E., DODGE, B. F.; *Ibid.* 1950 **42** 1112–1119. [30] TAYLOR, G. I.; Phil. Trans. 1923 **223** 289. [31] VERSCHOOR, H.; Trans. Inst. Chem. Engrs 1938 **16** 66–76. [32] WESTHAVER, J.; Ind. Eng. Chem. 1942 **34** 126–130. [33] WILKE, C. R.; Chem. Eng. Progr. 1949 **45** 218–224. [34] WILLIAMS, F. G.; Ind. Eng. Chem. 1947 **39** 779–782. [35] WILLINGHAM, C. B., SEDLAK, V. A., ROSSINI, F. D., WESTHAVER, J.; *Ibid.* 1947 **39** 706–712. [36] ZUIDERWEG, F. J.; Chem. Eng. Sci. 1952 **1** 167–177.

RESEARCH NOTE

A graphical method for computing the flow of compressible fluids in pipes

W. S. NORMAN

University College London

(Received 22 January 1952)

The flow of compressible fluids in pipes is governed by two relations which can be expressed mathematically as the energy balance or Bernoulli equation and the equation of state of the fluid. The energy balance is represented by the equation

$$\left.\begin{aligned}(Z_2-Z_1)+(p_2v_2-p_1v_1)+\left(\frac{V_2^2-V_1^2}{2g_c}\right)+\\+J(u_2-u_1)=JQ+W_0\end{aligned}\right\} \quad (1)$$

or in the differential form

$$dZ+d(pv)+\frac{V\,dV}{g_c}+J\,du=J\,dQ+dW_0. \quad (2)$$

When a fluid is flowing in a pipe or nozzle the external work term W_0 is zero, but friction causes a degradation of mechanical energy into heat and from the first law of thermodynamics

$$J\,dQ+dF=J\,du+p\,dv. \quad (3)$$

The frictional loss in a pipe is usually expressed by the equation

$$dF=\frac{4fV^2\,dL}{2g_cD} \quad (4)$$

and from eqs. (2), (3) and (4) the mechanical energy balance is obtained:

$$dZ+v\,dp+\frac{V\,dV}{g_c}+\frac{4fV^2\,dL}{2g_cD}=0. \quad (5)$$

The friction factor f is a function of the Reynolds number and of the roughness of the pipe surface. The Reynolds number for the isothermal flow of a perfect gas in a uniform pipe is constant along the pipe since the mass flow rate $G=\varrho V$ is constant and the viscosity of a perfect gas is independent of its pressure. Any change in the temperature of the gas will alter its viscosity and therefore the Reynolds number and friction factor, but for fully turbulent flow (Reynolds numbers greater than 10000) the change in the friction factor is relatively small and may usually be ignored.

Eq. (5) may be written, substituting $V=Gv$, as

$$dZ+v\,dp+\frac{G^2}{g_c}v\,dv+\frac{4fG^2}{2g_cD}v^2\,dL=0. \quad (6)$$

This equation can be integrated only if the relation between p and v is known. For isothermal flow $pv=$ constant, and since the term dZ can usually be neglected when dealing with gases, eq. (6) may be rearranged as

$$\frac{p}{p_1v_1}\,dp+\frac{G^2}{g_c}\times\frac{dv}{v}+\frac{4fG^2}{2g_cD}\,dL=0. \quad (7)$$

Integrating between state 1 and state 2 for a pipe of length L gives

$$\frac{1}{p_1v_1}\int_1^2 p\,dp+\frac{G^2}{g_c}\int_1^2\frac{dv}{v}+\frac{4fG^2}{2g_cD}\int_0^L dL=0$$

$$p_1^2-p_2^2=\frac{p_1v_1G^2}{g_c}\left(2\,ln\,\frac{v_2}{v_1}+\frac{4fL}{D}\right) \quad (8)$$

$$\left.\begin{aligned}p_1-p_2&=\frac{p_1v_1G^2}{g_c(p_1+p_2)}\left(2\,ln\,\frac{v_2}{v_1}+\frac{4fL}{D}\right)\\&=\frac{G^2}{g_c\left(\frac{1}{v_1}+\frac{1}{v_2}\right)}\left(2\,ln\,\frac{v_2}{v_1}+\frac{4fL}{D}\right)\\&=\frac{G^2}{2g_c\varrho_{av}}\left(2\,ln\,\frac{v_2}{v_1}+\frac{4fL}{D}\right)\end{aligned}\right\} \quad (9)$$

where ϱ_{av} is the average density of the gas at the average pressure $(p_1+p_2)/2$. When the term $4fL/D$ is large in comparison with $2\,ln(v_2/v_1)$, so that the latter may be ignored, eq. (9) is identical to the friction factor equation for an incompressible fluid, with the gas density taken as the average between the initial and final states.

The equation of state for the adiabatic flow of a perfect gas, derived from the thermodynamic relations, is

$$d(pv)+\frac{\varkappa-1}{\varkappa}\frac{V\,dV}{g_c}=0 \quad (10)$$

$$\left.\begin{aligned}pv+\frac{\varkappa-1}{\varkappa}\frac{V^2}{2g_c}&=\text{constant}\\&=p_1v_1+\left(\frac{\varkappa-1}{\varkappa}\right)\frac{G^2v_1^2}{2g_c}\end{aligned}\right\} \quad (11)$$

$$\left.\begin{aligned}v\,dp&=d(pv)-(pv)\frac{dv}{v}\\&=-\frac{1}{2}\left(\frac{\varkappa-1}{\varkappa}\right)\frac{G^2}{g_c}v\,dv-\\&\quad-\left\{p_1v_1+\left(\frac{\varkappa-1}{\varkappa}\right)\frac{G^2v_1^2}{2g_c}\right\}\frac{dv}{v}.\end{aligned}\right\} \quad (12)$$

VOL. 1 1952

Substituting in eq. (6) and dividing by v^2 gives

$$\left(\frac{\varkappa+1}{\varkappa}\right)\frac{G^2}{2g_c}\frac{dv}{v} - \left\{p_1 v_1 + \left(\frac{\varkappa-1}{\varkappa}\right)\frac{G^2 v_1^2}{2g_c}\right\}\frac{dv}{v^3} + \frac{4fG^2}{2g_c D}\,dL = 0$$

$$\left(\frac{\varkappa+1}{\varkappa}\right)\frac{G^2}{2g_c} ln\,\frac{v_2}{v_1} + \frac{1}{2}\left\{p_1 v_1 + \left(\frac{\varkappa-1}{\varkappa}\right)\frac{G^2 v_1^2}{2g_c}\right\}\left\{\frac{1}{v_2^2} - \frac{1}{v_1^2}\right\} + \frac{4fG^2 L}{2g_c D} = 0.$$

Dividing by $G^2/2g_c$,

$$\left.\begin{aligned}\left(\frac{\varkappa+1}{\varkappa}\right) ln\,\frac{v_2}{v_1} + \\ + \left\{\frac{p_1 v_1 g_c}{G^2} + \left(\frac{\varkappa-1}{\varkappa}\right)\frac{v_1^2}{2}\right\}\left\{\frac{1}{v_2^2} - \frac{1}{v_1^2}\right\} + \frac{4fL}{D} = 0.\end{aligned}\right\} \quad (13)$$

The flow conditions must satisfy the equation of state, eq. (11), and the energy balance, eq. (13), but owing to the complicated nature of these equations, a direct mathematical solution is out of the question and a numerical trial-and-error method must be followed. For example, if it was required to calculate the pressure drop for a known flow rate G in a pipe of specified dimensions, it would first be necessary to assume a value for the specific volume of the gas at the exit of the pipe, v_2, and substituting the known values of p_1, v_1, G, D and f, to calculate the pressure at the exit, p_2, from eq. (11), and then the length of pipe L, necessary to give this pressure drop using eq. (13). Then if the calculated pipe length differed from that specified, it would be necessary to assume other values of v_2, and repeat the calculation until the correct conditions were found.

A convenient graphical solution to these equations has been developed in terms of three dimensionless ratios, $(p_1 - p_2)/p_1$, $4fL/D$ and the initial Mach number Ma_1, where

$$\left.\begin{aligned}Ma_1 &= \frac{V_1}{V_{a1}} \\ &= \frac{G v_1}{\sqrt{\varkappa g_c p_1 v_1}}.\end{aligned}\right\} \quad (14)$$

Substituting in eq. (13)

$$\frac{4fL}{D} = \frac{1}{\varkappa}\left\{\frac{1}{Ma_1^2} + \frac{\varkappa-1}{2}\right\}\left\{1 - \left(\frac{v_1}{v_2}\right)^2\right\} - \left(\frac{\varkappa+1}{\varkappa}\right) ln\,\frac{v_2}{v_1}. \quad (15)$$

Also from eq. (11)

$$p_1 v_1 - p_2 v_2 = \frac{(\varkappa-1)}{\varkappa}\,\frac{G^2}{2g_c}\,(v_2^2 - v_1^2)$$

$$\frac{p_1 - p_2}{p_1} = 1 - \frac{v_1}{v_2}\left\{1 + \frac{(\varkappa-1)\,Ma_1^2}{2}\left[1 - \left(\frac{v_2}{v_1}\right)^2\right]\right\}. \quad (16)$$

The chart shows the pressure drop ratio $(p_1 - p_2/p_1$ as a function of the initial Mach number Ma_1 and the friction number $4fL/D$ for adiabatic flow when the ratio of the specific heats $\varkappa$ is 1·4. The pressure drop ratio has also been calculated for isothermal flow using eq. (9) which may be written as

$$\frac{p_1 - p_2}{p_1} = \frac{G^2}{2g_c p_1 \varrho_{a\,v}}\left\{2\,ln\,\frac{v_2}{v_1} + \frac{4fL}{D}\right\} = \frac{\varkappa Ma_1^2}{2}\,\frac{\varrho_1}{\varrho_{a\,v}}\left\{2\,ln\,\frac{v_2}{v_1} + \frac{4fL}{D}\right\}.$$

For values of Ma_1 below 0·25 the calculated pressure drops for adiabatic and isothermal flow are almost

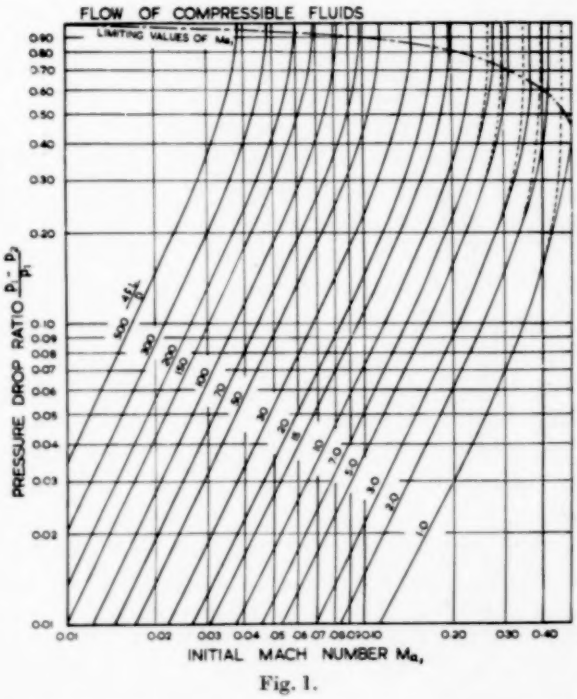

Fig. 1.

identical and are represented by single lines on the chart. Appreciable deviations occur between adiabatic and isothermal flow in the top right hand corner of the chart, when the full curves represent adiabatic flow and the broken curves the isothermal state.

For each value of $4fL/D$ there is a critical pressure drop at which the velocity at the discharge end of the pipe reaches the velocity of sound in the gas. At this point the discharge rate and initial Mach number Ma_1 attain their limiting values. The critical pressure drop and the limiting value of Ma_1 for adiabatic flow are indicated by the broken curve across the top of the chart.

The chart may be used, in conjunction with eq. (14), to calculate the pressure drop in a pipe for a given rate of flow, or the rate of flow when the pressure drop and dimensions of the pipe are known. The resistance due to pipe bends and fittings may be

evaluated in terms of the equivalent length of straight pipe, or in terms of the number of "velocity heads" lost, as recommended by LAPPLE [1].

The friction number $4fL/D$ represents the number of "velocity heads" lost through friction, since from the friction factor equation

$$\Delta p = \frac{4fL\varrho V^2}{2g_c D}$$

$$\frac{4fL}{D} = \frac{\Delta p}{(\varrho V^2/2g_c)}$$

where $\varrho V^2/2g_c$ represents the "velocity head" or pressure equivalent to the kinetic energy of the fluid.

When the chart is used to calculate the rate of flow of gas through a pipe connected to a vessel, the initial pressure p_1 must be taken as the pressure within the pipe at the inlet, this pressure being lower than the pressure p_0 in the vessel by an amount equivalent to the velocity head of the gas, plus any frictional losses at the inlet. In the case of a rounded inlet the frictional losses are small and the pressure drop is equivalent to the kinetic energy gained by the gas. Since this is a reversible process the pressure drop at the pipe inlet should be evaluated separately and added to the irreversible pressure loss due to friction in the pipe, to obtain the total drop from the receiver to the pipe outlet.

However, for many purposes, a sufficiently accurate result is obtained by assuming that the pressure drop at the inlet is an irreversible loss, and adding 1·0 velocity head for a rounded inlet, or 1·5 for an abrupt inlet, to the friction number $4fL/D$.

An exact method for calculating the pressure drop for a gas flowing from a vessel through a pipe with a rounded inlet has been presented by LAPPLE [1]. A detailed comparison of results calculated by LAPPLE's method and using the present chart with an allowance of 1·0 velocity head for the inlet shows that the deviation is appreciable only when the friction number for the pipe is less than 2·0. When the friction number for the pipe is 1·0 the maximum discharge rate calculated by LAPPLE's method is 4% higher than that calculated from this chart, assuming a loss of 1 velocity head at the inlet.

Example

Calculate the rate of discharge of air from a reservoir at 150 lb/in² gauge and 70° F through 33 ft of pipe, 2·067 in. internal diameter, with an abrupt inlet and three elbows.

Assumed friction factor, f =	0·0040
Friction number, $4fL/d$	
Pipe =	3·06
Inlet (equivalent) =	1·5
Elbows (equivalent) =	1·44
Total	6·0

$$\frac{p_1 - p_2}{p_1} = \frac{150}{164{\cdot}7} = 0{\cdot}907$$

$$v_1 = 1{\cdot}19 \text{ ft}^3/\text{lb}.$$

From chart $Ma_1 = 0{\cdot}295$

$$G = \frac{Ma_1}{v_1}\sqrt{\varkappa g_c p_1 v_1}$$

$$= \frac{0{\cdot}295}{1{\cdot}19}\sqrt{1{\cdot}4 \times 32{\cdot}2 \times 164{\cdot}7 \times 144 \times 1{\cdot}19}$$

$$= 279 \text{ (lb)/(sec)} \times (\text{ft}^2).$$

Cross section of pipe = 0·0233 ft².

Rate of flow = 6·49 lb/sec.

For the same problem the rate of flow calculated by LAPPLE [1] (page 423), was 6·41 lb/sec.

List of symbols

D = Pipe diameter
f = Friction factor
g_c = Gravitational constant
G = Mass flow rate
J = Mechanical equivalent of heat
L = Pipe length
Ma_1 = Mach number at inlet of pipe
p = Pressure
Q = Heat added to system
W_0 = Work done on system
u = Internal Energy
v = Specific volume
V = Velocity
V_a = Velocity of sound
Z = Height above a datum plane
ϱ = Gas density
$\varkappa$ = Ratio of specific heats (c_p/c_v)

REFERENCE

[1] LAPPLE, C. E.; Trans. Amer. Inst. Chem. Engrs 1943 **39** 385.

VOL. 1 1952